



HELLENIC REPUBLIC
National and Kapodistrian
University of Athens
EST. 1837



"ALEXANDER FLEMING"
Biomedical Sciences Research Center

**International M.Sc. in "Molecular Biomedicine - Disease Mechanisms,
Molecular and Cellular therapies, and Bioinnovation"**

Medical School, University of Athens – BSRC "Alexander Fleming"

**"Investigation of the molecular mechanisms
stimulated by exosomes in the treatment of acute
hepatic failure"**

Christos Karakostas

Supervisor

Maria Roubelakis, Associate Professor of Biology and Applications of Regenerative Medicine, Medical School, National and Kapodistrian University of Athens

Members of the Committee

Maria Gazouli, Professor of Biology – Nanomedicine, Medical School, NKUA

Aristeides Eliopoulos, Professor of Biology and Genetics, Medical School, NKUA

Athens, 2021

Acknowledgements

The present dissertation was conducted in the context of the Master in Science (M.Sc.) program “Molecular Biomedicine – Disease Mechanisms, Molecular and Cellular therapies and Bioinnovation”, jointly organized by the Medical School of the National and Kapodistrian University of Athens and the Biomedical Sciences Research Center “Alexander Fleming”. I would like to thank the selection committee and its president George Kollias for selecting me to be part of the 2019-2021 class. Throughout all the courses and the two laboratory rotations, I was offered a thorough view of the mechanisms of diseases and bioinnovation concepts, as well as technical skills, and I had the pleasant opportunity to meet and collaborate with many different insightful people.

The dissertation thesis took place at the Laboratory of Biology, at the Medical School of the National and Kapodistrian University of Athens. I would like to thank Professor Maria Roubelakis for appointing to me this project, the valuable feedback and the chance to work in the laboratory. In addition, I am thankful to doctoral student Adriana Psaraki and postdoctoral researcher Lydia Ntari for their guidance and collaboration during my presence in the laboratory. Kiki Pavlou, Nikos Andreou, Hector Katifelis, Farida Giakoub and Maria Nikou from the laboratory of Prof. Maria Gazouli team were also very eager to help with any issue that came up. Furthermore, the rotation students Despoina Korrou-Karava and Maria Martinou were very cooperative and a great company. I would like also to thank Prof. Aristeidis Eliopoulos and Prof. Maria Gazouli for their co-supervision and cooperation.

Finally, I would like to thank my family, my parents and my friends for their love and support during this dissertation thesis and beyond that.

Contents

Acknowledgements.....	2
Abstract.....	5
Σύνοψη.....	6
1. Introduction	7
1.1. Liver anatomy.....	7
1.2. Liver regeneration	8
1.3. Acute Hepatic Failure	9
1.3.1 Clinical features and pathology	9
1.3.2 Epidemiology and etiology	10
1.3.3 Therapeutic approaches of AHF	12
1.3.4 Experimental models of AHF	12
1.4. Stem Cells	13
1.5 Mesenchymal Stem/Stromal Cells	15
1.5.1 Amniotic-Fluid MSCs (AF-MSCs)	17
1.6 Applications of MSCs in Regenerative Medicine	18
1.6.1 Homing / Cell transplantation	18
1.6.2 Paracrine action.....	18
1.6.3 MSC-Exosomes and their use in regenerative medicine.....	19
1.6.4 Applications of MSC-exosomes in liver	20
2. Aim of study	21
2.1 Background.....	21
2.2 Goals of the project.....	21
3. Materials and methods	23
3.1 Cell culture and differentiation	23
3.1.1 Isolation of AF-MSCs.....	23
3.1.2 Thawing of AF-MSCs	23
3.1.3 AF-MSCs culture	23
3.1.4 Cell count using Neubauer counting chamber	23
3.1.5 AF-MSCs freezing.....	24
3.1.6 Differentiation of AF-MSCs into hepatic progenitors (HPL and HL cells)	24
3.1.6 Exosome collection.....	24
3.2 Proteomics	25

3.2.1	Sample preparation for proteomic analysis	25
3.2.2	Liquid Chromatography – Mass Spectrometry/Mass Spectrometry (LC-MS/MS) ..	25
3.3	Liver tissues molecular profile	26
3.3.1	In vivo exosomes/CM treatment	26
3.3.2	Exosomes imaging in the murine liver using Xenogen IVIS system	27
3.3.3	RNA extraction from FFPE tissues	27
3.3.4	Protein extraction from FFPE tissues	27
3.3.5	Bradford assay	28
3.3.6	cDNA synthesis	28
3.3.7	Real-Time PCR.....	28
3.3.8	Western Blot.....	29
3.3.9	Hematoxylin/Eosin (H&E) staining	31
3.3.10	TUNEL assay.....	31
3.3.11	Immunofluorescence.....	31
4	Results.....	33
4.1	Differentiation of AF-MSCs to HPL and HL cells.....	33
4.2	Characterization of exosomes isolated from AF-MSCs, HPL and HL cells.....	34
4.3	Proteomic characterization of AF-MSC, HPL and HL exosomes.....	35
4.4	Pathway analysis	39
4.5	Protein detection in the exosome cargo.....	42
4.6	Evaluation of exosome efficacy against AHF by administration in an <i>in vivo</i> mouse model.....	42
4.7	Profiling of liver tissues upon exosomes or CM treatment	45
4.7.1	Inflammation	45
4.7.2	Apoptosis	47
4.7.3	PI3K/AKT and ERK pathways	49
4.7.4	TGFβ.....	53
4.7.5	Matrix metalloproteinases (MMPs)	55
4.7.6	VEGFA	57
4.8	Evaluation of MFGE8 effectiveness against AHF by administration of exogenous rMFGE8 in an <i>in vivo</i> mouse model	57
5.	Discussion.....	59
6.	Bibliography	62

Abstract

Acute Hepatic Failure (AHF) is a very serious clinical malignancy, manifested with rapid and massive hepatic necrosis which cannot be restored by the endogenous liver regeneration mechanisms and as a result it has a mortal outcome in many cases. Unfortunately, the available therapeutic options are limited to orthotopic liver transplantation, which presents several restrictions and low efficacy. In order to propose novel treatment options, the mechanisms of pathology of AHF as well as of the liver regeneration should be further investigated.

Stem cells are undifferentiated cells which can be specialized and differentiated to almost any cell type. Mesenchymal Stem/Stromal Cells (MSCs) are multipotent, self-renewable adult or fetal stem cells that can exhibit a therapeutic value in the context of several diseases, including AHF. Instead of cell transplantation, which shows many setbacks, such as possible rejection or immunogenicity, the exploitation of their paracrine effects as a part of cell-free therapy could be proven promising as a therapy. It is generally suggested that secreted biomolecules, such as proteins, lipids and RNA, are transferred in extracellular vesicles – such as exosomes – originating from fetal MSCs, such as amniotic-fluid MSCs (AF-MSCs), or their hepatic derivatives (Hepatocyte progenitor-like cells (HPL) and Hepatocyte-like cells (HL)). These biomolecules end up at their targets, inducing hepatocyte proliferation and, thus, liver regeneration, as well as ameliorate the clinical phenotype of AHF, reducing inflammation and apoptosis. Previous work in our laboratory has provided evidence of the therapeutic potential of secretome and exosomes derived from the three cell categories in vivo utilizing immunosuppressed Rag1^{-/-} mouse models of AHF, and has also underlined, through proteomic analysis, the importance of specific proteins, contained in both exosomes and secretome of all three cell types, which proved to be statistically significant (MFGE8, Emilin1, Gas6).

The aim of the present study is (a) to investigate the molecular mechanisms triggered by the exosomes and secretome action, responsible for the induction of proliferation, and reduction of apoptosis and inflammation in the CCl₄-induced murine AHF model, as well as (b) to study the importance of MFGE8 in this context. AF-MSCs were cultured and differentiated into HPL and HL cells, and conditioned media (CM) as well as exosomes were isolated from each cell type. Exosomes or CM were administered to AHF mice, and the liver tissues were isolated, in order to investigate the gene expression pattern and protein levels of mediators and effectors of molecular, as well as to localize specific markers in liver tissues.

Σύνοψη

Η Οξεία Ηπατική Ανεπάρκεια είναι ένα πολύ σοβαρό κλινικό σύνδρομο που εκδηλώνεται ως ταχεία και μαζική νέκρωση του ήπατος που οι ενδογενείς μηχανισμοί ηπατικής αναγέννησης δεν είναι σε θέση να την ανατρέψουν, και έχει ως αποτέλεσμα τον θάνατο στις περισσότερες περιπτώσεις. Δυστυχώς, η μόνη διαθέσιμη θεραπευτική λύση είναι η ορθοτοπική ηπατική μεταμόσχευση, η οποία όμως ενέχει πολλούς περιορισμούς και χαμηλή αποτελεσματικότητα. Για να προταθούν καινοτόμες θεραπευτικές επιλογές, οι μηχανισμοί παθολογίας της οξείας ηπατικής ανεπάρκειας, όπως και της ηπατικής αναγέννησης θα πρέπει να διερευνηθούν περαιτέρω.

Τα βλαστικά κύτταρα είναι μη διαφοροποιημένα κύτταρα, τα οποία μπορούν να διαφοροποιηθούν σχεδόν σε οποιονδήποτε κυτταρικό τύπο. Τα Μεσεγχυματικά Βλαστικά/Στρωματικά Κύτταρα (MSCs) είναι πολυδύναμα, ενήλικα ή εμβρυικά βλαστικά κύτταρα, που έχουν θεραπευτική αξία σε αρκετές ασθένειες, συμπεριλαμβανομένης και της οξείας ηπατικής ανεπάρκειας. Αντί για την εμφύτευση βλαστικών κυττάρων που έχει αρκετά μειονεκτήματα, όπως πιθανή απόρριψη ή ανοσοαπόκριση, η αξιοποίηση της παρακρινούς τους δράσης ως βάση μιας μη κυτταρικής θεραπείας θα μπορούσε να αποδειχθεί υποσχόμενη. Είναι γνωστό πως εκκρινόμενα βιομόρια – όπως πρωτεΐνες, λιπίδια και RNA – μεταφέρονται εντός εξωκυττάρων κυστιδίων (πχ εξωσωμάτια) που προκύπτουν από εμβρυϊκά MSCs, όπως τα AF-MSCs ή σε ηπατικές προβαθμίδες αυτών. Αυτά τα βιομόρια καταλήγουν στους στόχους τους και επάγουν ηπατοκυτταρικό πολλαπλασιασμό και, εντέλει, ηπατική αναγέννηση, όπως και επίσης βελτιώνουν τον κλινικό φαινότυπο της οξείας κυτταρικής ανεπάρκειας, μειώνοντας την φλεγμονή και την απόπτωση. Προηγούμενες μελέτες στο δικό μας εργαστήριο έδωσαν στοιχεία για τη θεραπευτική αξία του εκκριτώματος και των εξωσωματίων και από τις τρεις προαναφερθείσες κατηγορίες κυττάρων *in vivo*, χρησιμοποιώντας ανοσοκατεσταλμένα Rag1^{-/-} ποντίκια, και επίσης υπογράμμισαν, μέσω πρωτεομικής ανάλυσης, την σημασία συγκεκριμένων πρωτεϊνών που περιέχονται σε όλα τα εξωσωμάτια και το εκκρίτωμα και των τριών κυτταρικών τύπων και είναι στατιστικά σημαντική η έκφρασή τους (MFGE8, Emilin1, Gas6).

Ο σκοπός της παρούσας μελέτης είναι (α) να διερευνήσει τους μοριακούς μηχανισμούς που κινητοποιούνται από τη δράση εξωσωματίων ή/και εκκριτώματος και είναι υπεύθυνοι για την επαγωγή του κυτταρικού πολλαπλασιασμού και για τη μείωση της απόπτωσης και της φλεγμονής σε μοντέλο ποντικού οξείας ηπατικής ανεπάρκειας, επαγόμενης από τετραχλωράνθρακα (CCl₄), και (β) να μελετήσουμε τον ρόλο της MFGE8. Τα AF-MSCs καλλιεργήθηκαν *in vitro* και διαφοροποιήθηκαν σε ηπατικές προβαθμίδες (HPL) και ηπατικά κύτταρα (HL), ενώ τόσο το εκκρίτωμα, όσο και τα εξωσωμάτια απομονώθηκαν και από τους τρεις κυτταρικούς τύπους, και κατόπιν χορηγήθηκαν στα ποντίκια ως θεραπεία μετά από την επαγωγή οξείας ηπατικής ανεπάρκειας. Στη συνέχεια το ήπαρ των ποντικών απομονώθηκε ώστε να μελετηθεί τόσο η γονιδιακή έκφραση, όσο και τα επίπεδα πρωτεϊνών των μορίων των επιλεγμένων μοριακών μονοπατιών.

1. Introduction

1.1. Liver anatomy

Liver is an essential organ of our organism, because it conducts a significant number of functions, such as metabolism of macronutrients, aminoacids and lipids, blood volume regulation, lipid and cholesterol homeostasis and breakdown of xenobiotics – including drugs (1). Liver accounts for 2% to 3% of the total body weight, making it one of the largest organs (2). Although it is thought to be consisted of two main lobes (3), the liver is composed of repeating units, 1 mm in diameter in humans, called lobules, which have a hexagonal column shape (4). Its local circulatory system is also complex; liver receives oxygenated blood originating from the heart through the main hepatic artery, and nutrient-rich blood originating from the gastrointestinal tract through the portal vein. The blood flows through the lobules via terminal vessels, called sinusoids, which all end up at the central vein, and finally blood exits liver through hepatic veins (5).

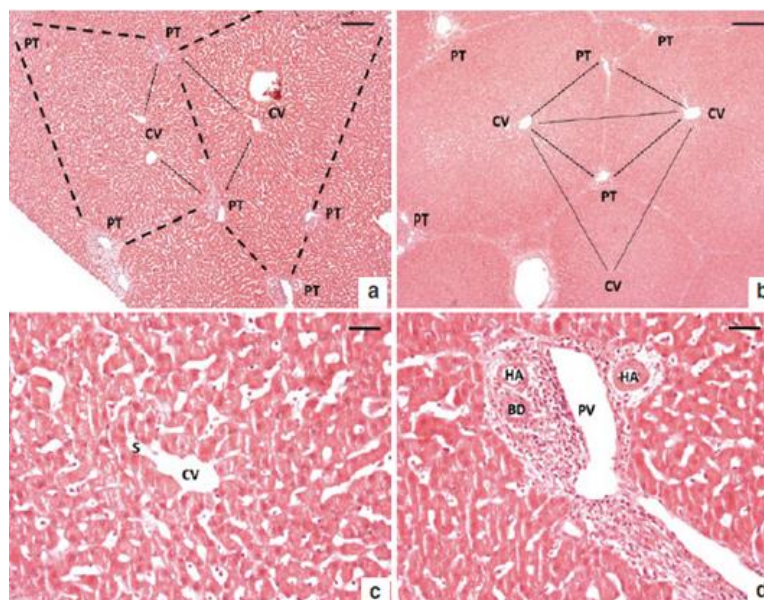


Figure 1: (a,b) Normal liver histology, indicating the hexagonal lobules with their central vein (CV), and the portal triads (PT). (c,d) Branches of the sinusoid capillaries, the portal vein (PV), the hepatic artery (HA) and the bile interlobular ducts (BD) (a,b) x40 magnification, (c,d) x200 magnification (*Liver Diseases A Multidisciplinary Textbook / edited by Radu-Ionita et al.*)

The liver is composed of various cell types, which are classified as parenchymal and non-parenchymal. Hepatic parenchyma is arranged in hexagonal lobules, each one of them has attached on them branches of the hepatic artery, portal vein and bile duct, forming a portal triad at the periphery of every lobule. The lobules have sinusoidal capillaries, which are lined with specialized endothelial cells through which the portal blood can communicate with the adjacent hepatocytes (6). Hepatocytes, the main parenchymal cells, account for the 80-85% of the total liver mass, and are arranged in thin, hexagonal pattern, plates. They are responsible for a wide range of hepatic functions, including liver homeostasis, metabolism of lipids, proteins, detoxification of drugs and immune activation (7).

The second most significant and abundant cells of the liver are the hepatic resident macrophages, known as Kupffer cells. Their main functions are immunological and phagocytic, as well as making an immunological barrier against gut microbiota, and playing a role in the removal of senescent red blood cells and iron recovery (8). Kupffer cells are generally known as tolerogenic during normal conditions, but their immune response may sometimes enhance liver injury, such as during alcoholic liver disease, highlighting the importance of the regulation of macrophages, such as Kupffer cells, between proinflammatory M1 state and immune-modulatory M2 state (9).

Hepatic stellate cells (HSCs), which make up approximately 5% of the total liver cell population, are predominantly responsible for fibrosis. HSCs reside in the perisinusoidal space, and under normal circumstances remain quiescent (10). They start to proliferate and differentiate into myofibroblasts when stimulated by nearby Kupffer cells during liver injury of infection, ultimately contributing to fibrosis by producing an abnormal extracellular matrix (ECM) that makes up fibrous scar tissue in liver fibrosis (7).

In mice, hepatoblasts, hepatic progenitor cells, or oval cells, are bi-potent stem cells, capable of self-renewal and differentiation into both hepatocytes and cholangiocytes (11). Several signaling pathways, such as the WNT, hepatocyte growth factor (HGF), fibroblast growth factor (FGF), transforming growth factor β (TGF β) and MAPK regulate hepatoblast proliferation, and eventually differentiation is stimulated by transcription factors such as TBX3, CEBPa, PROX1 and HNF4a (12). Hepatoblasts contribute to liver regeneration, as the properties of self-renewal, proliferation and differentiation are crucial for the restoration of the liver after injury, infection or rapid necrosis.

1.2. Liver regeneration

The liver is the only solid organ to use regenerative mechanisms in order to ensure that its liver-to-bodyweight ratio is the perfect for maintaining homeostasis. For instance, liver is enlarged during pregnancy and is shrunk in cachexia. Liver possesses mechanisms which can be activated following loss of hepatocytes, hepatectomy or liver injury, and they are capable of restoring the initial state of the liver (13). One of the most studied animal models of liver regeneration is the 2/3PH model in rodents. Immediately after partial hepatectomy (PH), hepatocytes in the remaining liver enter into the cell cycle. 12-16 hours post-PH, DNA synthesis takes place, peaking at 24 hours, and finally 1 to 2 weeks post-PH, the initial liver mass is completely restored (14). Liver regeneration is a complex network regulated by various growth factors and cytokines expressed at the site of the liver injury, and is consisted of three main phases. At the beginning, after stimulations, G0 hepatocytes convert to G1 phase of the cell cycle (priming phase). Consequently, mitogens induce hepatocyte proliferation (proliferative phase), and finally negative regulating factors terminate proliferation (termination phase) (15).

Priming phase is the first step in hepatic regeneration. During this step, nearby liver macrophages, known as Kupffer cells, are activated by LPS and complement proteins, and respond to the stimulation of hepatocyte loss – for instance an injury or an infection – producing cytokines such as TNF α and IL-6. As a result of cytokine stimulation, quiescent hepatocytes rapidly re-enter the cell cycle into the G1 phase, in order to get ready to proliferate. Various pathways are playing a key role in this activation, such as JAK/STAT, MAPK/ERK and PI3K/AKT. (16). The second step of regeneration is called proliferative phase, which has as its outcome the mitotic process of hepatocytes. Mitogens involved in this phase are divided in two categories; complete mitogens and auxiliary mitogens. Complete mitogens have direct mitogenic properties, stimulating DNA synthesis and cell proliferation, and include HGF, TGF β , epidermal growth factor (EGF) and heparin-binding EGF (HB-EGF). Auxiliary mitogens are not mitogenic, but can contribute in the proliferative process by enhancing the action of complete mitogens, and include TNF and TNFR1, vascular endothelial growth factor (VEGF) and its receptors, serotonin, norepinephrine, leptin, insulin and fibroblast growth factors 1 and 2 (FGF1 and FGF2) (15, 17). The final phase of regeneration, known as termination phase, is essential in order to prevent uncontrolled proliferation of hepatocytes. Despite its importance, the exact mechanisms and pathways mediating the termination of liver regeneration have not been yet well investigated, though several key factors have been under research, such as hepatocyte nuclear factor 4 (HNF4a), (18), various microRNAs (19) and TGF β family members (15).

1.3. Acute Hepatic Failure

The first attempt to define the Acute Hepatic Failure (AHF) was made by Trey and Davidson in 1970, assuming that AHF was “*a potentially reversible clinical entity, arising from severe liver injury and resulting in hepatic encephalopathy (HE) within 8 weeks since symptoms started in a person without chronic liver disease*” (20). Currently, AHF is defined as a clinical condition in which an acute hepatic insult, leads to rapid clinical deterioration, with HE occurring within 26 weeks since the appearance of the initial symptoms of liver dysfunction (21).

1.3.1 Clinical features and pathology

AHF is a rare, life-threatening condition, with a high mortality rate, manifested through serious hepatic injury, coagulopathy, hepatic encephalopathy, jaundice and in some instances, multisystem organ failure (22). AHF initiates with a severe acute hepatic injury (AHI), which is characterized by a 2-fold to 3-fold increase of transaminase levels, associated with impaired liver function (23). In general, hepatocyte death occurs via two well-conserved processes, the apoptotic and the necrotic pathway [Fig. 2]. AHF via the apoptotic pathway, is generally less inflammatory, as the cellular membrane of the hepatocytes is maintained, thus holding any triggering signal into the apoptotic cell. On the other hand, AHF via the necrotic pathway is quite inflammatory, as ATP depletion triggers cell swelling and ruptures the membrane, inducing a massive inflammation response (24). The most

severe AHI causing AHF, is identified as diffuse, massive and zonal, with massive hepatic, and near-complete parenchymal necrosis, associated with inflammation (25).

As mentioned above, immune system plays a very significant and dynamic role in AHF development and outcome. AHF exhibits a wide, systemic inflammatory response, which has a very similar clinical phenotype with Systemic Inflammatory Response Syndrome (SIRS), centered around inflammatory response and immune activation (26). Patients with AHF who develop SIRS, have a worse outcome, mainly because they progress to encephalopathy more often than the patients who do not (25).

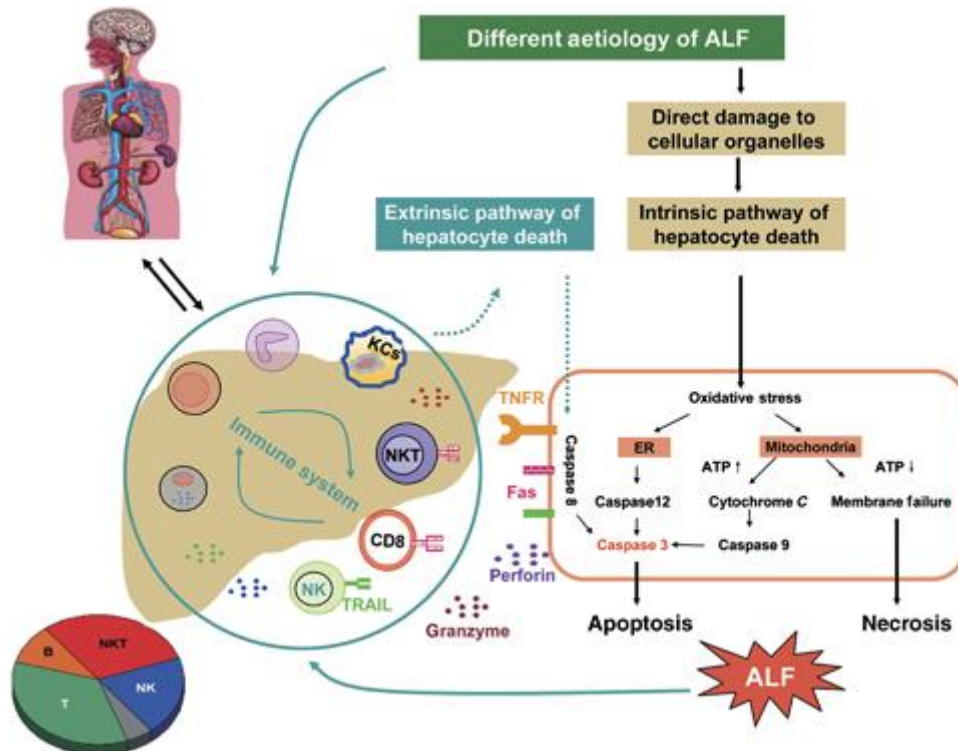


Figure 2: The overall mechanism of Acute Hepatic Failure (AHF), triggered by either cellular damage (intrinsic pathway) or by acute inflammation (extrinsic pathway), leading to either apoptosis or necrosis of hepatocytes. (27)

1.3.2 Epidemiology and etiology

AHF is a rare condition, with very low incidence ranging from 1 to 6 cases per million people annually in the developed world, which represents about 2000 cases per year. AHF is responsible for 6% of all liver-related deaths and 7% of orthotopic liver transplants in the USA annually (28). Although there is a limited guide management, due to the rarity and heterogeneity of AHF, its survival rates have been increased in recent years because of the advances in critical care management and the advent of liver transplantation (28, 29).

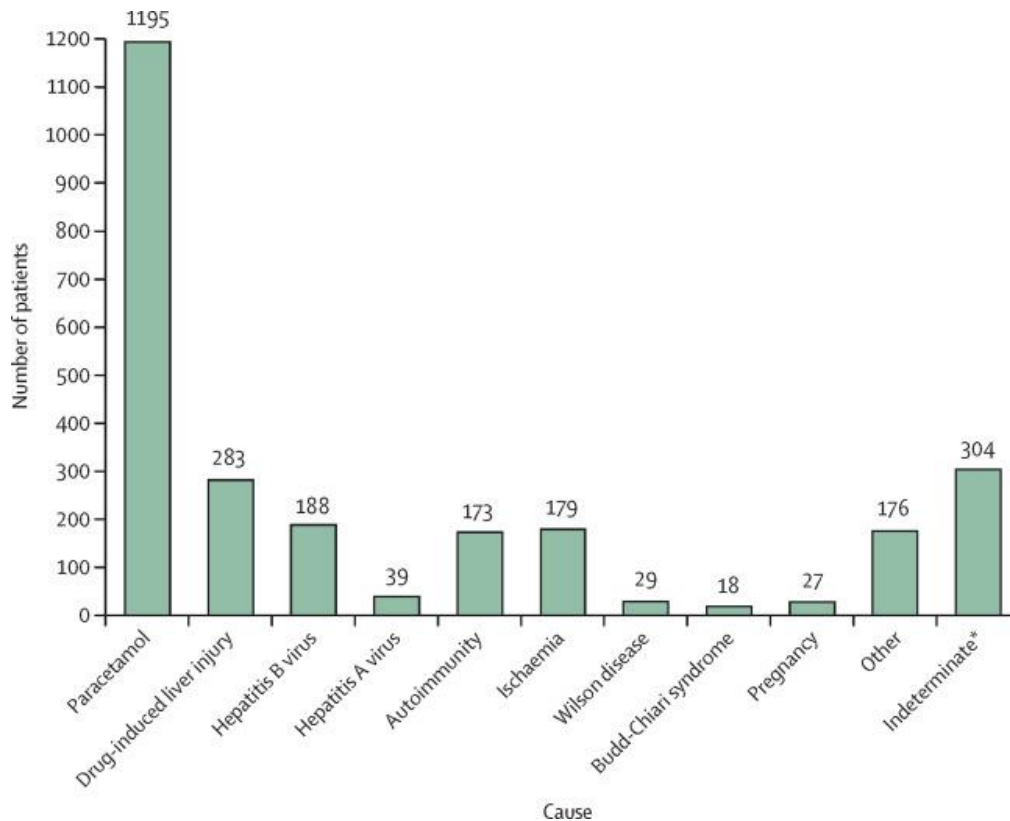


Figure 3: The most common etiologies of AHF, in a study involving a number of patients with AHF. Paracetamol overdose is the leading cause, followed by other drug-induced injuries, infections (hepatitis A and B viruses) and autoimmune hepatitis (32)

The most common cause of AHF is drug intake, with the most cases caused from paracetamol overdosing, accounting for almost half of the total cases of AHF in North America and the UK, and in a lower rate in Asia and Africa (30). Drug-induced liver injury (DILI) causing AHF (except paracetamol overdose) is the second most common etiology of AHF and is linked to drug intake, mainly antibiotics. Since DILI appears in a very small proportion of those who are treated with these drugs, nearly all cases in the clinical setting are considered idiosyncratic. The pathogenesis of DILI is thought to be immune based, with some individuals having a genetic predisposition (31). Autoimmune hepatitis is another relatively common cause of AHF, which has – similarly to DILI – an immune-based background. It is more common in women, has poor outcome and needs liver transplantation (32). Viruses are included also in the etiologies of AHF. Approximately 1% of hepatitis B patients will develop AHF. The exact molecular mechanism of HBV-associated AHF is not fully understood, though it is inferred that this is associated with expression of genes related to hepatic stellate cell (HSC) activation and fibrogenesis, along with an overriding cell proliferation and tumorigenesis gene signature (33). Hepatitis A patients also could develop AHF, also rarely (about 1% of all HAV patients), especially patients with nonalcoholic fatty liver disease (NAFLD), and is loosely associated with high rates of substitutions in the 5' untranslated region of the HAV genome (34). The remaining, rarest causes of acute liver failure comprise fewer than 15% of the total and include heat stroke, pregnancy-associated injury, HELLP (hemolysis, elevated liver enzyme, and low platelet) syndrome, other viruses such as herpes simplex virus, and tumors (32).

1.3.3 Therapeutic approaches of AHF

AHF is a potentially deadly condition, rendering the research on its treatment an urgent necessity. Orthotopic liver transplantation (OLT) is currently the main therapeutic option for AHF patients, having dramatically improved the one and five year survival rates, from 15-20% to over 80% and 75% respectively (35). OLT was performed on a human in 1963, and is the golden standard in terms of AHF treatment since 1983 (36). Despite the overall success of OLT treatment, there are several potential complications, such as infections, biliary complications (15%), hepatic artery thrombosis (2-5%), and poor functionality of the new transplant (1-5%) leading to a 7% rate of mortality (37). In addition, the most common obstacle regarding OLT is graft rejection within weeks or months after the surgery, being the main cause of death after OLT treatment. Finally, there is another significant drawback of liver transplantation, since there is a global organ donor shortage, as the demand for organs, including livers, is higher than their supply, resulting in a number of patients waiting for a transplant, to die (38).

In an urge to overcome all these complications and obstacles emerging from liver transplantation, there is a continuous research on different therapeutic approaches to combat AHF. Extracorporeal artificial liver support, mediated by a device, could be a valuable tool which is able to assist hepatic functions until a suitable liver transplant is found, resulting in a decrease of mortality before OLT (39). Most attempts to find an effective device have been based on dialysis techniques, correcting the blood composition, though large toxins and protein-bound molecules need alternative bioartificial liver support devices, which until now have shown disappointing results in clinical trials (40).

1.3.4 Experimental models of AHF

Due to the mortal outcome of AHF, it could not be studied on humans. As a result, many attempts have been made in order to develop a suitable animal model, using a wide variety of species, the most common being mice, rats, rabbits and pigs, and approaches, from surgical models to the use of hepatotoxic drugs (41). A number of animal AHF models are shown in **Table 1**, including chemical, drug-induced such as Galactosamine/Lipopolysaccharide (Gal/LPS). Tetrachlorocarbon (CCl₄), Azoxymethane, Acetaminophen.

The main criteria for developing a suitable AHF animal model were set by Terblanche and Hickman in 1991. According to them, a model should have reproducible end-points to standardize the model, treatments should reverse AHF and improve survival, should reflect biochemical, histological and clinical changes including death from AHF, should clarify the exact time for treatment between insult and death, should have size large enough to allow blood and tissue analysis to be conducted, and should expose personnel to minimal hazard (42).

Table 1: Main drug-induced animal experimental models used to study acute hepatic failure

Model	Species	Result	Ref.
D-galactosamine/ Lipopolysaccharide (Gal/LPS)	Mouse Rat	Galactosamine drives Kupffer cells to promote inflammation LPS disrupts RNA and protein synthesis Wide hepatotoxicity, hepatic encephalopathy	(43)
Tetrachlorocarbon (CCl ₄)	Mouse Rat Rabbit Pig	Tetrachlorocarbon is transformed at the liver and produces reactive oxygen species (ROS) Damage by macromolecule binding Enhancement of lipid peroxidation Disturbance of calcium homeostasis	(44, 45)
Azoxymethane	Mouse	Azoxymethane induces microvesicular steatosis and centrilobular necrosis Mitochondrial injury Hepatic encephalopathy Increased reproducibility	(46, 47)
Acetaminophen	Mouse Rat Rabbit Pig	Excess acetaminophen is converted to a toxic compound, called N-acetyl-p-benzoquinoneimine (NAPQI) NAPQI interrupts mitochondrial calcium flux which produces ROS and other radicals Cell necrosis and apoptosis	(48, 49)

1.4. Stem Cells

Stem cells are unspecialized cells, which are able to self-renew and differentiate, and are found in embryos and adult organisms. Their ability to differentiate is described as a “step” in their specialization, describing them as totipotent, pluripotent, multipotent or unipotent (50). After fertilization, zygotes are able to develop into an adult organism beginning from a single cell, a feature called totipotency. Totipotent stem cells are able to differentiate into embryonic, extra-embryonic and adult cells (51), but their exclusive source is the embryonic morula (52). The next step of specialization is pluripotency, which refers to the ability of a cell to differentiate into cell types derived from one of the three germ layers – ectoderm, mesoderm and endoderm – as well as early embryonic tissues, but not extra-embryonic structures (53). The two most used and characterized examples of pluripotent stem cells (PSCs) are embryonic stem cells (ESCs) and induced pluripotent stem cells (iPSCs) (50).

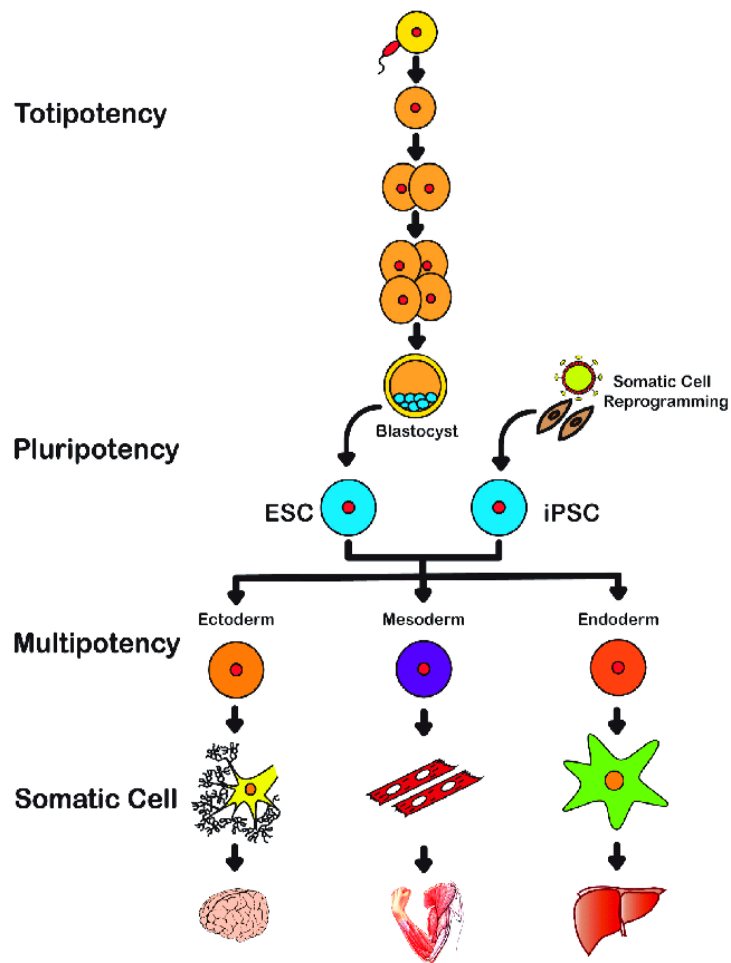


Figure 4: Stages of stem cells according to their ability to differentiate (54)

ESCs are harvested from the inner cell mass of a blastocyst, and since their first derivation from murine blastocysts in 1981 they have been quite promising in regenerative medicine, mainly due to their beneficial biological traits (indefinite proliferation, genotypic normalcy and pluripotency). (55). Unfortunately, since the early days of their identification, human ESC (hESC) research has faced a vast amount of ethical obstacles and challenges; the main one being the fact that in order to establish hESC cell lines, the destruction of the embryo is needed (56). In addition, all attempts to employ ESCs in clinical trials have failed, due to incomplete differentiation into fully functional cells, tumorigenicity, and genomic instability (57). Despite the discouraging results, another type of pluripotent stem cells has been discovered, known as very small embryonic-like stem cells (VSELs), which may overcome the obstacles of the ESCs, as it may hold a potential advantage of being able to differentiate across germ layers in adult animals or human subjects. Such cells may function as an alternative to monopotent tissue-committed stem cells in adults (53, 57).

More recently, scientists managed to reprogram adult cells into embryonic-like behaving cells, by inducing pluripotency in somatic cells. These are known as induced pluripotent stem cells (iPSCs) (58). This technique traces back to 2006, when Yamanaka and Takahashi managed for the first time to reprogram differentiated cells by expressing Oct4, Sox2, Klf4 and c-Myc factors (59). In general, iPSCs have advantages over ESCs, such as lack

of ethical concerns, and the fact that they are able to generate autologous PSCs, which means that it is possible to obtain pluripotent stem cells derived from the patient's own cells (60). All of the aforementioned rendered iPSCs to be viewed as a novel, promising stem cell technology, and in 2014, the first human clinical trial involving iPSCs was conducted. Though, the transplantations ceased due to genetic aberrations detected in iPSCs, hampering the initial excitement about this new stem cell technology (61). iPSCs could be potentially used as a treatment in various diseases, such as neurodegenerative diseases (62, 63), hepatic diseases (64), heart diseases (65), even in cancer research (66).

Multipotent stem cells are known as the main class of adult stem cells which can differentiate into more than one cell type, but are more limited than PSCs, and include hematopoietic stem cells (HSCs), endothelial progenitor cells (EPCs), mesenchymal stem cells (MSCs) and skeletal myoblasts, with their main advantages being their genomic stability, low immunogenicity, low metabolic status, small risks of tumorigenesis and rejection and easy access and isolation (67).

1.5 Mesenchymal Stem/Stromal Cells

Mesenchymal Stem/Stromal Cells (MSCs) are adult multipotent progenitor cells, with self-renewal potential and able to differentiate into several cell types. More specifically, there have been "*minimal criteria*" set in 2006 by the International Society for Cellular Therapy (68), and include:

- a) The ability of self-renewal
- b) The multipotency with osteogenic, chondrogenic and adipogenic potentials
- c) The expression of surface markers, such as CD73, CD90, CD105
- d) The lack of expression of lineage surface markers, such as CD14, CD34, CD45, HLA-DR

Human MSCs can be isolated from multiple tissues, mainly from bone marrow (BM-MSCs), amniotic fluid (AF-MSCs), adipose tissue (AT-MSCs), dental tissues, skin, salivary glands, menstrual blood, perinatal tissues and many other mesoderm-derived sources and can be differentiated into almost every mesodermal tissue, including muscle, nerve, liver, skin, bone and cartilage tissues (69).

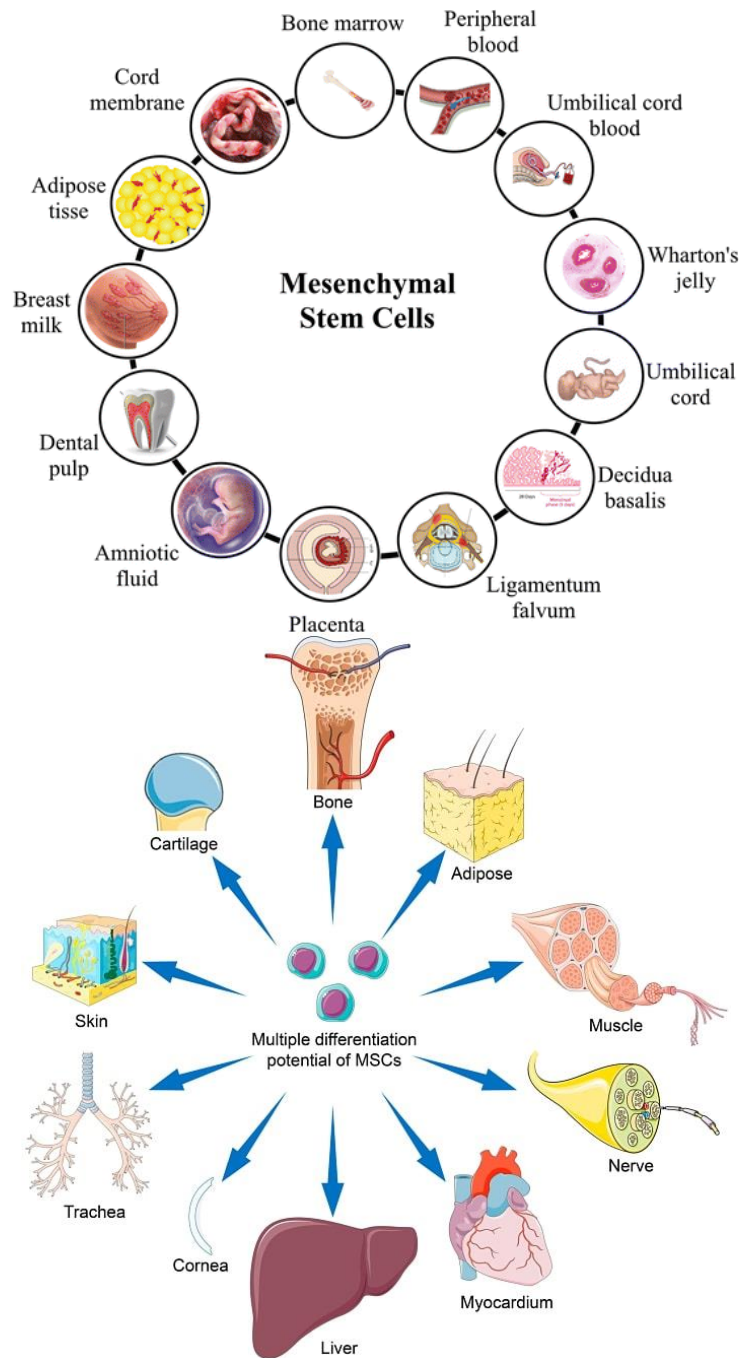


Figure 5: Sources (top) of MSCs and tissues that MSCs are capable to be differentiated to (bottom). (top – (70)) (bottom - <https://www.dvcstem.com/post/what-are-mesenchymal-stem-cells>)

In comparison to ESCs, mesenchymal stem/stromal cells do not pose moral or ethical concerns. This has led researchers to use MSCs in a growing number of therapies. Despite their advantages, therapeutic use of adult MSCs has been hampered due to several reasons. First of all, MSC isolation from adult sources is often painful and requires invasive procedures (71). Moreover, MSCs have variable proliferation and differentiation capabilities, which are further reduced upon in vitro passaging (72). In addition, several factors concerning the donor can affect the self-renewal and differentiation capabilities of MSCs, such as age, genetics and exposure to environmental stress (73). Due to these restrictions exhibited by adult MSCs, perinatal and fetal sources are preferred, such as

umbilical cord and umbilical cord blood, placenta and amniotic fluid. Perinatal and fetal MSCs meet the minimal criteria for MSCs as mentioned above, and are very promising as they overcome the donor background and painful isolation procedures (71).

Table 2: Advantages and disadvantages of stem cell types used in clinical (NSCs, MSCs, ESCs, iPSCs)
(source: https://www.nrronline.org/viewimage.asp?img=NeuralRegenRes_2020_15_2_242_265544_t4.jpg)

Cells	Source	Advantages	Disadvantages
Neural stem cells	Primary tissues, (fetal, neonatal, and adult brain) or embryonic stem cells and induced pluripotent stem cells	(1) Easy to access; (2) No ethical issues; (3) No histocompatibility.	(1) Strong immunogenicity; (2) The mechanism of cell proliferation, differentiation, and migration is unclear.
Mesenchymal stem cells	Bone marrow, adipose tissue, and umbilical cord	(1) Widespread sources; (2) Secrete multiple bioactive factors; (3) Directional migration.	(1) Bone marrow mesenchymal stem cells-limited raw materials, poor proliferation, and traumatic; (2) No unified identification standard for umbilical cord blood mesenchymal stem cells, and the culture technology <i>in vitro</i> and differentiation are not yet mature.
Embryonic stem cells	Early embryo	(1) Strong proliferation ability; (2) Abundant sources; (3) Can be passed on.	(1) Ethical issues; (2) The allograft produces a great rejection reaction; (3) Unrestrained differentiation; (4) Tumorigenicity.
Induced pluripotent stem cells	Gene recombination	(1) No ethical issues; (2) No histocompatibility.	(1) Complex operation process; (2) Low reprogramming efficiency; (3) Mutation induction; (4) Tumorigenicity.

Each stem cell has a specific neurogenic potential and can achieve certain results, but there are still many problems to be solved before they can be used for clinical applications.

1.5.1 Amniotic-Fluid MSCs (AF-MSCs)

The amniotic sac is consisted of a pair of membranes which hold the fetus during pregnancy. Amniotic fluid (AF) fills the inner membrane, which contains the embryo, protects it, ensures symmetrical development and growth, maintains a stable temperature and permits free fetal movement into the sac, enabling normal musculoskeletal development and blood flow (74). AF is collected between the 15th and the 19th week of pregnancy, during amniocentesis, a routine procedure used for the prenatal diagnosis of fetal abnormalities and genetic diseases (75). AF is a novel source of stem cells, known as Amniotic fluid-derived mesenchymal stem cells (AF-MSCs), which are primitive mesodermal progenitors exhibiting great self-renewal and differentiation potential (76).

In addition to the mesenchymal stem cell markers, AF-MSCs also express a number of pluripotency-related markers as well as transcriptional factors, such as Oct4, Sox2, c-Kit, Nanog, TRA-1-60 and TRA-1-80, exposing their intermediate stage between embryonic and adult stem cells (76). AF-MSCs express various unique proteins in comparison with BM-MSCs, related to primitive stemness, making them more distinct as a cell population (77). Furthermore, AF-MSCs possess greater immunomodulatory properties than BM-MSCs, suppressing inflammation and promoting T regulatory cells and M2 polarization, regulating the immune system. Along with the lack of ethical and safety concerns, AF-MSCs are a great candidate for clinical applications (78).

1.6 Applications of MSCs in Regenerative Medicine

1.6.1 Homing / Cell transplantation

MSCs have been studied for their therapeutic potential, since their main properties of self-renewal and differentiation render them quite promising for being used in regenerative medicine. In addition to these beneficial properties, MSCs are capable of migrating preferentially to injured and damaged tissues, and exerting their benefits there, a characteristic known as homing (79). Thus, transplanted MSCs are able to target specific injured tissues, gravitated by chemokine signals.

Initially, MSC-based therapies were anticipated to act through direct cell replacement, utilizing the homing property in order to be delivered to the injured tissue, and exhibited quite beneficial outcomes. Despite the promising results, it became clear that only few MSCs manage to reach their destination; most of the cells are caught in the vascular system and cleared, with only a small proportion of the initial MSC population administered to be engrafted at the site of injury (80). Furthermore, recent studies suggest that a large number of bioactive factors secreted from MSCs might play a quite important role in the regulation of various physiological processes, highlighting the importance of the paracrine action of MSCs (81).

1.6.2 Paracrine action

As mentioned above, despite the beneficial homing property of MSCs, exogenously administered cells exhibit low survival rates, and do not persist at the damaged area. Therefore, it is proposed that paracrine action, with the MSC-secreted soluble factors, known as the MSC secretome, as mediators, may be their most efficient way of action (82). Secretome is defined as the set of cell-derived bioactive factors, such as proteins, lipids, nucleic acids and extracellular vesicles, and is gaining attention because of its potential therapeutic effects, similar to those induced by cell transplantation but with no transplant-related side effects (83).

Conditioned media (CM) derived from MSCs (MSC-CM) contains numerous growth factors, such as insulin growth factor 1 (IGF-1), vascular endothelial growth factor (VEGF), nerve growth factor (NGF), hepatocyte growth factor (HGF) and transforming growth factor β (TGF β) (84, 85), as well as various immunomodulatory molecules, though the majority of beneficial factors is included in the extracellular vesicles (EVs). Extracellular vesicles derived from MSCs (MSC-EVs) are consisted of a lipid bilayer enriched in proteins, enabling their trafficking and adhesion properties, and they include a great number of bioactive molecules, such as proteins, lipids, DNA, mRNA, miRNA, enzymes, immunomodulatory factors and growth factors (86).

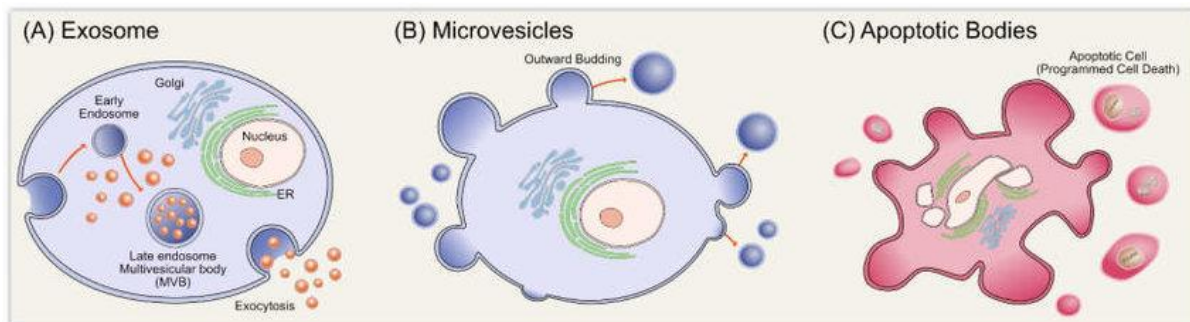


Figure 6: Production of all of the three types of EVs (exosomes, microvesicles, apoptotic bodies). (87)

Depending on their size and origin, EVs are categorized into three types: apoptotic bodies, microvesicles and exosomes. Apoptotic bodies are the biggest in size (>1000 nm) and are generated from the dissolution of the MSCs during apoptosis, and are engulfed by several cell types, resulting in the digestion of their components and possible intracellular communication, though the exact role and mechanism is largely unknown (88). Microvesicles (MVs) are the medium-sized EVs (100-1000 nm), which originate from direct budding from the plasma membrane. MVs (mainly by BM-MSCs) possess the ability to mediate tissue regeneration, and they have been used for gene therapy, as they are able to transfer genetic information, such as miRNAs and siRNAs (89). MSC-MVs have been studied as potential, cell-free therapeutic tool against medical condition, such as neurodegenerative and lung diseases, as they mediate intracellular communication and regenerative action, carrying soluble biofactors and lacking MHC molecules, facilitating their allogeneic transfusion (90, 91).

1.6.3 MSC-Exosomes and their use in regenerative medicine

Exosomes are the smallest (30-200 nm) and most important EVs derived from MSCs and , unlike MVs, they are produced from endosome-like structures, known as multivesicular bodies (MVBs). Exosomes produced from a single cell may be vastly heterogeneous, with every vesicle being composed of different markers, factors and having different functions. This heterogeneity of exosomes, along with their stable physical features, render them very promising for therapeutic applications (83, 92). MSC-derived exosomes exhibit great immunomodulatory properties, downregulating pro-inflammatory cytokines, such as interleukin (IL)-1b, IL-6 and tumor necrosis factor (TNF) a, upregulating anti-inflammatory factors, such as IL-10 and switching macrophages from the M1 phenotype towards the immunoregulating M2 phenotype (93). Apart from their immunoregulating properties, exosomes hold great tissue repair and regenerative capability due to their cargo, composed of growth factors, enzymes and nucleic acids (94).

MSC-exosomes are currently being under investigation for their potential efficacy as a cell-free therapy against various diseases (95). Components of MSC-exosomes have been observed to promote skin regeneration (96), cartilage repair (97), proliferation of chondrocytes (88), skeletal muscle regeneration (98), to suppress myocardial injury (99), cardiac apoptosis (100), and they are being under investigation in cancer, whether they facilitate cancer immunotherapy (101) or target directly cancer cells (102) and even as a

potential therapeutic option for COVID-19 patients (**103**) and against their lung injury induced by SARS-CoV-2 (**104**).

1.6.4 Applications of MSC-exosomes in liver

As we discussed in our review (**95**), the therapeutic effects of MSC-exosomes in liver are also studied in liver diseases, although less than in other conditions. Liver fibrosis can be induced by a variety of factors, such as chronic injuries, viral hepatitis, alcohol, drugs and autoimmunities. Fibrosis can be improved by exosomes administration in carbon tetrachloride (CCl₄)-induced fibrotic liver, restoring liver functions (**105**). MSC-exosomes have been proved to hold great proliferative, regenerative and anti-apoptotic properties when administered as a therapy to drug-induced liver injury models, suggesting that exosomes can potentially elicit hepatoprotective effects against injury (**106**). Furthermore, MSC-exosomes have been observed to suppress directly CCl₄-induced liver injury development through antioxidant potentials, decreasing oxidative stress levels (**107**).

MSC-exosomes have been studied against AHF. Exosome administration has been observed to successfully ameliorate AHF phenotype in drug-induced models, reducing inflammatory factor secretion and inflammasome activation (**108**), with several factors like miRNAs being noticed as important (**109**). Furthermore, autophagy is promoted when MSC-exosomes are administered in drug-induced AHF models, attenuating hepatocyte apoptosis and ultimately reducing hepatocyte loss (**110**). In conclusion, there is a growing number of promising studies involving MSC-exosomes as a cell-free therapy against liver diseases, which could result in clinical trials in the near future in order to be evaluated as a potential approved therapy for AHF and other liver conditions.

2. Aim of study

2.1 Background

Cell-free therapeutic approaches against a growing number of medical conditions have been under investigation lately, with the use of MSCs being one of the main therapeutic tools. Different sources of MSCs have been used against AHF, such as bone marrow (BM-MSCs), adipose tissue (AD-MSCs), umbilical cord (UC-MSCs) and amniotic fluid (AF-MSCs). AF-MSCs, though, exhibit a low immunogenic profile reducing rejection risk, are easier to be obtained and present no ethical concern, rendering amniotic fluid collected during amniocentesis a promising source of therapeutical stem cells.

Our group has successfully isolated AF-MSCs from routine amniocentesis of women during their second trimester of pregnancy. These cells, under proper conditions and under the effect of specific growth factors can be differentiated into HPL cells and HL cells. Recent evidence suggest that the therapeutic potential of these cells is primarily paracrine, underlining that biomolecules secreted from AF-MSCs, HPL cells and HL cells could act as the main mediators of liver restoration after the induction of AHF. Our team has also proved that AHF could be reversed through the mobilization of hepatic progenitors (oval cells) in mice (**111, 112**).

As mentioned above, AF-MSCs, HPL cells and HL cells secretome is worth being studied as the main mediators of improving AHF clinical phenotype. Extracellular vesicles, and primarily exosomes are currently being widely investigated as the main vehicles, delivering active biomolecules, such as proteins, lipids and RNA, to their target and eventually trigger molecular mechanisms which end up in liver repopulation with hepatocytes and finally restore the liver and reverse AHF. Our team has revealed that secreted molecules of AF-MSCs, as well as of HPL and HL cells have a therapeutic potential in mice with AHF, reversing their disease phenotype (**111**). This led to further functional secretome analysis, which highlighted Annexin-A1 as an important protein, playing key role in liver regeneration (**112**). As a next step, exosomes and CM were underwent proteomic analysis and specific proteins included in them, exhibited abundant presence and statistically significant differential expression between the samples. Milk-fat globule EGF factor VIII (MFGE8) protein was found through proteomic analysis as a key factor in many pathways. MFGE8 has been proven to be a pro-proliferative, anti-apoptotic, anti-inflammatory and anti-fibrotic protein, playing a key role in protection and restoration of the liver (**113-116**) and it is suggested that, as a key part of exosomes and CM could trigger specific molecular mechanisms which reverse ultimately AHF.

2.2 Goals of the project

In the present study, we firstly aimed to analyze the proteomic profile of the exosomes derived from all cell types (AF-MSCs, HPL, HL), in order to highlight any significant protein component of the exosomes cargo. As mentioned before, exosomes contain a diverse set of proteins, each of them having its role. Through proteomic analysis, we are able to identify

and characterize the protein components and select a number of them according to their significance and involvement in main pathways. The second aim of this project is to examine the molecular pathways initiated by the exosomes treatment. Significant proteins of exosomes trigger downstream signaling, which might play a key role in the accomplishment of the therapeutic effect of exosomes against AHF phenotype. Gene expression, protein levels and visual detection of specific molecules involved in specific pathways are identified, in order to propose a mechanism of action triggered by exosomes. Finally, we aimed to assess the role of one of the main proteins identified in the exosomes, MFGE8, as its anti-inflammatory, proliferative and anti-apoptotic properties, known from several studies, match the exosomes effect on AHF, and it is worth evaluating as a key protein to our proposed mechanism.

3. Materials and methods

3.1 Cell culture and differentiation

3.1.1 Isolation of AF-MSCs

Human AF-MSCs were isolated from amniotic fluid samples, collected during scheduled amniocentesis between the 15th and 18th week of gestation. Samples were obtained, following a written informed consent, approved by the Ethical Committee of the Alexandra Hospital, Athens and the Bioethics Committee of the University of Athens, School of Medicine, during scheduled amniocenteses. Amniocentesis was performed under aseptic conditions. Using a 22G needle and under ultrasonographic control, 10–15 ml of AF was aspirated for each sample. Samples were collected and 10 ml of each were centrifuged at 1300rpm for 10 minutes. The pellet was resuspended in DMEM (Sigma-Aldrich, St. Louis, MO, USA) supplemented with 20% (v/v) fetal bovine serum (FBS; Gibco-BRL, Paisley, Scotland, UK), in a 25cm² tissue culture-treated flask and incubated at 37°C in a 5% humidified CO₂ chamber for approximately 20 days, where the first colonies appeared. The medium was then changed every five days. The cells were expanded into higher passages and frozen until use.

3.1.2 Thawing of AF-MSCs

Vials containing AF-MSCs preserved at -80°C, are put initially on ice and then, their content is mixed with 1 mL DMEM + 1% a/a + 20% fetal bovine serum (FBS; Gibco) and centrifuged at 1200 rpm for 5'. The pellet is resuspended with DMEM + 1% a/a + 20% FBS and is distributed in 6-well plate.

3.1.3 AF-MSCs culture

When reached 80% confluency, culture media were removed and the cells were rinsed once with phosphate-buffered saline (PBS; Gibco) solution and then detached from the culture plate of flask, by a 37°C, 5% CO₂ incubation for 5', with 0.5% Trypsin/EDTA. The cells were centrifuged in Dulbecco's Modified Eagle's Medium (DMEM; Gibco, Paisley, Scotland) at 1200 rpm for 5', and the pellet was resuspended in DMEM.

3.1.4 Cell count using Neubauer counting chamber

10 µL of resuspended cells in DMEM (see 3.1.3) were mixed with 10 µL of Trypan-Blue dye, reaching a final volume of 20 µL. The mixture was inserted into the gap between the Neubauer counting chamber and the cover slip. Cells found at the central 5x5 square (**fig. 7**)

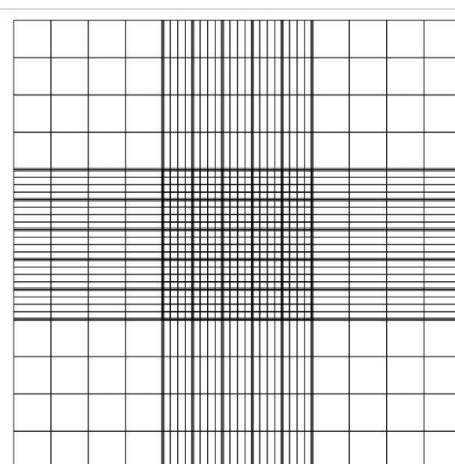


Figure 7: Cells are counted at the center 5x5 square

were counted. In order to calculate the total cell number, the following formula was used:

$$\text{Total cells} = 2 * (\text{DMEM volume}) * 10^4$$

Knowing the total cell number is useful in plating precisely the cells into the flasks or plates. 1.5×10^6 and 1.2×10^6 cells were plated in a 75cm^2 flask and a 6-well plate, respectively.

3.1.5 AF-MSCs freezing

Cell pellet (see 3.1.3) was resuspended in freezing medium (50% FBS/Dimethylsulfoxide (DMSO; Sigma-Aldrich Ltd., St. Louis, MO USA) 9:1, 50% DMEM+1% a/a), aliquoting 1 mL of cell/freezing medium mixture per vial. Vials were put on ice and subsequently were cryopreserved at -80°C .

3.1.6 Differentiation of AF-MSCs into hepatic progenitors (HPL and HL cells)

Hepatic differentiation was a three-step process: AF-MSCs > HPL0 > HPL > HL. 90% confluent AF-MSCs are incubated with 9 mL Hepato0 solution for 2-3 days (HPL0 step) and 9 mL Hepato1 solution for 7 days with a change of medium at the middle day (HPL1 step).

Hepato0 solution: Iscove's Modified Dulbecco Medium (IMDM; Gibco, Paisley, Scotland) + 20 ng/mL Epidermal Growth Factor (EGF; Peptidech) + 10 ng/mL Fibroblast Growth Factor (FGF; Peptidech) + 1% a/a.

Hepato1 solution: IMDM + 20 ng/mL Hepatocyte Growth Factor (HGF; Peptidech) + 10 ng/mL FGF (Peptidech) + 0.1% DMSO (Sigma-Aldrich Ltd., St. Louis, MO USA) + 1% a/a

At this stage, cells were fully differentiated into Hepatic Progenitor-like (HPL) cells. In order to continue with the differentiation to HL cells, HPL cells are incubated in Hepato2 solution for 14 days, with a change of medium at the Day 7 (HL step). At this stage, cells were fully differentiated into Hepatocyte-like (HL) cells.

Hepato2 solution: IMDM + 20 ng/mL Oncostatin M (Peptidech),+ 1 mM Dexamethasone (Sigma-Aldrich Ltd.) + 50 $\mu\text{g}/\text{mL}$ ITS (Sigma-Aldrich Ltd.) + 1% a/a

3.1.6 Exosome collection

Cells (AF-MSCs, HPL or HL) at 90% confluency, were cultured into 40-fold diluted "exosome-depleted" medium (DMEM +20% FBS +1% a/a), which was previously ultracentrifuged overnight at 37500 rpm in order to remove FBS-derived exosomes, and was subsequently 40x concentrated using a 30 kDa cutoff filter. After a 2-day incubation at 37°C , the medium was collected and centrifuged at 12000 rpm for 5', and the supernatant was stored at 4°C .

In order to isolate the exosomes, the supernatant was ultracentrifuged (Fixed Angle Rotor T865, Thermo Fischer Scientific) at 37500 rpm, 4°C for 2 hours. The supernatant was filtered by using a 0.2 μm cutoff filter, and was kept at 4°C as negative control. The pellet was resuspended in PBS, followed by 30' bath sonication, and stored at -80°C .

3.2 Proteomics

3.2.1 Sample preparation for proteomic analysis

GeLC-MS method was performed to prepare the samples for proteomic analysis. 10 mg of each sample were analyzed in SDS-PAGE. Electrophoresis was terminated when samples just entered the separating gel. Gels were stained with Coomassie colloidal blue overnight. Each band was excised from the gel and further sliced to small pieces (1-2 mm). Gel pieces were destained with 40% Acetonitrile (Sigma), 50 mM NH₄HCO₃ (Fluka), reduced with 10 mM DTE (Sigma) in 100 mM NH₄HCO₃ for 20 min RT and alkylated with 54 mM Iodoacetamide (Applichem) in 100 mM NH₄HCO₃ for 20 min RT in the dark. Samples were then washed with 100 mM NH₄HCO₃ for 20 min at RT, followed by another wash with 40% Acetonitrile, 50 mM NH₄HCO₃ for 20 min at RT and a final wash with ultrapure water under the same conditions was performed. Gel pieces were dried in a centrifugal vacuum concentrator and trypsinized overnight in the dark, RT, by adding 600 ng of trypsin (Roche) per sample (trypsin stock solution: 10 ng/μl in 10 mM NH₄HCO₃, pH 8.5). Peptides were extracted after incubation with the following buffers: 50 mM NH₄HCO₃ for 15 min, RT followed by two incubations with 10% Formic Acid, Acetonitrile (1:1) for 15 min, RT. Peptides were eluted in a final volume of 600 μl and filtered with PVDF filters (Merck Millipore) before dried in a centrifugal vacuum concentrator. Dried peptides were reconstituted in mobile phase A buffer (0.1% formic acid, pH 3) and processed with LC-MS/MS analysis.

3.2.2 Liquid Chromatography – Mass Spectrometry/Mass Spectrometry (LC-MS/MS)

LC-MS/MS experiments were performed on the Dionex Ultimate 3000 UHPLC (Thermo Fisher Scientific, Bremen, Germany) system coupled with the high-resolution nano-ESIOrbitrap-Elite mass spectrometer (Thermo Fisher Scientific). Each sample was reconstituted in 10 μl loading solution consisted of 0.1% v/v formic acid. A 5 μl volume was injected and loaded on the Acclaim PepMap 100 (100 μm × 2 cm C18, 5 μm, 100 Å) trapping column with the ul-Pick-Up Injection mode with the loading pump operating at a flow rate of 5 μl/min. For the peptide separation the Acclaim PepMapRSLC, 75 μm × 50 cm, nanoViper, C18, 2 μm, 100 Å column (Thermo Fisher Scientific) retrofitted to a PicoTip (New Objective Woburn, MA, USA) emitter was used for multi-step gradient elution. Mobile phase (A) was composed of 0.1% formic acid and mobile phase (B) was composed of 100% acetonitrile, 0.1% formic acid. The peptides were eluted under a 240 min gradient from 2% (B) to 33% (B). Flow rate was 300 nl/min and column temperature was set at 35 °C. Gaseous phase transition of the separated peptides was achieved with positive ion electrospray ionization applying a voltage of 2.5 kV. For every MS survey scan, the top 10 most abundant multiply charged precursor ions between m/z ratio 300 and 2200 and intensity threshold 500 counts were selected with FT mass resolution of 60,000 and subjected to HCD fragmentation. Tandem mass spectra were acquired with FT resolution of 15,000. Normalized collision energy was set to 33 and already targeted precursors were dynamically excluded for further isolation and activation for 30 s with 5 ppm mass tolerance.

3.3 Liver tissues molecular profile

3.3.1 In vivo exosomes/CM treatment

In order to analyze the profile of the liver tissue upon AHF induction and exosomes or CM treatment in a murine model, Rag1^{-/-} mice, 6-8 weeks old, were housed and maintained at the Animal Facility of the Biomedical Research Foundation of the Academy of Athens according to the institutional guidelines, which follow the guidelines of the Association for Assessment and Accreditation of Laboratory Animal Care, the recommendations of the Federation of European Laboratory Animal Science Associations and of the National Institute of Health.

Mice of the AHF group were intraperitoneally injected with one dose of 100 μ L sun oil per 20g of body weight, containing 10 μ L of CCl₄. The control group mice were administered one dose of 100 μ L sun oil per 20g of body weight, containing 10 μ L of PBS. The next day, AHF mice were intrahepatically injected with the six treatments (20 μ g exosomes or 200 μ L CM) collected from AF-MSCs, HPL or HL (**table 3**) or with rMFGE8 (**table 4**).

Table 3: Grouping of mice per treatment in the *in vivo* administration of exosomes and CM experiment (see section 4.6)

Group label	AHF injection	Treatment
Control	PBS – no AHF induction	no treatment
CCl ₄	CCl ₄ – AHF induction	
AF-exo		20 μ g exosomes derived from AF-MSCs
AF-CM		200 μ L CM derived from AF-MSCs
HPL-exo		20 μ g exosomes derived from HPL cells
HPL-CM		200 μ L CM derived from HPL cells
HL-exo		20 μ g exosomes derived from HL cells
HL-CM		200 μ L CM derived from HL cells

Table 4: Grouping of mice per treatment in the *in vivo* administration of exogenous rMFGE8 experiment (see section 4.7)

Group label	AHF injection	Treatment
Control	PBS – no AHF induction	no treatment
CCl ₄	CCl ₄ – AHF induction	
rMFGE8		6.5 μ g of rMFGE8

One day later, all the mice were sacrificed, and blood sample and liver tissue were collected. The blood samples were collected in tubes containing heparin, centrifuged at 13000 rpm for 5', and the blood serum was isolated and sent for biochemical analysis, in order to measure the transaminase levels. Hepatic tissue slices were obtained from all mice and were formalin-fixed and paraffin-embedded (FFPE) in blocks.

3.3.2 Exosomes imaging in the murine liver using Xenogen IVIS system

PKH26-stained exosomes were administered to murine livers one day post CCl₄-induced AHF (see 3.3.1). 20 µg of stained exosomes were administered intrahepatically (IH), or 10 µg of stained exosomes were administered intravenously (IV) to the mice. Live animal imaging was performed using Xenogen IVIS imaging system, during which PKH26 marker was detected. The following day the mice were sacrificed, and their livers were dissected, along with the liver of a control mouse, without having administered exosomes.

3.3.3 RNA extraction from FFPE tissues

In order to extract the total RNA from FFPE liver tissues, the NucleoSpin totalRNA FFPE XS (Macherey-Nagel) kit was used. At the beginning, 1 mL of Paraffin Dissolver was added to the FFPE sections and they were incubated at 56°C for 15 minutes to melt the paraffin. Then, the sample was vortexed and centrifuged at 16000g for 2 minutes, followed by addition of 140 µL MLF buffer and a centrifugation at 16000g for 2 minutes. Paraffin Dissolver was removed by pipetting and the sample was lysed by adding 12 µL Proteinase K and incubated at least for 90 minutes, up to overnight, until the sample was lysed. 12 µL of MKA buffer was then added and the lysate was incubated for 5 minutes on ice, then centrifuged at 16000g for 5 minutes.

The next step was to bind the RNA onto the columns. 400 µL of MX buffer was added to the supernatant of the lysate and then was mixed and left to incubate for 1 minute at room temperature. The lysate was loaded into a NucleoSpin® RNA FFPE XS Column, placed on a 2mL tube, and then centrifuged at 16000g for 1 minute. Flow-through was discarded and the same procedure was repeated, by adding 400 µL MW2 buffer and once again by adding 200 µL MW2 buffer, in order to rinse the membrane.

After the final centrifugation, 25 µL rDNase was added directly onto the silica membrane of the column, in order to digest any DNA present in the lysate. Columns were incubated at room temperature for 15 minutes, and then the same procedure was followed as previously in order to rinse the membrane from the rDNase. A final centrifugation of 5 minutes followed in order to completely dry the membrane.

The final step involved the elution of total RNA. The columns were placed into a new 1.5 mL tube, and 30 µL RNase was added to the columns. The samples were incubated for 1 minute at room temperature and centrifuged at 16000g for 1 minute. RNA concentration and purity were measured in spectrophotometer. The eluted RNA was stored at -20 °C for short-term storage.

3.3.4 Protein extraction from FFPE tissues

The first step of the protein extraction was the deparaffinization of FFPE samples, by a 5 minutes incubation in 1 mL xylene (twice) and washing once for 1 minute in xylene, with a 3-minute centrifugation in 13000g between the steps. Rehydration of the tissue pellets was conducted by serial incubations of the samples in ethanol 100%, 95%, 70% and H₂O, with a

3-minute centrifugation in 13000g between the incubations. A 5-minute centrifugation in 13000g was then followed, and the pellets were dried in open air for at least 30 minutes.

Pellets were resuspended in 200 μ L of FASP protein extraction buffer (100mM Tris-HCl pH 7.6, SDS 4%, 100mM DTE) and then homogenized by sonication. Sonication was applied for three 10-second cycles with a 10-second pause between them, with a 60-minute incubation at 90°C following next, and a centrifugation at 13000 rpm for 10 minutes.

In order to concentrate the protein, 10-fold quantity of ammonium bicarbonate was added, so that the solution could pass through the concentration columns (Ultracel 3k, Amicon Ultra, UFC500396), 500 μ L at a time, with a centrifugation applied after each time at 13000 rpm for 30-45 minutes. When all of the solution had passed through, the remaining solution was collected and protease inhibitors were added to the supernatant of the lysate in a final concentration of 3.6%. Protein concentration was measured by performing Bradford assay and protein was stored at -20°C.

3.3.5 Bradford assay

Concentrated proteins were diluted 1:20 in H₂O. In a 96well ELISA plate, 2.5 μ L of the diluted protein sample was added along with 250 μ L Bradford solution. Apart from the samples, a negative sample was also included (without protein). The ELISA plate was left in dark for 10 minutes and the absorbance was counted at 595 nm, using a standard curve to specify the concentrations.

3.3.6 cDNA synthesis

In order to synthesize mRNA from the extracted RNA (**see 3.2.2**) and reverse transcribe it into cDNA, we used FIREScript RT cDNA Synthesis kit (Solis Biodyne). A total of 0.2-1 μ g RNA, 1 μ L oligo(dT) primers and nuclease-free H₂O were added, up to 16 μ L volume. The mix was heated at 65°C for 5 minutes, for the primers to bind to the RNA. Then, a mastermix containing 2 μ L 10x RT Reaction Buffer, 0.5 μ L dNTP mix, 0.5 μ L RiboGrip RNase Inhibitor (40 U/ μ L) and 1 μ L FIREScript RTase for each sample was prepared, and 4 μ L of MasterMix was added to each sample. The samples were incubated at 37°C for 30 minutes and at 85°C for 5 minutes

3.3.7 Real-Time PCR

The protocol for 5x HOT FIREPol EvaGreen qPCR Supermix was used to perform real-time PCR. For each sample, 2.5 μ L cDNA, 0.4 μ L of each primer (**Table 5**), 4 μ L of 5x HOT FIREPol EvaGreen qPCR Supermix and water for injections were added up to 20 μ L. The PCR protocol included 12-minute incubation at 95°C, followed by 40 cycles of 15-second incubation at 95°C, a 20-second incubation at 60°C and a 20-second incubation at 72°C.

Table 5: Primers used for the RT-PCR experiments

Gene	Forward (5' – 3')	Reverse (5' – 3')	Size (bp)
PI3K	GCAGAGGGCTACCAGTACAGA	CTGAATCCAAGTGCCACTAAGG	122
mTOR	ACCGGCACACATTTGAAGAAG	CTCGTTGAGGATCAGCAAGG	110
FOXO1	ATGCTCAATCCAGAGGGAGG	ACTCGCAGGCCACTTAGAAAA	183
PTEN	TTTGCTAGTGAGTGGAATCCTCT	TGTGACAAAAGTGACACAGATCA	155
IL-1b	CAGGTCGCTCAGGGTCACA	CAGAGGCAAGGAGGAAACACA	
IL-6	GTTCTCTGGGAAATCGTGGA	TCCAGTTTGGTAGCATCCATC	138
CD68	GGACCCACAACCTGTCACCTCAT	AAGCCCCACTTTAGCTTTACC	296
VEGFA	GCAGCGACAAGGCAGACTAT	AACCTCCTCAAACCGTTGGC	169
BCL-2	GTCGCTACCGTCGTGACTTC	CAGACATGCACCTACCCAGC	284
BAX	TGAAGACAGGGGCCTTTTTG	AATTCGCCGGAGACACTCG	140
ERK1	TCCGCCATGAGAATGTTATAGGC	GGTGGTGTGATAAGCAGATTGG	248
c-MET	GTGAACATGAAGTATCAGCTCCC	TGTAGTTTGTGGCTCCGAGAT	100
MFGE8	GTATGTGGCGTCCTACAAGG	GTGATGCGGTTATGCCAG	189
MMP2	CCTGGACCCTGAAACCGTG	TCCCCATCATGGATTCGAGAA	96
MMP9	CTGGACAGCCAGACACTAAAG	CTCGCGGCAAGTCTTCAGAG	145
TGFB1	CTCCCGTGGCTTCTAGTGC	GCCTTAGTTTGGACAGGATCTG	133
p21	CCTGGTGATGTCCGACCTG	CCATGAGCGCATCGCAATC	103

3.3.8 Western Blot

Two polyacrylamide gels were prepared, in order to perform an SDS-PAGE electrophoresis: a 12% separating gel (375 mM Tris-HCl pH=8.8, 0.1% SDS, 12% Bis/Acrylamid (Bio-Rad), 5 μ L Temed, 0.05% AP) and a 4% stacking gel (125 mM Tris-HCl, pH=6.8, 0.1% SDS, 4% Bis/Acrylamid (Bio-Rad), 5 μ L Temed, 0.1% AP). A comb was added above the stacking gel and the two gels were left to become solid.

Protein samples were added in a tube (~ 60 μ g) along with 6x loading dye, 3 mL β -mercaptoethanol and dH₂O up to the final volume (40-60 μ L). The samples were incubated at 95°C for 10-20 minutes. The SDS-PAGE gel electrophoresis device was set up and the gels were clasped on a plastic plate. Running buffer 1x (14.4 g glycine, 3 g Tris base, 0.1% SDS) was added into the device until half of it is covered. The samples were then loaded on the wells shaped by the comb (max volume ~30 μ L) and the electrophoresis device was set at about 45V for 15' (until the samples reach the stacking-separating gel border) and then at 120 V for 1-1.5 hour.

PVDF membranes and the Whatmann's papers were cut at 9 * 5.5 mm dimensions. The Whatmann's papers along with two sponges were placed into the Transfer buffer (14.4 g glycine, 3 g Tris base, 20% methanol). PVDF membranes are dipped for 10 seconds in methanol, 2 minutes in dH2O and 15 minutes in the Transfer buffer subsequently. The Transfer device was placed on ice, and both membranes and gel were placed into its inside cassette in the following order (cathode – sponge - whatmann's – separating gel - PVDF membrane - whatmann's – sponge - anode) (**fig. 8**).

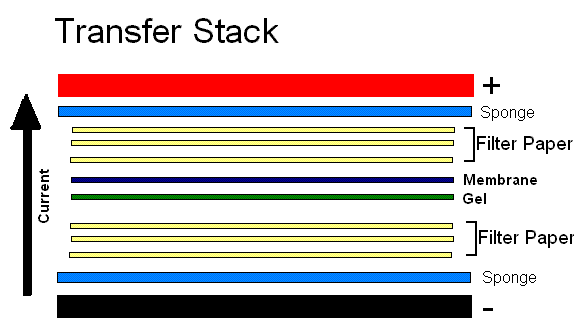


Figure 8: Setting of the Transfer cassette

The cassette was placed into the Transfer device along with the Transfer buffer, two icepacks and a stirring magnet, placed over a stirrer at 4°C and left at 100 V for 1-2 hours.

After the transfer, Blocking buffer (5% w/v milk, 0.1% Tween-20 in TBS) was applied on the membrane, and incubated under shaking for 1-1.5 hour at room temperature, and followed by three 10-minute washes with Wash buffer (0.1% Tween-20 in TBS). The membrane was split depending on the molecular weight of the proteins under investigation. Each piece was enclosed in a case containing 1-2 mL of the diluted (in 5% w/v milk in TBS) primary antibody (**Table 6**), incubating them on the shaker at 4°C overnight.

Table 6: Primary antibodies used in the Western blot experiments

Antibody	Code	Company	Size (kDa)
Mouse anti-MFGE8	SC-271574	Santa Cruz	46
Mouse anti-PTEN	SC-7974	Santa Cruz	55
Rabbit anti-AKT	#9272	Cell Signaling	56
Rabbit anti-p-AKT	#9271	Cell Signaling	60
Rabbit anti-ERK1	#9102	Cell Signaling	42
Rabbit anti-p-ERK1	#9101	Cell Signaling	44
Mouse anti-CD63	SC-5275	Santa Cruz	50
Mouse anti-CD9	SC-13118	Santa Cruz	24
Mouse anti-EMILIN-1	SC-365737	Santa Cruz	115
Mouse anti-GAPDH	MAB374	Millipore	38

Membranes were rinsed three times using Wash buffer for 10 minutes on the shaker, and then, the corresponding secondary antibody (**Table 7**) is diluted 1:1000 in 5% milk + 0.1% Tween-20 in TBS.

Table 7: Secondary antibodies used in the Western blot experiments

Antibody	Code	Trademark
Anti-mouse HRP	AP130P	Millipore
Anti-rabbit HRP	#7074	Cell Signaling

The membranes were enclosed with 1-2 mL of the secondary antibody and were incubated in the shaker in room temperature for 1 hour. Following the incubation, membranes were washed two times with Wash buffer and once with TBS. Membranes were placed in such an order, according to molecular weight, and 2 mL of Luminata Forte Western HRP substrate (Millipore, Burlington, Massachusetts, USA) was added on the membranes, incubating for 5 minutes in dark. Following this step, membranes were ready for exposure, in order to acquire the results.

In order to use the same samples again, attaching different antibodies, the membranes were placed into Stripping buffer (2% SDS, 62.4 mM Tris-HCl pH=6.8, 0.8% β -mercaptoethanol) and incubated at 50°C for 20 minutes, followed by wash three times using Wash buffer. The protocol is then followed from Blocking buffer (5% w/v milk, 0.1% Tween-20 in TBS) and continues as above.

3.3.9 Hematoxylin/Eosin (H&E) staining

The formaldehyde-fixed tissues which undergo H/E staining were placed into 70% ethanol, and subsequently were immersed into increasing concentrations of ethanol, in order to dehydrate, and then the tissues were paraffinized. Sections of paraffinized liver tissues were immersed at 70% ethanol for 30 minutes, followed by washes with dH₂O. Tissues were then incubated with Hematoxylin (Sigma-Aldrich) for 30-45 seconds, followed by a short wash and then incubated with Eosin (Sigma-Aldrich) for 30-45 seconds, followed by another short wash. Finally, the tissues were immersed into 70% ethanol for 30 seconds and subsequently into 100% ethanol for 1 minute and into xylene (Carlo-Erba Reagents, Italy) for 7 minutes.

3.3.10 TUNEL assay

TUNEL assay was performed according to the manufacturers' instructions of TUNEL apoptosis Assay Kit (HRP-DAB) (ES00331-20, AssayGenie, Ireland) in FFPE liver sections of AHF mice treated with CM or exosomes derived from AF-MSC, HPL, HL cells (n=3 per group). Liver sections of mice injected with PBS were used as negative controls (n=3 per group). Positive apoptotic cells were counted with ImageJ v1.43m software.

3.3.11 Immunofluorescence

The paraffin-embedded tissue slides were placed into Xylene (Carlo-Erba Reagents, Italy) for 3 times of 3 minutes each, and subsequently are immersed into decreasing concentrations of ethanol (100%, 95%, 70%) for 3 minutes each, and finally slides were rinsed twice in dH₂O for 5 minutes. Following that, slides were soaked into citrate buffer (10.5g citric acid and

14.7g sodium citrate in 500 mL dH₂O), covered with a lid, and microwaved until citrate buffer boiled. Slides were then removed from heat and were left for 20 minutes to stand, washed 3 times for 5 minutes and liquid was removed. A PAP pen was used to make a hydrophobic circle around the tissue, and 5% BSA was applied on the sample. Slides were incubated at 4°C overnight.

The following day, slides were incubated with the diluted primary antibody (in 1% BSA/PBS) for 1 hour. Slides were washed 3 times and the diluted secondary antibody was applied (1:200 in 1% BSA) for 1 hour in dark. Slides were then rinsed 3 times and 50% glycerol/PBS is applied on the sample, coverslip was placed and slides were stored at 4°C until viewed using confocal microscopy.

Table 8: Antibodies used in the immunofluorescence experiments

Antibody	Code	Trademark
Mouse anti-MMP2	AM00257AF-N	Acris
Mouse anti-MMP9	sc-10737	Santa Cruz
Rabbit anti-TGFb	APO6350PU-N	Origene
Donkey anti-mouse AlexaFluor 488	A-11029	Invitrogen
Donkey anti-rabbit AlexaFluor 594	A-32754	Invitrogen

4 Results

4.1 Differentiation of AF-MSCs to HPL and HL cells

AF-MSCs were initially differentiated into Hepatocyte Progenitor-like cells (HPL), enriching their culture medium with EGF and FGF growth factors, followed by HGF, EGF, FGF and DMSO, in order to give rise to HPL cells. In the following step, HPL cells were differentiated into Hepatocyte-like cells (HL), providing them with a differentiation medium consisted of Dexamethasone, ITS and Oncostatin M. Throughout the differentiation process, the spindle-shaped morphology of AF-MSCs, through an intermediate shape of HPL, was changed into the characteristic polygonal shape of HL cells in optical microscopy (**fig. 9A**), and upon periodic acid-schiff (PAS) staining (**fig. 9B**). HL cells are closer to fetal liver by tyrosine aminotransferase and albumin levels than AF-MSCs (**fig. 9C**).

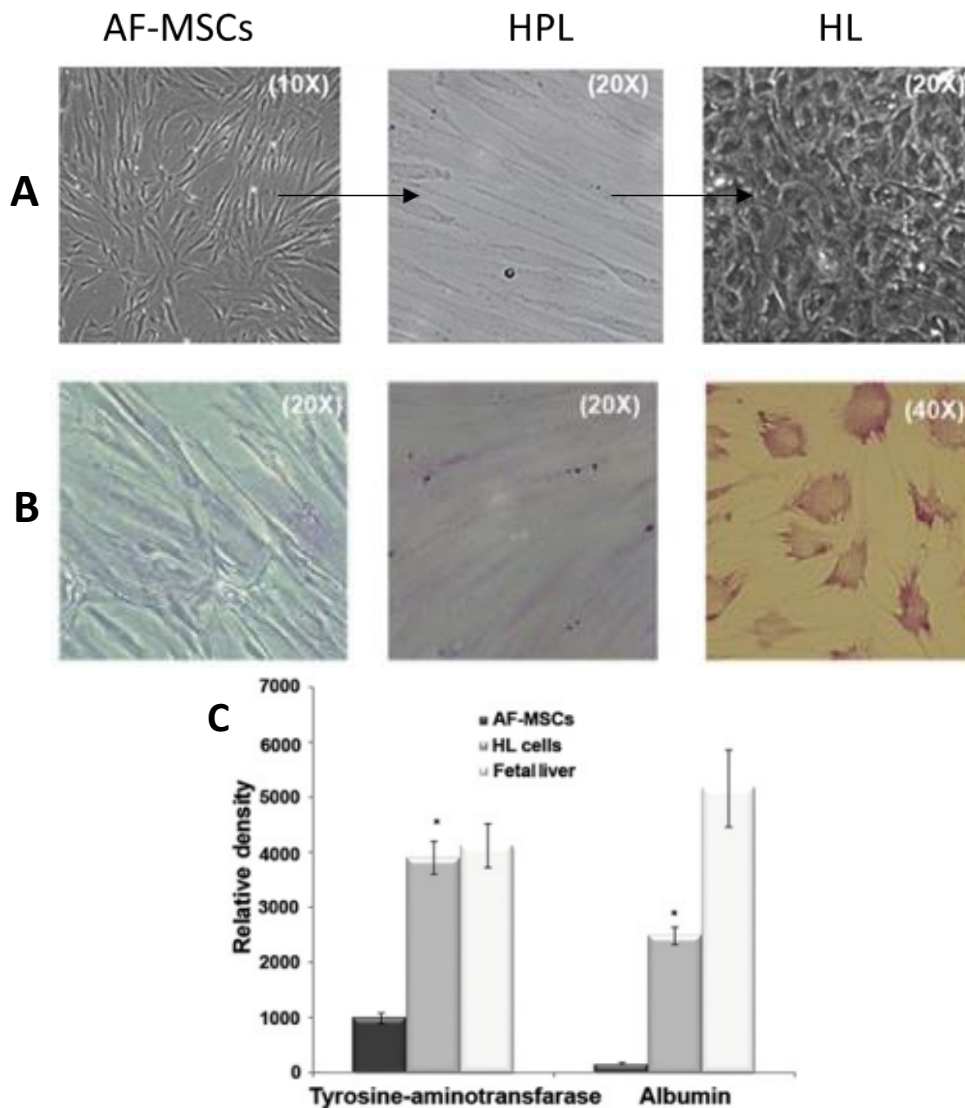


Figure 9: (A) Light microscope images of AF-MSCs, HPL and HL cells (right, 20x zoom). Characteristic spindle-shaped morphology of AF-MSCs is changed into the polygonal shape of HL cells. (B) Periodic Acid-Schiff (PAS) staining of AF-MSCs, HPL and HL cells. (C) Semi-quantitative PCR of tyrosine aminotransferase and albumin of AF-MSCs and HL cells relatively to fetal liver levels. [111]

4.2 Characterization of exosomes isolated from AF-MSCs, HPL and HL cells

In previous results from our laboratory, AF-MSCs, as well as their derivatives, HPL and HL cells, showed a significant therapeutic effect against CCl₄-induced AHF in NOD/SCID mice through their conditioned media (CM), which contains a wide variety of secreted molecules. This project is mostly focused on an important component of the secretome, exosomes, so we sought to isolate the exosomes of these three cell types and investigate their effect against AHF.

Throughout the whole differentiation process (see 4.1), the cells were cultured using 0.5% FBS exosome-depleted medium which, after 2-3 days of culture, it was collected and ultracentrifuged, in order to isolate the exosomes. Exosomes were characterized by identifying tetraspanins CD63 and CD9, which are specific membrane molecular markers, by Western blot on exosomes samples (fig. 10). Exosomes were visualized using electron microscopy (fig. 11).

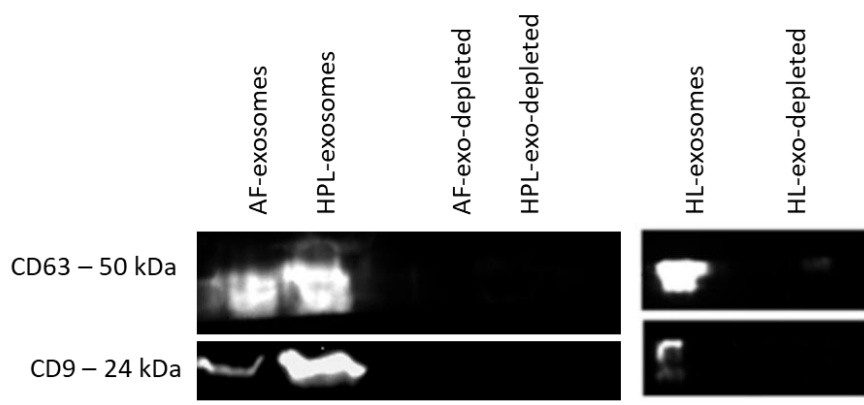


Figure 10: Western blot images, depicting CD63 (anti-human CD63; 50kDa) and CD9 (anti-human CD9; 24 kDa) on exosomes isolated from Af-MSCs, HPL, HL cells versus their correspondent CM without exosomes

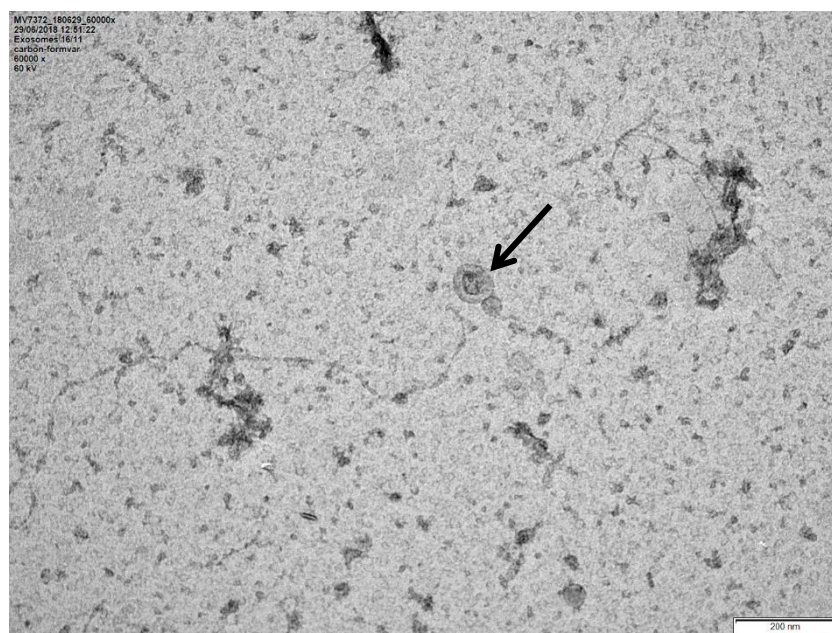


Figure 11: Electron microscope of AF-exosomes. Black arrow indicates an exosome.

4.3 Proteomic characterization of AF-MSC, HPL and HL exosomes

LC-MS/MS analysis was performed in BRFAA, in cooperation with former member of our laboratory Ioanna Angelioudaki, in order to conduct the proteomic analysis of the exosomes, in 18 exosomes samples, six from each cell type (AF-MSCs, HPL and HL cells). Initially, we examined the number of proteins expressed in our samples that were also present in the two major databases, which include information about exosomes and, generally about EVs – Exocarta and Vesiclepedia, respectively. Both of these databases include a list of the top 100 most found proteins in exosomes and EVs.

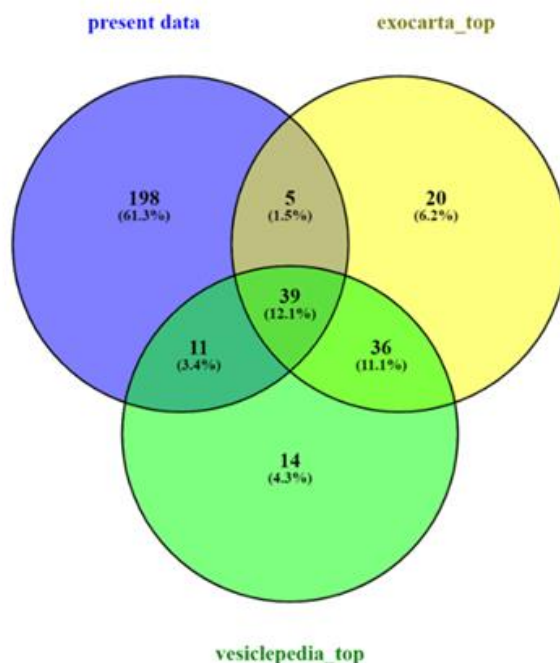


Figure 12: Venn diagram depicting the overlap between the proteins of our samples and the top 100 proteins of Exocarta and Vesiclepedia

The analysis showed that 39 proteins were present in our samples and also in Exocarta and Vesiclepedia databases (**fig. 12**). These proteins include Serum albumin (ALB), Glyceraldehyde-3-phosphate dehydrogenase (GAPDH), Annexin A2 (ANXA2), Actin, cytoplasmic 1 (ACTB), Histone H4 (HIST1H4A), Elongation factor 1-alpha 1 (EEF1A1), Fructose-bisphosphate aldolase A (ALDOA), Heat shock cognate 71 kDa protein (HSPA8), Peroxiredoxin-1 (PRDX1), Heat shock protein HSP 90-beta (HSP90AB1), L-lactate dehydrogenase A chain (LDHA), Alpha-2-macroglobulin (A2M), Alpha-enolase (ENO1), Annexin A5 (ANXA5), Pyruvate kinase PKM, Syntenin-1 (SDCBP), Phosphoglycerate kinase 1 (PGK1), Myosin-9 (MYH9), Annexin A1 (ANXA1), Heat shock protein HSP 90-alpha (HSP90AA1), 4F2 cell-surface antigen heavy chain (SLC3A2), T-complex protein 1 subunit alpha (TCP1), Filamin-A (FLNA), Adenosylhomocysteinase (AHCY), Moesin (MSN), CD81 antigen (CD81), Triosephosphate isomerase (TPI1), Ras-related protein Rap-1b (RAP1B), Galectin-3-binding protein (LGALS3BP), 14-3-3 protein theta (YWHAQ), Annexin A6 (ANXA6), T-complex protein 1 subunit gamma (CCT3), Transitional endoplasmic reticulum ATPase (VCP), GTP-binding nuclear protein Ran (RAN), Clathrin heavy chain 1 (CLTC), CD9 antigen

(CD9), Programmed cell death 6-interacting protein (PDCD6IP), CD63 antigen (CD63) and Elongation factor 2 (EEF2).

Then, we filtered out the protein data, leaving only the proteins that were present in all six samples of AF-MSCs, HPL and/or HL cells. We found that only 7 proteins were uniquely present in all AF-MSC exosomes samples, 17 in all HPL exosomes samples, 11 in all HL exosomes samples, 7 common in all AF and HL exosomes samples, 15 in all HPL and HL samples, and 8 in all AF and HPL samples (**fig. 13**).

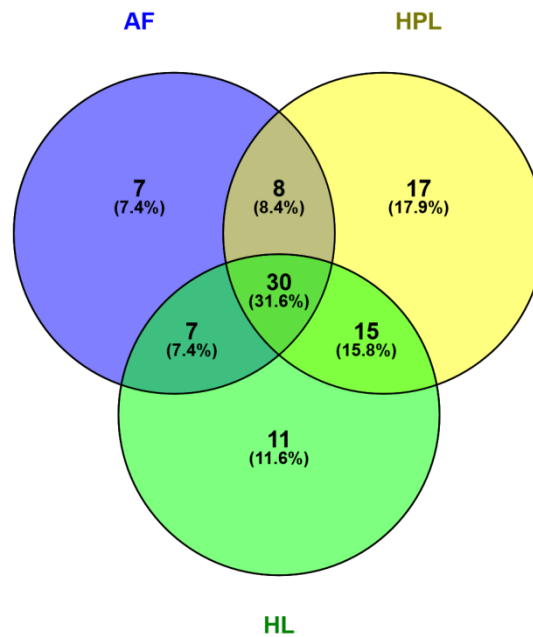


Figure 13: Venn diagram depicting the number of proteins being present in all exosomes samples of each cell type, and their overlaps

Most importantly, there were 30 proteins that were present in all samples of all cell types (**fig. 13**), which included various collagen (COL) and keratin (KRT) types, glyceraldehyde 3-phosphate dehydrogenase (GAPDH), fibronectin, thrombospondin (THBS), periostin (POSTN), lactadherin (MFG8), elongation factor 1-A1 (EEF1A1), matrix metalloproteinase 2 (MMP2), annexin-A2 (ANXA2), SPARC, actin (ACTB), histone H4 (HIST1H4A), peroxidase (PXD), lysyl oxidase homolog 2 (LOXL2), elastin microfibril interfacier 1 (EMILIN1), HTRA1 and TGF β -induced protein ig-h3 (TGF β i). The mean intensity of these 30 proteins in each exosomes type is depicted in **fig. 14**.

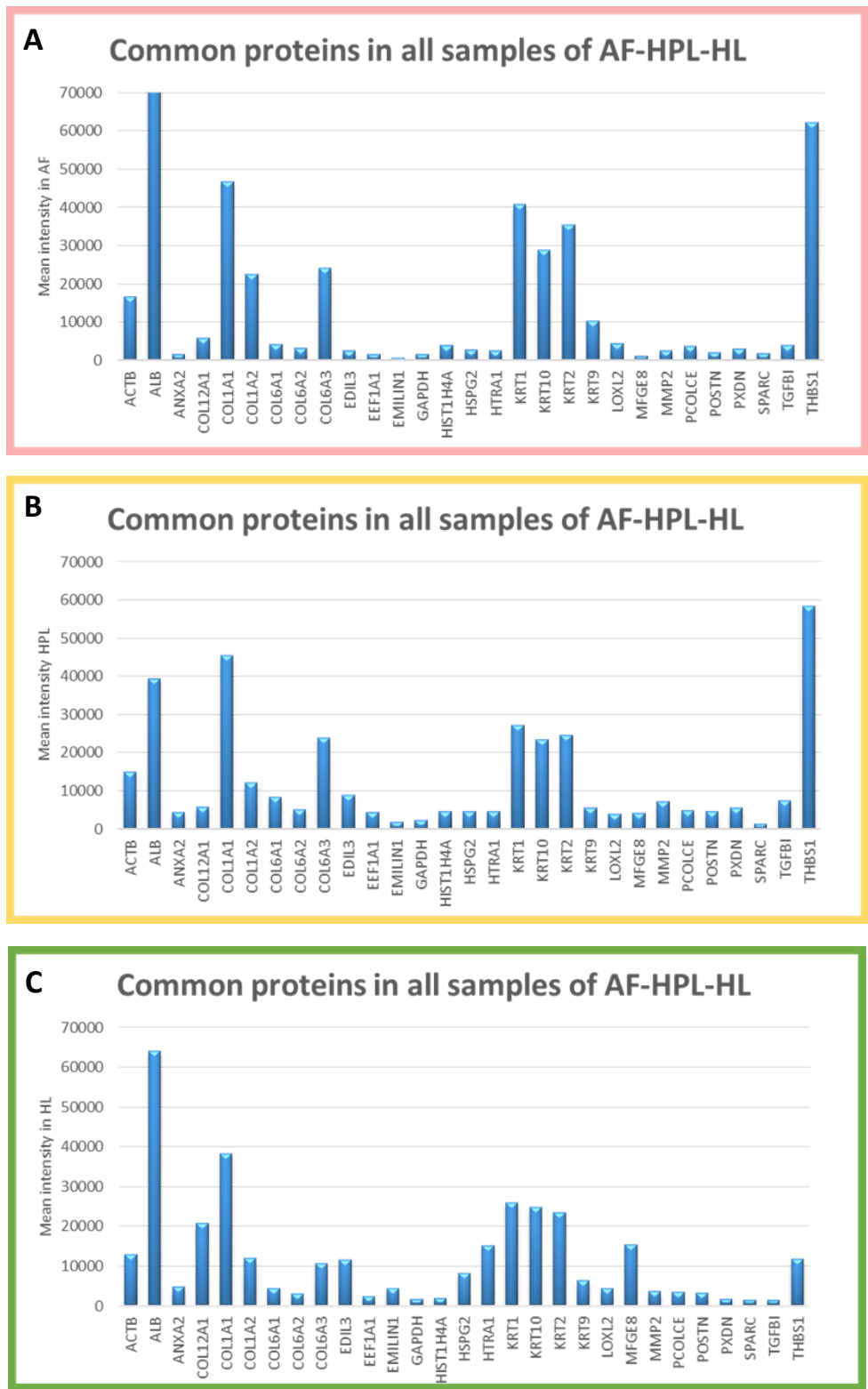


Figure 14: Mean intensity values of the 30 common proteins in all cell type exosomes, in AF-MSCs (A), HPL cells (B), HL cells (C)

Mean intensities were compared between each possible pair of the three cell types: AF vs HPL, AF vs HL, HPL vs HL. In each pair, all of the proteins identified in the exosome cargo of the samples were compared according to the level of expression between the two samples of each pair. Ratios greater than 1.5, or lower than 0.67, were determined as upregulation

4.4 Pathway analysis

The six common proteins, having statistically significant difference in intensity in every possible pair of samples (**fig. 15B-D**), include the C1s and C1r complement subcomponents (C1S, C1R), lactadherin (MFGE8), EMILIN-1, phosphoglycerate mutase (PGAM2) and TGF β -induced protein ig-h3 (TGF β i). These proteins were examined for pathway enrichment, using a built-in application of Cytoscape, ClueGo (apps.cytoscape.org/apps/cluego). A list including all the proteins exhibiting statistically significant difference in their expression between the exosomes of two cell types each time, was uploaded to the software, for each pair of cell types. The most highly represented pathways, which were common in every comparison, are Extracellular Matrix Organization (ECM)-associated pathways, regulation of complement cascade, as well as post-translational protein phosphorylation (**fig. 16**). Moreover, there was a number of important pathways enriched in one or two comparisons, including interleukin 4/13 signaling and regulation of IGF transport and uptake by IGFBPs.

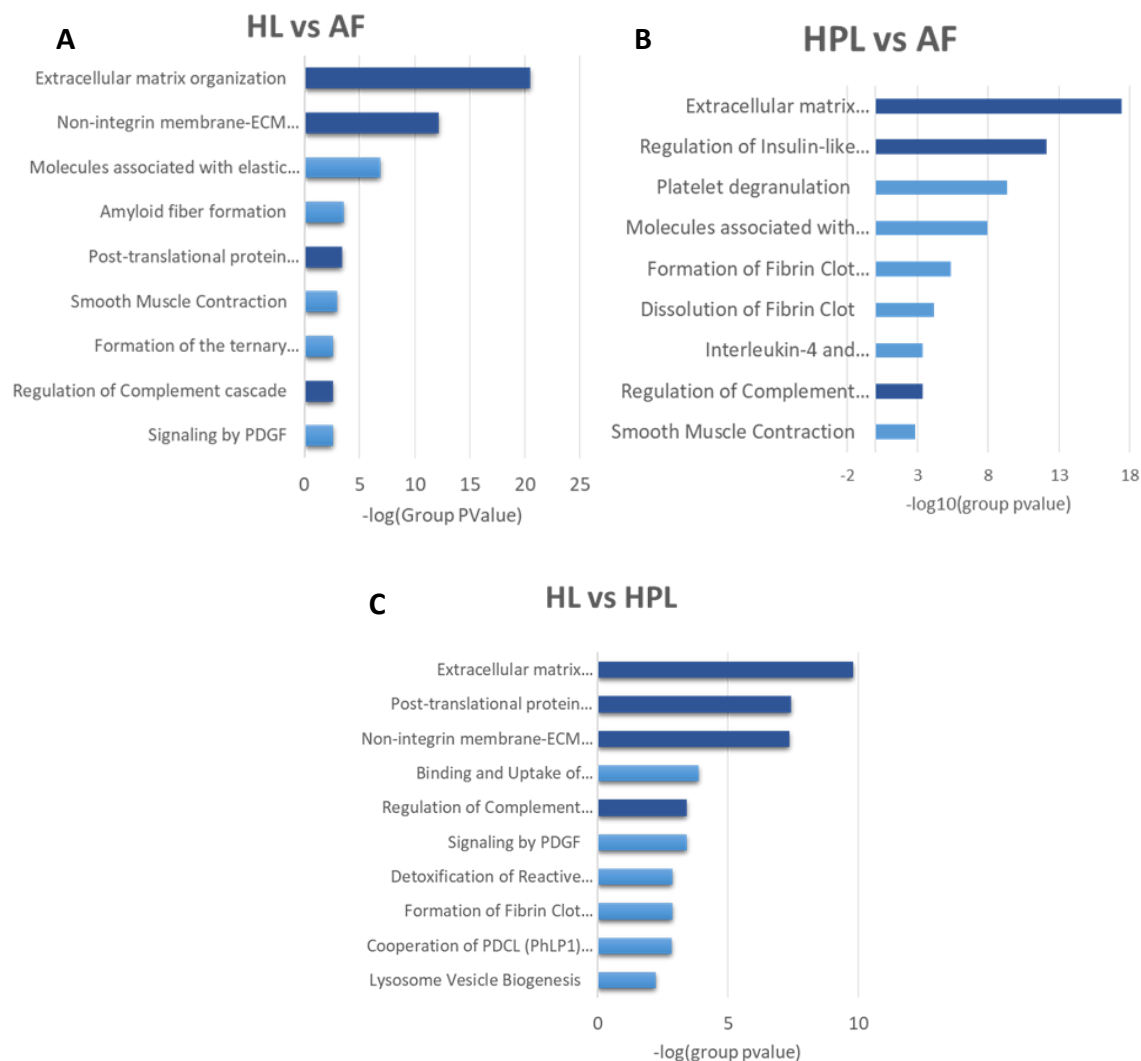


Figure 16: The 10 most represented pathways in which the common proteins with statistically significant difference in their expression between AF-MSCs and HL cells (A), AF-MSCs and HPL cells (B), and HPL and HL cells (C). Pathways are grouped by order of significance ($-\log(\text{group p-value})$): longer bars mean lower p values and higher significance.

As mentioned above, six of the proteins were common in all comparisons, C1s and C1r complement subcomponents, lactadherin (MFGE8), EMILIN1, phosphoglycerate mutase 2 (PGAM2) and TGFβ-induced gene ig-h3 (TGFβi). We aim to examine whether these proteins are responsible for the therapeutic potential of the exosomes, probably through activation of a reparatory mechanism, or deactivation of a disease-involving mechanism. ECM organization pathway, as well as some other significant pathways, such as interleukins 4/13 (IL4/IL13) signaling and regulation of insulin growth factor (IGF) transport and uptake by insulin growth factor binding proteins (IGFBPs), involve one or more of these six important proteins. The association of the aforementioned 6 proteins with each one of the selected pathways (ECM, IL4/13, signaling and regulation of IGF transport and uptake by IGFBPs) were clustered in heatmaps according to their expression patters, using Morpheus software (software.broadinstitute.org/morpheus/) (fig. 17).

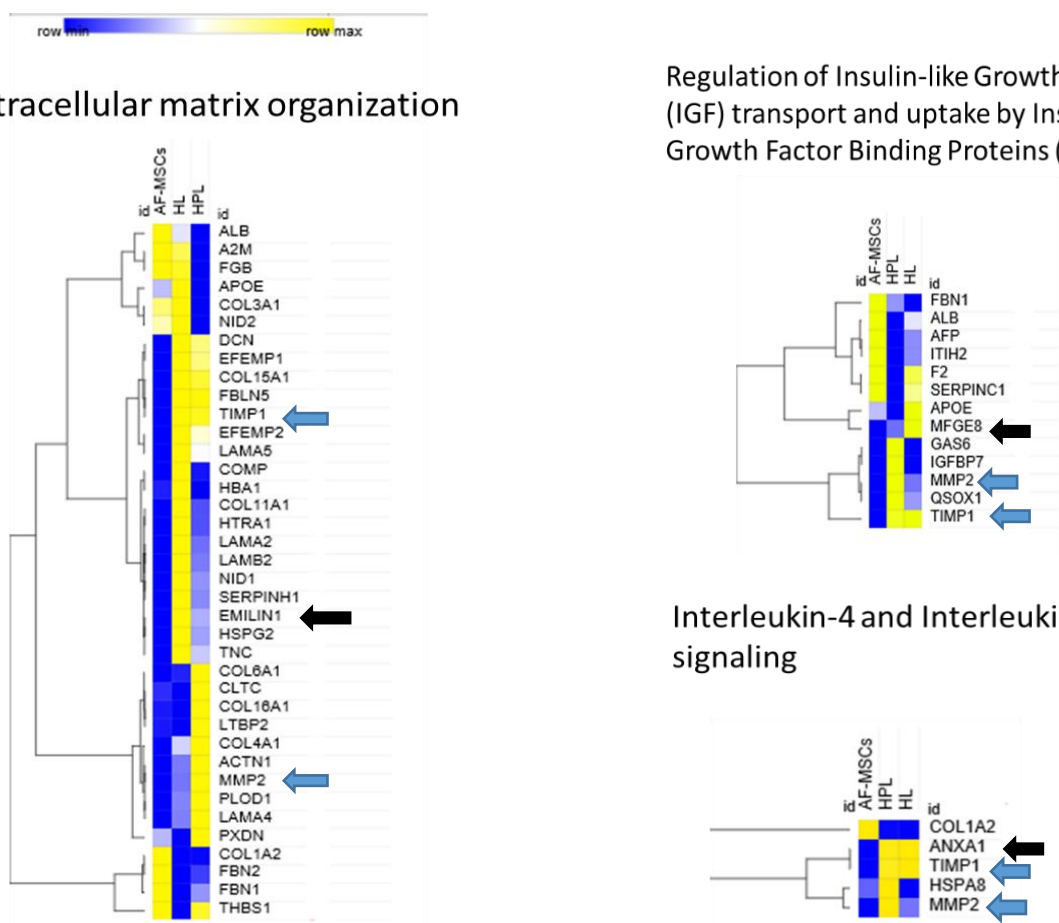


Figure 17: Heatmaps depicting the clustered proteins according to their expression pattern, for ECM organization pathway (left), regulation of IGF transport and uptake by IGFBP (top right) and IL4/IL13 signaling (bottom right). Black arrows represent statistically significant proteins from proteomics analysis. Blue arrows represent common proteins of all pathways.

To begin with, we noticed that Annexin-A1, which was described in a previous publication of our team as a very important paracrine factor of the AF-MSCs secretome, ameliorating AHF clinical phenotype (111), is associated with IL4/IL13 signaling. Other molecules associated with the same pathways were MMP2 and TIMP1. IL4/IL13 signaling is linked to Th2-type of inflammation resulting in tissue repair and remodeling, as well as in the reduction of

overexcessive inflammation (**117-120**). EMILIN1 is a homo-trimeric ECM component, which interacts with the $\alpha 4\beta 1$ integrin through its gC1q domain, playing a key role in ECM assembly and organization (**121, 122**). This is confirmed in our data, as it appears to be associated with ECM pathways, which are important in wound healing and scar formation. MMP2 and TIMP1 are also involved in the same pathways, as they play a major role in ECM degradation and regulation system (**123**). Finally, in IGF/IGFBPs signaling pathway a number of proteins are involved, such as MFGE8, which through its interaction with integrin $\alpha v\beta 5$ ($\alpha v\beta 5$) regulates the pathway (**124**), a fact that also appears in our analysis. MMP2 and TIMPs that are also involved in the respective pathway (**125**) are also reflected in our data.

All of the above indicate that MFGE8 and EMILIN1, as well as MMPs/TIMPs molecules might play a significant role in orchestrating these crucial pathways. PI3K/AKT and MAPK/ERK are basic signaling pathways regulated by MFGE8 and EMILIN1 and might play a key role, by activating or deactivating downstream signals connected to ECM or other signaling proteins. PI3K/AKT pathway is regulated by MFGE8 in a number of studies published in the bibliography (**126-128**), while MAPK/ERK pathway is also referred in literature to be regulated by MFGE8 (**129**) and EMILIN1 (**130**). In **fig. 18**, the pathways that are going to be studied mainly, are depicted.

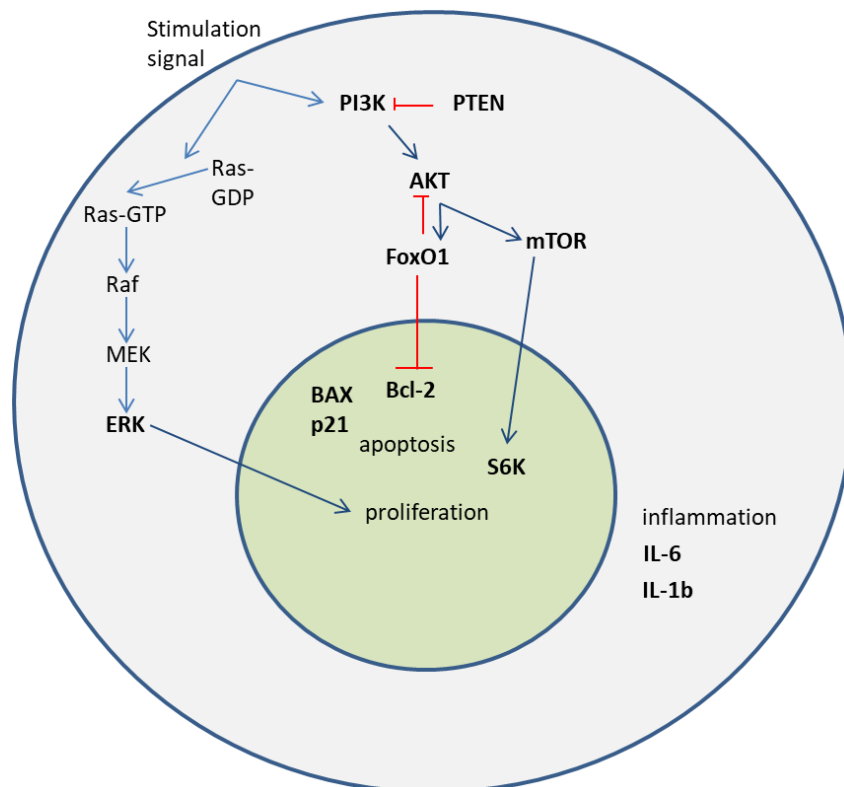


Figure 18: Sketch depicting the main molecules involved in the PI3K/AKT and MAPK/ERK pathways, as well as specific proteins connected to apoptosis, inflammation and proliferation which might be affected by upregulation or downregulation of these intermediate signal pathways

4.5 Protein detection in the exosome cargo

Proteomic analysis underlined MFGE8 and EMILIN1 as proteins of potentially high importance in our exosome samples. In order to detect whether the MFGE8 and EMILIN1 proteins are present in AF-MSC, HPL or HL exosomes' cargo, AF-MSCs were cultured in exosome-depleted DMEM, and then differentiated into HPL cells. In each step of differentiation, culture media were collected and stored at -20°C, until used. Protein extraction and subsequently Western blot were performed (**fig. 19**) in order to confirm or not the presence of EMILIN1 and MFGE8 in the exosomes' cargo of AF and HPL cells.

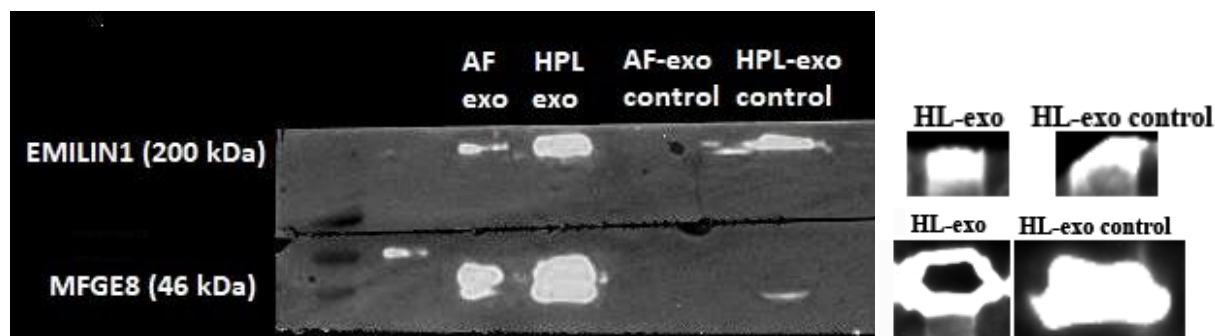


Figure 19: Western blot image indicating EMILIN1 (200 kDa) and MFGE8 (46 kDa) presence in AF-exosomes and HPL-exosomes (primary mouse anti-EMILIN1 and anti-MFGE8 antibodies) versus CM without exosomes (controls)

Western blot results showed that both EMILIN1 and MFGE8 proteins were present in the exosomes cargo, and absent, or in low levels, in CM without exosomes (control).

4.6 Evaluation of exosome efficacy against AHF by administration in an *in vivo* mouse model

Conditioned media secreted by AF-MSCs were proved to be effective against AHF, restoring clinical phenotype, in previous published study of our laboratory (**110**). Exosomes isolated from AF-MSCs, HPL and HL cells were studied in this project in order to evaluate their therapeutic effect in the context of AHF.

Rag1^{-/-} mice were initially injected intraperitoneally with CCl₄ in sun oil, in order to induce AHF phenotype, and control group Rag1^{-/-} mice were injected with PBS in sun oil. Extracellular vesicle dye PKH26 Red Fluorescent (Mini26, Merck/Millipore) was used to label the exosomes, in order to visualize them using Xenogen IVIS system (**see 3.3.2**), after being administered intravenously (IV) or intrahepatically (IH). A better integration of the exosomes in the liver was observed upon IH administration, for the AF-exosomes (**fig. 20**).

Exosomes or CM from the three cell types were administered the second day at the experimental group mice, except the "AHF" or "CCl₄" subgroup (**see 3.3.1**) which were administered with PBS.

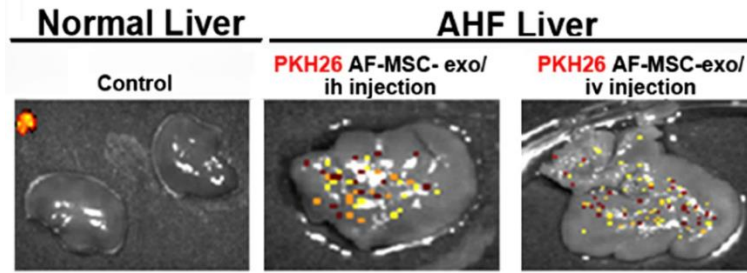
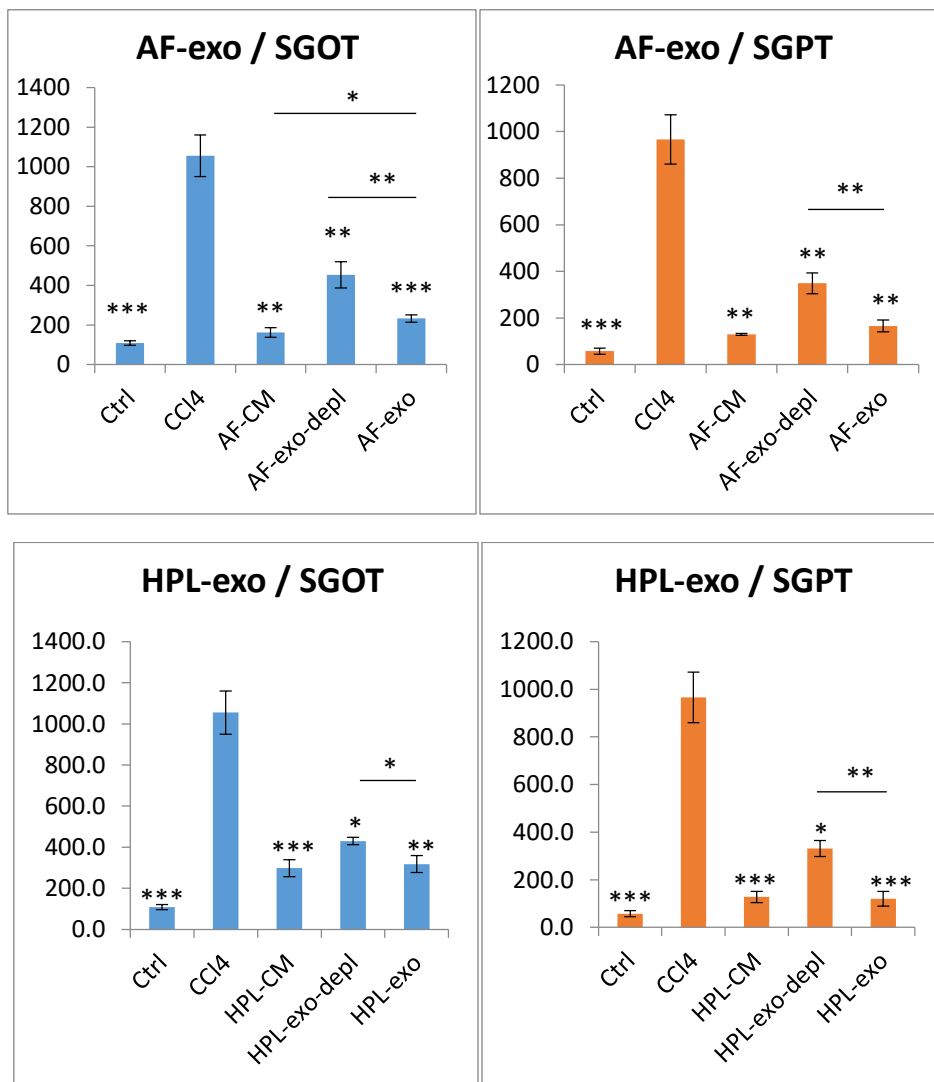


Figure 20: Images of liver tissue: normal (left) and treated with AF-MSc-exosomes via intrahepatic (middle) or intravenous (right) administration, visualized by Xenogen IVIS system. Coloured dots represent exosomes, with darker red colours representing higher intensity. PKH26 in orange to red color represents extracellular vesicles, including exosomes.

Next day after exosomes' administration, mice were sacrificed. Blood samples were collected from all mice and biochemical analyses were performed, where SGOT and SGPT transaminase levels were identified, in order to determine the levels of liver damage in each condition (**fig. 21**). Liver sections were isolated and stained with H&E, to visualize AHF phenotype in each condition (**fig. 22**).



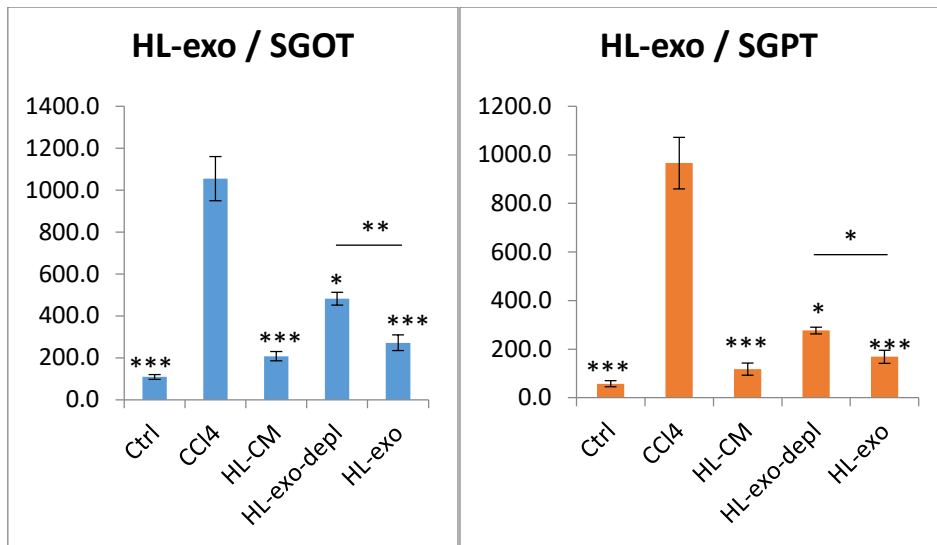


Figure 21: SGOT (left panels) and SGPT (right panels) transaminase levels (units/mL) average values and standard error (SEM) bars for each condition: healthy and AHF (CCl4) animals compared with CM, exosomes-depleted control and exosomes from each cell type. One-tailed t-test was performed, comparing each condition with CCl4 (stars above each bar) as well as exosomes with their control (exosomes-depleted) and with the correspondent CM (stars between correspondent bars). (* stands for $0.01 < p < 0.05$, ** stands for $0.001 < p < 0.01$, *** stands for $p < 0.001$).

AHF increases significantly the levels of transaminases, both SGOT (1055.0, SEM=105.3) and SGPT (966.2, SEM=106.0) in comparison with healthy mice SGOT (108.6, SEM=12.0, $p < 0.001$, ***) and SGPT (57.5, SEM=12.8, $p < 0.001$, ***). Conditioned media (CM) treatments decrease transaminases to near-healthy levels: AF-CM (SGOT: 162.0, SEM=24.4, $p = 0.001$, **); SGPT: 129.3, SEM=3.9, $p = 0.002$, **), HPL-CM (SGOT: 297.8, SEM=41.6, $p < 0.001$, **); SGPT: 127.6, SEM=23.7, $p < 0.001$, ***), HL-CM (SGOT: 207.7, SEM=22.5, $p < 0.001$, **); SGPT: 117.8, SEM=25.1, $p < 0.001$, **).

Exosome efficacy in reversing transaminase levels is also significant: AF-exo (SGOT: 232.5, SEM=19.1, $p < 0.001$, **); SGPT: 165.8, SEM=25.0, $p = 0.003$, **), HPL-exo (SGOT: 317.5, SEM=41.2, $p = 0.001$, **); SGPT: 120.0, SEM=31.1, $p < 0.001$, ***), HL-exo (SGOT: 271.8, SEM=37.5, $p < 0.001$, **); SGPT: 168.5, SEM=27.5, $p < 0.001$, **). Moreover, exosomes efficacy in all cases is greater than their controls (exosomes-depleted CM), in a statistically significant degree: AF-exo vs AF-exo-depleted (SGOT: $p = 0.003$, **); SGPT: $p = 0.006$, **), HPL-exo vs HPL-exo-depleted (SGOT: $p = 0.034$, *; SGPT: $p = 0.001$, **), HL-exo vs HL-exo-depleted (SGOT: $p = 0.005$, **; SGPT: $p = 0.023$, *).

All treatments, CM with exosomes, CM without exosomes and exosomes only, from all of three cell types were efficient in reversing AHF phenotype. In all cases, exosomes were more efficient in ameliorating the clinical image than the exosome-depleted CM (**fig. 21**). The direct effect of exosomes and CM resulted in improving the AHF phenotype in mice, as shown in H&E staining images of the liver tissue (**fig. 22**). Since, exosomes were proved efficient for improving the AHF and we sought to investigate the molecular mechanisms initiated in the target tissue by the exosomes.

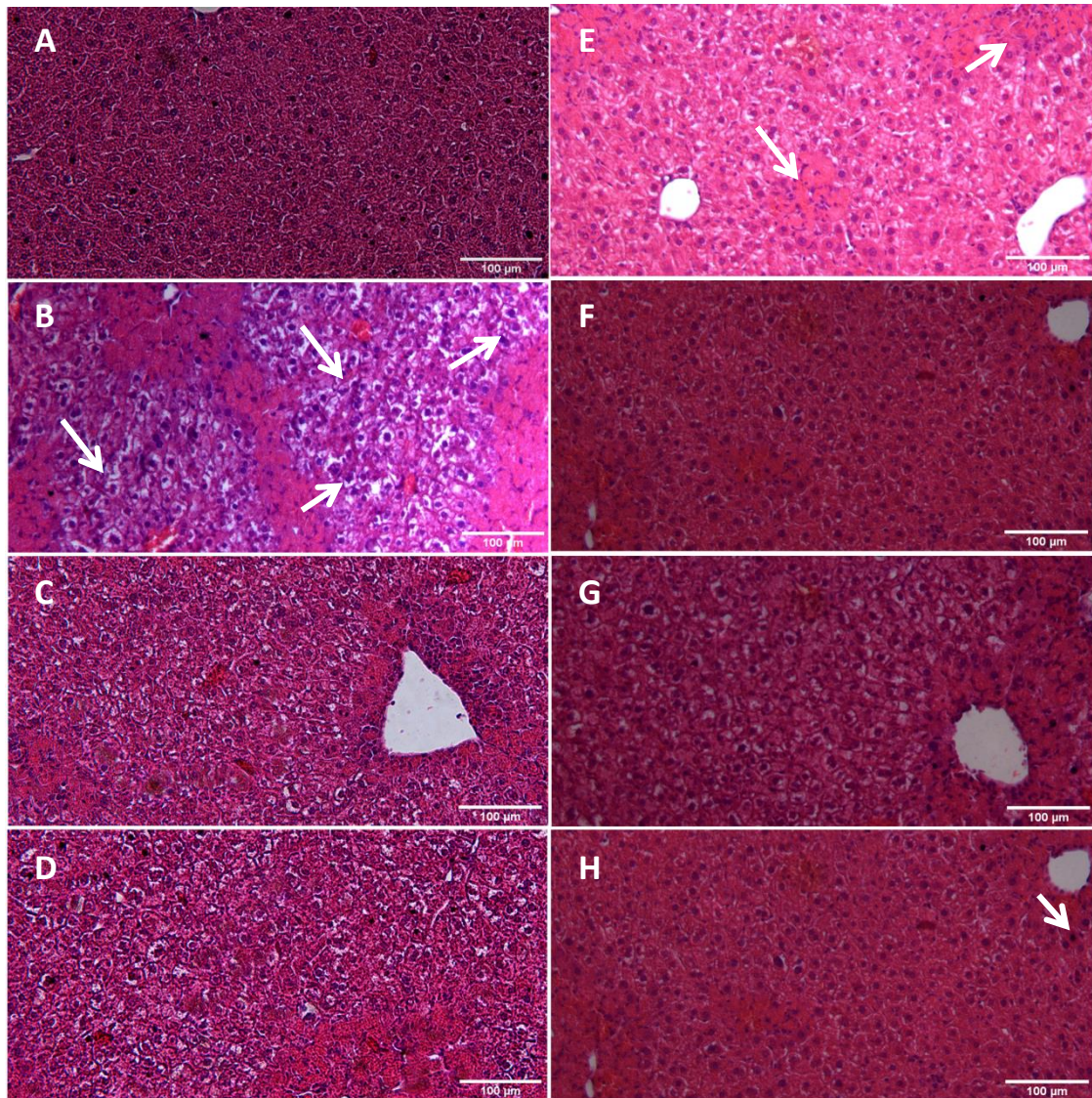


Figure 22: H&E staining of mouse liver tissues. (A) Healthy , (B) AHF, (C) AF-MSC-CM treated, (D) AF-MSC-exosomes treated, (E) HPL-CM treated, (F) HPL-exosomes treated, (G) HL-CM exosomes, (H) HL-exosomes treated. Inflammation areas are indicated by white arrows.

4.7 Profiling of liver tissues upon exosomes or CM treatment

Exosomes possess the capability of fusing with the cell membrane, and deliver their biological cargo into the cell (131, 132). Thus, we assume that this is the case for liver tissue (133). Following the results of exosomes treatments in the mouse AHF liver tissues, the next step was to analyze the mechanisms involved.

4.7.1 Inflammation

In order to investigate the effect of treatments on inflammation, gene expression of three crucial cytokines was determined using Real-Time PCR method; proinflammatory IL-1b and IL-6, as well as anti-inflammatory IL-10, the latter being currently under investigation.

Furthermore, hepatoprotective liver resident macrophages, Kupffer cells marker CD68 levels of expression were examined.

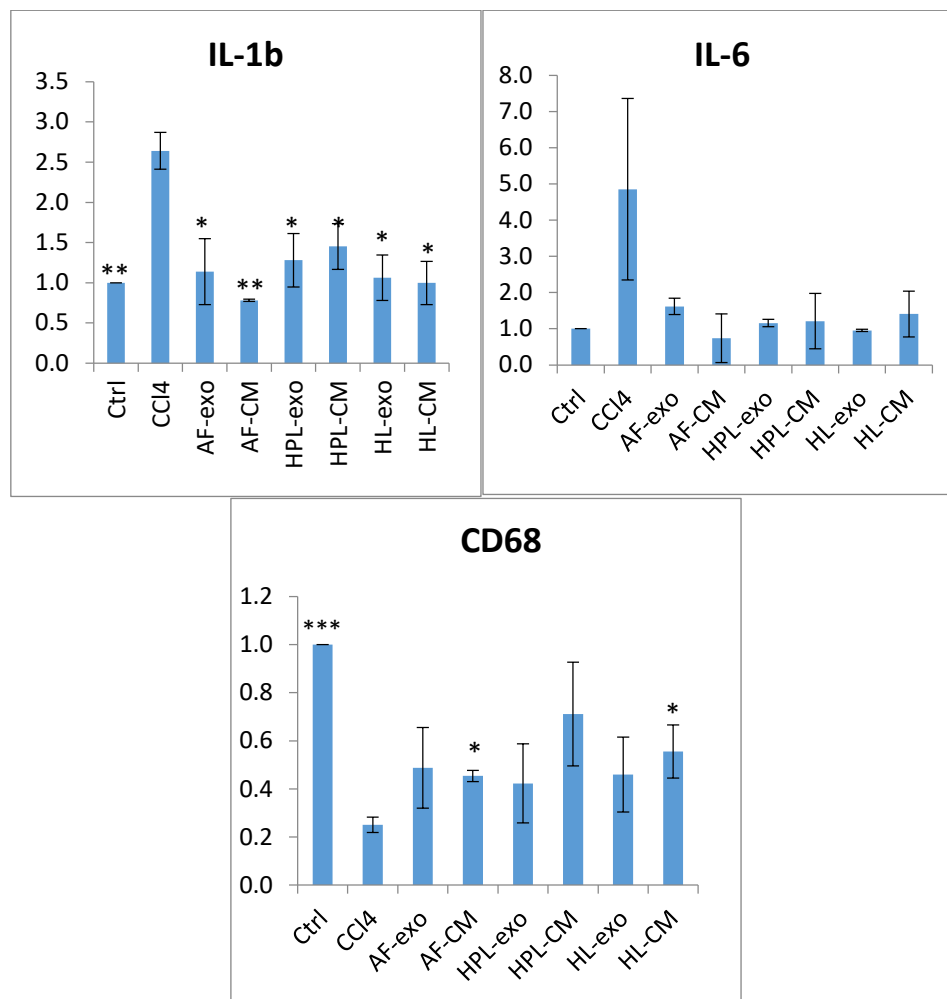


Figure 23: Fold change in expression levels of interleukin-1b (A), interleukin-6 (B) and CD68 (C) compared to healthy animals (ctrl). Bars represent fold change as emerged from average $\Delta\Delta Ct$ [$\Delta Ct(\text{gene}) - \text{average } \Delta Ct(\text{control})$] of all mice per condition. Error bars represent standard error margin (SEM). One-tailed T-test was performed, comparing each condition with CCl4 (stars above each bar). (* stands for $0.01 < p < 0.05$, ** stands for $0.001 < p < 0.01$, *** stands for $p < 0.001$). Number of samples = 3 (IL-1b, CD68), 2 (IL-6)

Both proinflammatory cytokines IL-1b (N=3) (2.64, SEM=0.23, $p=0.001$, ***) and IL-6 (N=2) (4.85, SEM=2.50, $p=0.132$, ns) were sharply increased in AHF mice and upon treatment with exosomes or CM, were reduced to near-healthy levels (**fig. 23A-B**). The reduction of IL-1b expression was statistically significant upon all exosomes treatments, AF-exo (1.13, SEM=0.41, $p=0.037$, *), HPL-exo (1.28, SEM=0.33, $p=0.030$, *), HL-exo (1.06, SEM=0.28, $p=0.015$, *) and upon CM treatments, AF-CM (0.78, SEM=0.01, $p=0.007$, **), HPL-CM (1.45, SEM=0.28, $p=0.030$, *), HL-CM (1.00, SEM=0.27, $p=0.011$, *). IL-6 was also reduced upon exosomes treatments, though the reduction was not statistically significant: AF-exo (1.62, SEM=0.22, $p=0.164$, ns), HPL-exo (1.16, SEM=0.10, $p=0.139$, ns), HL-exo (0.95, SEM=0.03, $p=0.130$, ns), as well as upon CM treatments: AF-CM (0.74, SEM=0.67, $p=0.124$, ns), HPL-CM (1.21, SEM=0.76, $p=0.149$, ns), HL-CM (1.41, SEM=0.63, $p=0.157$, ns). To summarize, the

reduction of gene expression of the pro-inflammatory cytokines IL-1b and IL-6 confirms the anti-inflammatory effect of both exosomes and CM treatments.

Kupffer cells are resident macrophages of the liver tissue, which play a main role in inflammation suppression and clearance of apoptosis and cell debris. CD68 is the main marker of these cells in hepatic tissue. Our results indicated a decrease in CD68 expression levels in AHF animals (0.25, SEM=0.03, $p < 0.001$, ***), while treatments manage to partly restore the healthy levels of expression (fig. 23C), [AF-exo (0.49, SEM=0.17, $p = 0.119$, ns), HPL-exo (0.42, SEM=0.16, $p = 0.182$, ns), HL-exo (0.46, SEM=0.16, $p = 0.129$, ns) and CM: AF-CM (0.45, SEM=0.02, $p = 0.010$, *), HPL-CM (0.71, SEM=0.22, $p = 0.051$, ns), HL-CM (0.55, SEM=0.11, $p = 0.028$, *)]. It is certain, though, that further experiments need to be conducted, in order to safely extract a conclusion about inflammation, however there is a clear tendency of direct effect towards resolution of inflammation upon all treatments.

4.7.2 Apoptosis

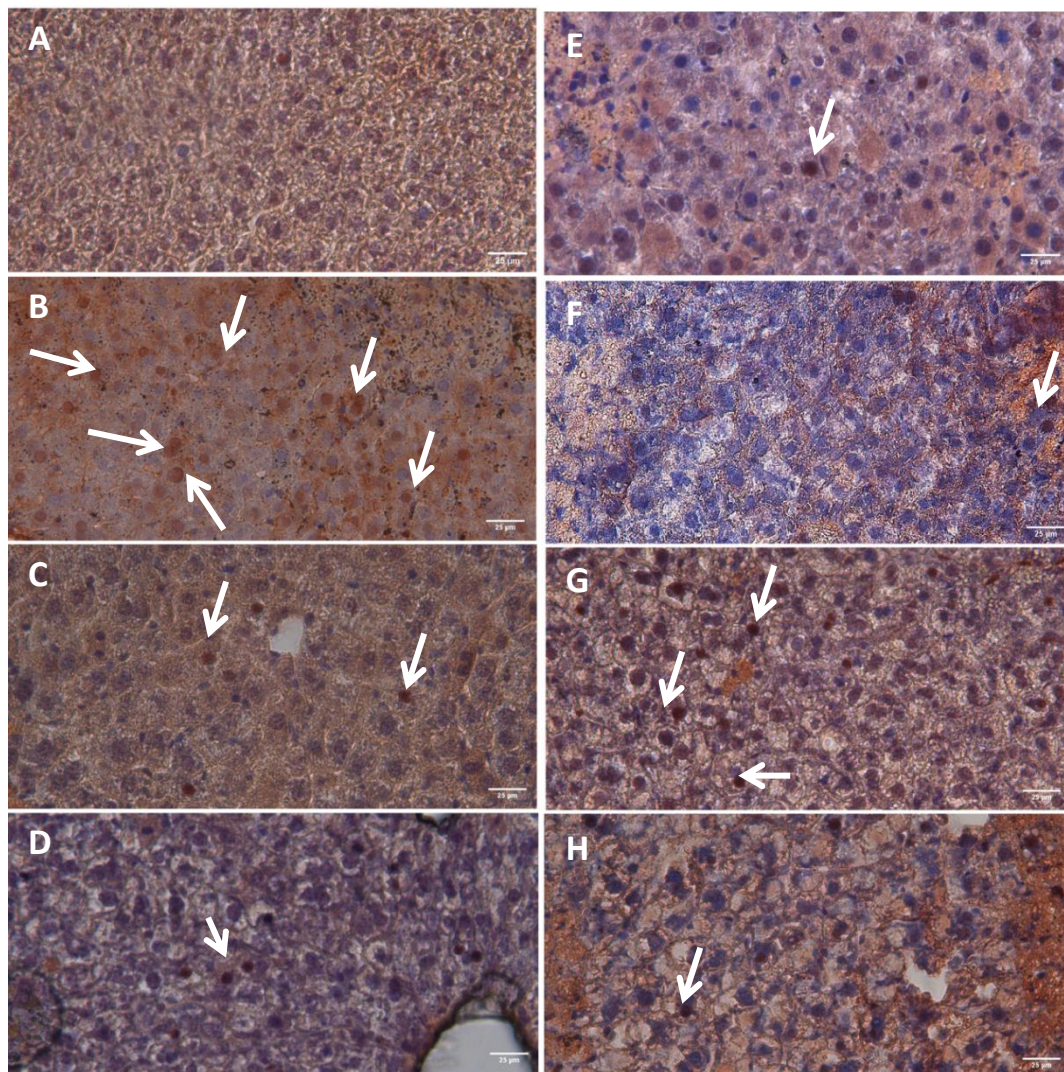


Figure 24: Mouse liver sections stained by TUNEL assay. (A) Healthy, (B) AHF, (C) AF-MSC-CM treated, (D) AF-MSC-exosomes treated, (E) HPL-CM treated, (F) HPL-exosomes treated, (G) HL-CM exosomes, (H) HL-exosome treated. White arrows show areas of apoptosis. Scale: 25 µm.

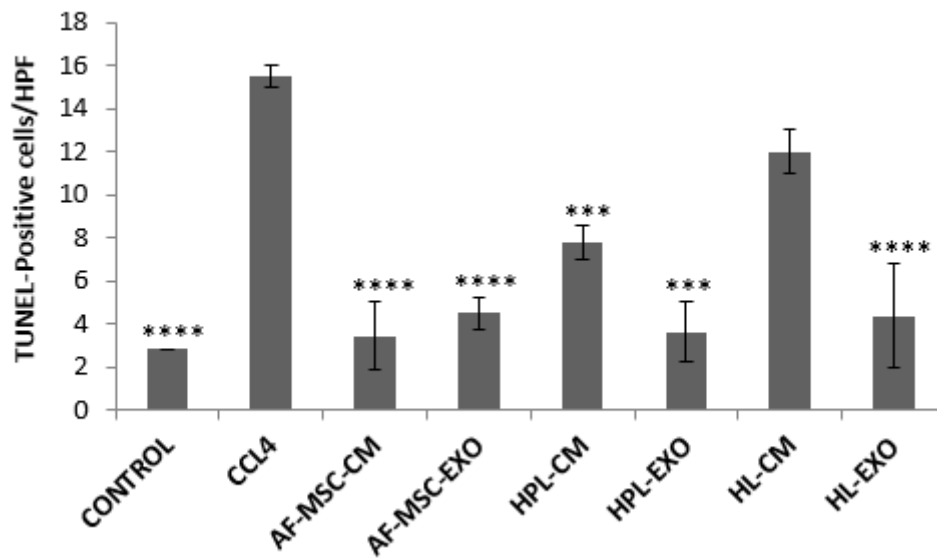


Figure 25: Average apoptotic cell count using TUNEL assay, in all experimental groups. Bars represent average TUNEL-positive cells per HPF. Error bars represent standard error margin (SEM). One-tailed T-test was performed, comparing each condition with CCL4 (stars above each bar). (* stands for $0.01 < p < 0.05$, ** stands for $0.001 < p < 0.01$, *** stands for $0.0001 < p < 0.001$, **** stands for $p < 0.0001$).

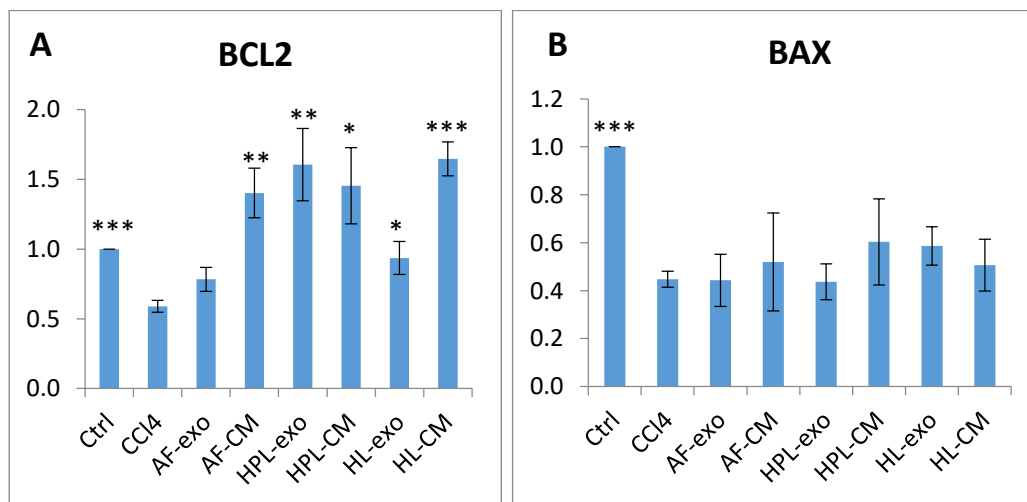
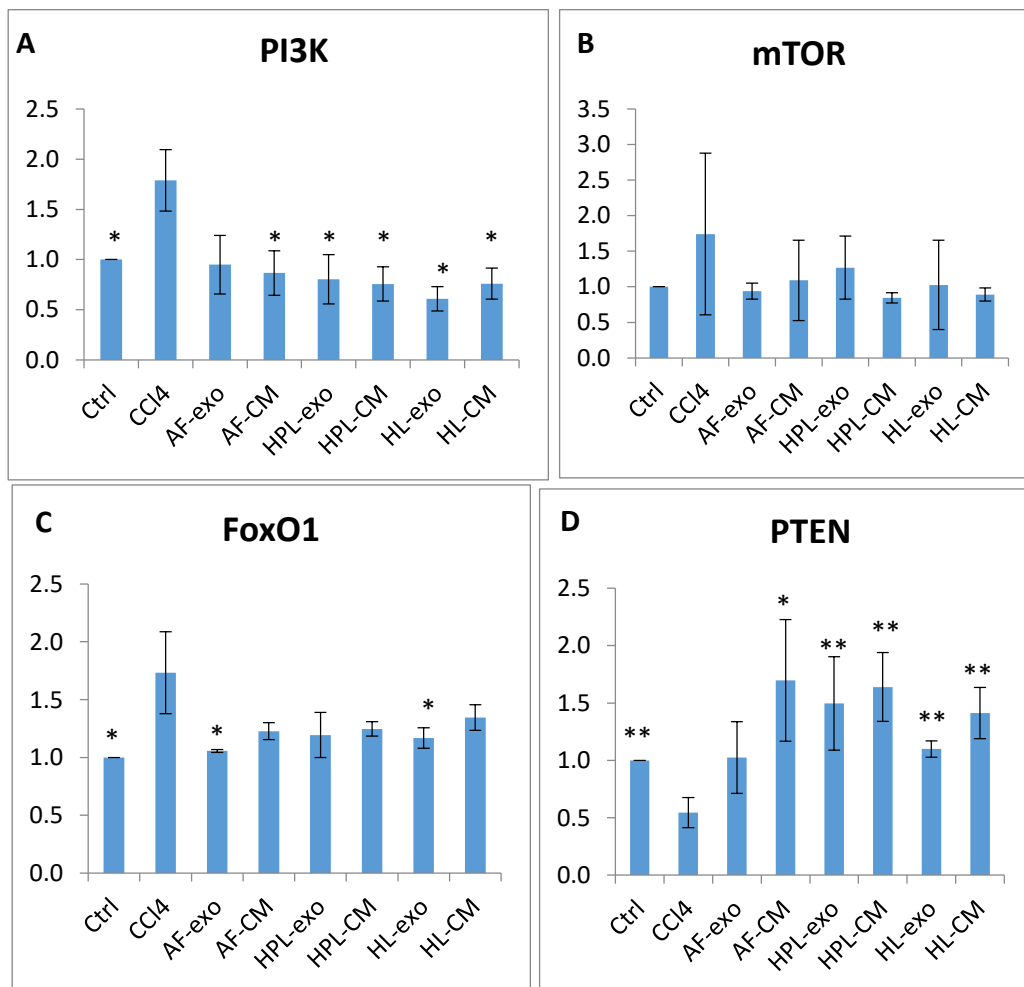


Figure 26: Fold change in expression levels of BCL-2 (left) and BAX (right) compared to healthy animals (ctrl). Bars represent fold change as emerged from average $\Delta\Delta Ct$ ($\Delta Ct(\text{gene}) - \text{average } \Delta Ct(\text{control})$) of all mice per condition. Error bars represent standard error margin (SEM). One-tailed T-test was performed, comparing each condition with CCL4 (stars above each bar). (* stands for $0.01 < p < 0.05$, ** stands for $0.001 < p < 0.01$, *** stands for $p < 0.001$). Number of samples = 3

In order to investigate the effect of the treatments on apoptosis, liver tissues were stained using TUNEL assay, in order to visualize apoptosis-related DNA fragmentation and apoptotic cells. Real-Time PCR was also performed in the liver tissues in order to determine the gene expression of BCL2 and BAX, an anti-apoptotic and pro-apoptotic gene, respectively, in all conditions tested. TUNEL assay detects high intensity of apoptotic cells, associated with apoptosis occurring in AHF in the mouse liver tissue (**fig. 24B**) compared to the healthy

animals (**fig. 24A**), determining apoptotic cell count around 5 times higher in CCL₄ mice than control group (**fig. 25**). The anti-apoptotic gene BCL2 is downregulated upon CCL₄ injection (0.59, SEM=0.04, p=0.000, ***), permitting apoptosis to occur in AHF (**fig. 26A**), confirming TUNEL results. Treatments altered the apoptosis phenotype as determined by TUNEL assay (**fig. 24C-H**), as apoptotic cell count is decreased to healthy levels in a statistically significant degree in all treatments, except HL-CM (**fig. 25**). RT-PCR confirmed TUNEL assay, as we observed upregulation of BCL2 gene expression to healthy levels upon treatments (**fig. 26A**). AF-exo (0.78, SEM=0.09, p=0.058, ns) appeared to be the least effective in BCL2 upregulation, followed by HL-exo (0.94, SEM=0.12, p=0.026, *). Among exosomes, HPL-exo was the most effective (1.61, SEM=0.26, p=0.009, **). CM treatments also showed a promising effect: AF-CM (1.40, SEM=0.18, p=0.006, **), HPL-CM (1.45, SEM=0.27, p=0.017, *), HL-CM (1.64, SEM=0.12, p<0.001, ***). BAX gene expression was also downregulated upon AHF induction (0.45, SEM=0.33, p<0.001, ***), which was not expected, as BAX is a pro-apoptotic gene. Thus, BAX was, posing an issue of its appropriateness in measuring apoptosis (**fig. 26B**). The above results, indicated that AHF-related apoptosis is altered upon exosomes and CM treatments.

4.7.3 PI3K/AKT and ERK pathways



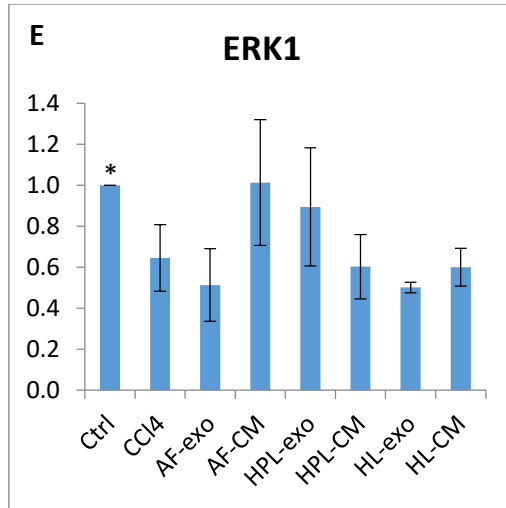
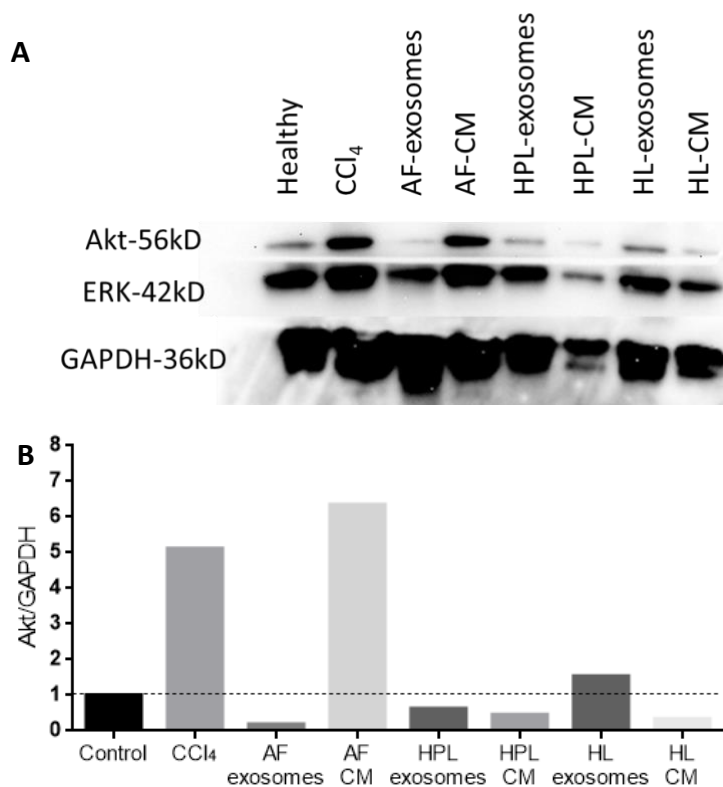
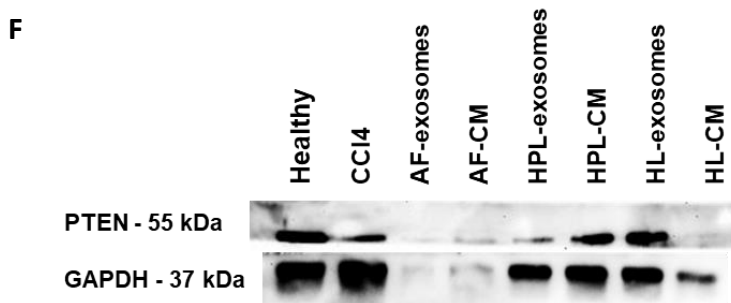
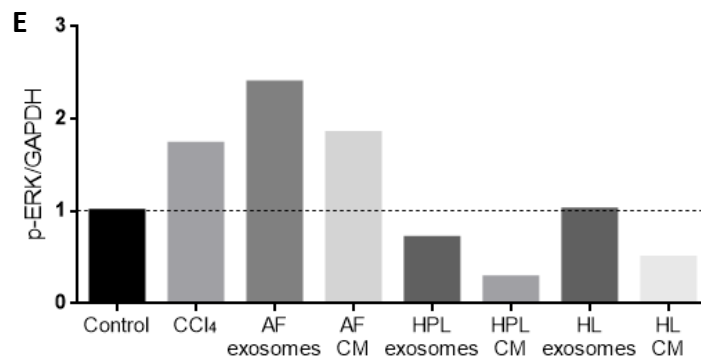
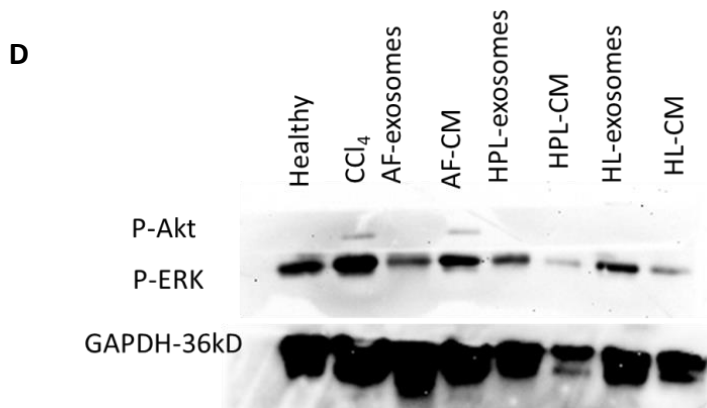
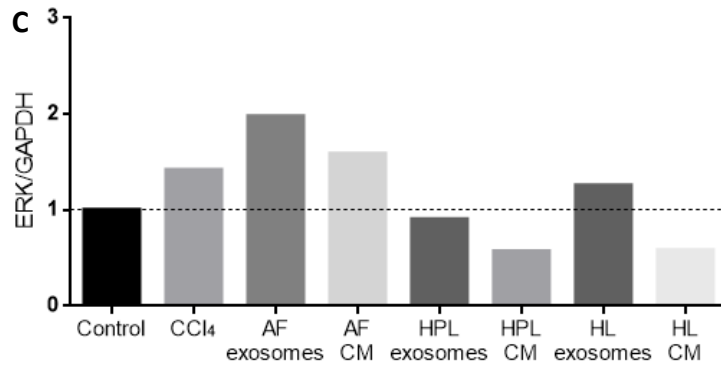


Figure 27: Fold change in expression levels of PI3K (a), mTOR (b), FoxO1 (c), PTEN (d), ERK1 (e) compared to healthy animals (ctrl). Bars represent fold change as emerged from average $\Delta\Delta Ct$ ($\Delta Ct(\text{gene}) - \text{average } \Delta Ct(\text{control})$) of all mice per condition. Error bars represent standard error margin (SEM). One-tailed T-test was performed, comparing each condition with CCl4 (stars above each bar). (* stands for $0.01 < p < 0.05$, ** stands for $0.001 < p < 0.01$, *** stands for $p < 0.001$). Number of samples = 3





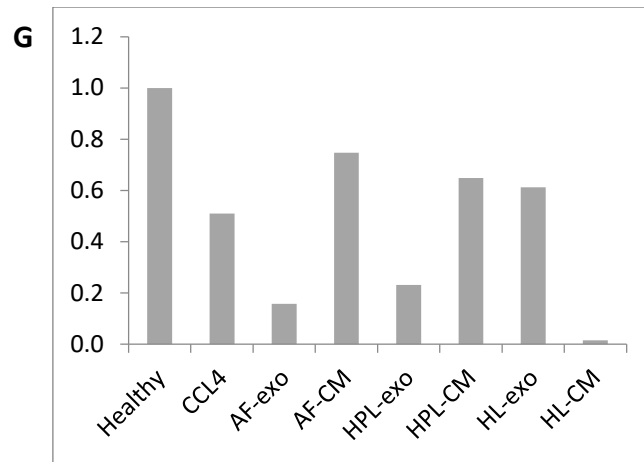


Figure 28: Western blot images of AKT and ERK compared to GAPDH (A) and respective quantification graphs (B-C), pAKT and pERK compared to GAPDH (D) and respective quantification graphs (E), PTEN compared to GAPDH (F) and respective quantification graph (G).

As depicted at the pathway analysis, two of the most significant pathways that the selected proteins in our exosomes samples are PI3K/AKT and MAPK/ERK pathways. MFGE8 and EMILIN1 bind on their receptors, integrin $\alpha v \beta 3$ and integrin $\alpha 4 / \alpha 9 \beta 1$ respectively, stimulating several signaling cascades inside the target cell. Gene expression of a number of components of the pathways is investigated by Real-Time PCR (**fig. 27**), in order to define up-regulation or down-regulation of enzymes and downstream molecules. Levels of specific proteins, as well as inactivated or activated isoforms of kinases are investigated by Western blot (**fig. 28**).

PI3K is the main activator of AKT, which transmits the signal phosphorylating the next molecules. During AHF, PI3K is upregulated (1.79, SEM=0.31, $p=0.021$, *) , while all treatments effectively reduce its levels, both exosomes, AF-exo (0.95, SEM=0.29, $p=0.077$, ns), HPL-exo (0.80, SEM=0.25, $p=0.043$, *), HL-exo (0.61, SEM=0.12, $p=0.012$, *) and CM, AF-CM (0.87, SEM=0.22, $p=0.043$, *), HPL-CM (0.76, SEM=0.25, $p=0.043$, *), HL-CM (0.76, SEM=0.15, $p=0.021$, *) (**fig. 27A**).

mTOR and FoxO1 (**fig. 27B-C**), downstream molecules of PI3K/AKT signaling follow a similar pattern with PI3K, as PI3K might activate the downstream signaling cascade during AHF and deactivate it upon treatments. They are upregulated in AHF (1.74, SEM=1.14, $p=0.222$, ns) and (1.73, SEM=0.35, $p=0.014$, *) respectively. Gene expression of mTOR is restored at near-healthy levels upon exosomes: AF-exo (0.94, SEM=0.11, $p=0.277$, ns), HPL-exo (1.27, SEM=0.44, $p=0.368$, ns), HL-exo (1.03, SEM=0.62, $p=0.318$, ns) or CM: AF-CM (1.09, SEM=0.56, $p=0.329$, ns), HPL-CM (0.84, SEM=0.07, $p=0.256$, ns), HL-CM (0.89, SEM=0.09, $p=0.267$, ns). Gene expression of FoxO1 follows the same trend upon all treatments: AF-exo (1.06, SEM=0.01, $p=0.042$, *), HPL-exo (1.19, SEM=0.19, $p=0.118$, ns), HL-exo (1.17, SEM=0.08, $p=0.046$, *), AF-CM (1.22, SEM=0.07, $p=0.053$, ns), HPL-CM (1.25, SEM=0.06, $p=0.054$, ns), HL-CM (1.34, SEM=0.11, $p=0.115$, ns).

Akt protein levels (**fig. 28A, B**) are also increased in AHF animals, compared to healthy animals, with treatments resulting to the decrease of the expression levels at near to

normal, except from the case of AF-CM. In contrary, pAkt was almost undetected in 2 samples, so currently this experiment is repeated.

PTEN, which represents an inhibitory molecule of the PI3K pathway, was downregulated in the context of AHF (0.54, SEM=0.13, p=0.003, **) compared to healthy animals, as expected. All treatments resulted in the upregulation of the expression of PTEN to healthy levels: AF-exo (1.02, SEM=0.31, p=0.071, ns), HPL-exo (1.49, SEM=0.40, p=0.026, *), HL-exo (1.10, SEM=0.07, p=0.005, **), AF-CM (1.70, SEM=0.53, p=0.029, *), HPL-CM (1.64, SEM=0.30, p=0.008, **), HL-CM (1.42, SEM=0.22, p=0.008, **) (**fig. 27D**). The above results indicated that PTEN might play a key role in this shift. Western blot confirmed the PTEN protein levels in the case of AHF (**fig. 28F, G**) and the upregulation upon , AF-CM, HPL-CM and HL-exo treatments.

ERK1 is one of the key molecules in the MAPK/ERK pathway. Results obtained from Real-Time PCR (**fig. 27E**) demonstrated a decrease of ERK1 gene expression in the context of AHF (0.65, SEM=0.16, p=0.036, *). The only effective treatment resulting the upregulation of the ERK1 expression levels was the AF-CM administration (1.01, SEM=0.30, p=0.149, ns), while the rest do not alter the AHF phenotype: AF-exo (0.51, SEM=0.18, p=0.304, ns), HPL-exo (0.89, SEM=0.29, p=0.228, ns), HL-exo (0.50, SEM=0.03, p=0.244, ns), HPL-CM (0.60, SEM=0.16, p=0.430, ns), HL-CM (0.60, SEM=0.09, p=0.418, ns). Protein expression profile of ERK1 and pERK1, though, exhibited an opposite effect: both molecules are increased during AHF and upon treatments (HPL-exo, HPL-CM, HL-exo, HL-CM) their expression profile is similar to healthy (**fig. 28E, F**). It is certain that further investigation is needed in order to draw conclusions about the role of ERK in the amelioration of AHF.

4.7.4 TGFβ

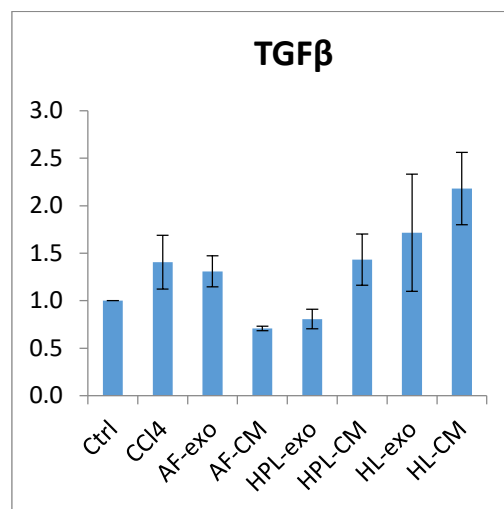


Figure 29: Fold change in expression levels of TGFβ compared to healthy animals (ctrl). Bars represent fold change as emerged from average $\Delta\Delta Ct$ ($\Delta Ct(\text{gene}) - \text{average } \Delta Ct(\text{control})$) of all mice per condition. Error bars represent standard error margin (SEM). One-tailed T-test was performed, comparing each condition with CCl4 (stars above each bar). (* stands for $0.01 < p < 0.05$, ** stands for $0.001 < p < 0.01$, *** stands for $p < 0.001$). Number of samples = 3

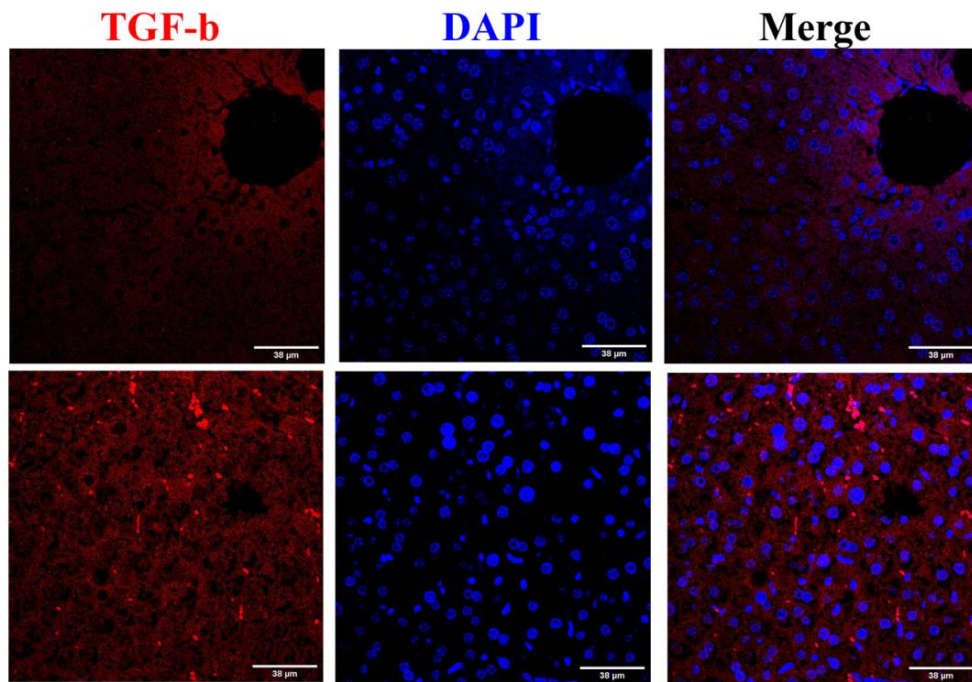


Figure 30: Confocal microscopy images of Control (upper images) and CCl₄ (lower images) mice. Immunofluorescence staining was performed on mouse liver sections using rabbit anti-TGF β and donkey anti-rabbit Alexa Fluor 594 (left images) and DAPI solution (middle images). Merged images are depicted at the right images. Scale 30 μ m.

TGF β is a multifunctional cytokine, which is produced in a latent pro-TGF β form and a proteolysis is essential in order to be activated. The proteolysis has been shown to be inhibited by MFGE8 (134, 135) and EMILIN1 (136), rendering it inactive and blocking the TGF β signaling pathway. Real-Time PCR and immunofluorescence assay were performed in mouse liver tissues as shown in figures 28 and 29.

Gene expression of TGF β is increased upon CCl₄ induction of AHF (1.41, SEM=0.28, p=0.112, ns), though no statistical significance is observed (fig. 29). Upon AF-CM and HPL-exosomes treatments, there is an expected downregulation of TGF β expression levels (0.71, SEM=0.02, p=0.076, ns and 0.81, SEM=0.10, p=0.059, ns), as MFGE8 and EMILIN1 inhibit the cleavage of the pro-TGF β molecule, though, the other treatments do not show the expected results: AF-exo (1.31, SEM=0.16, p=0.391, ns), HL-exo (1.72, SEM=0.62, p=0.336, ns), HPL-CM (1.43, SEM=0.27, p=0.474, ns), HL-CM (2.18, SEM=0.38, p=0.089, ns). Immunofluorescence (fig. 30) confirms the overexpression of TGF β in AHF.

4.7.5 Matrix metalloproteinases (MMPs)

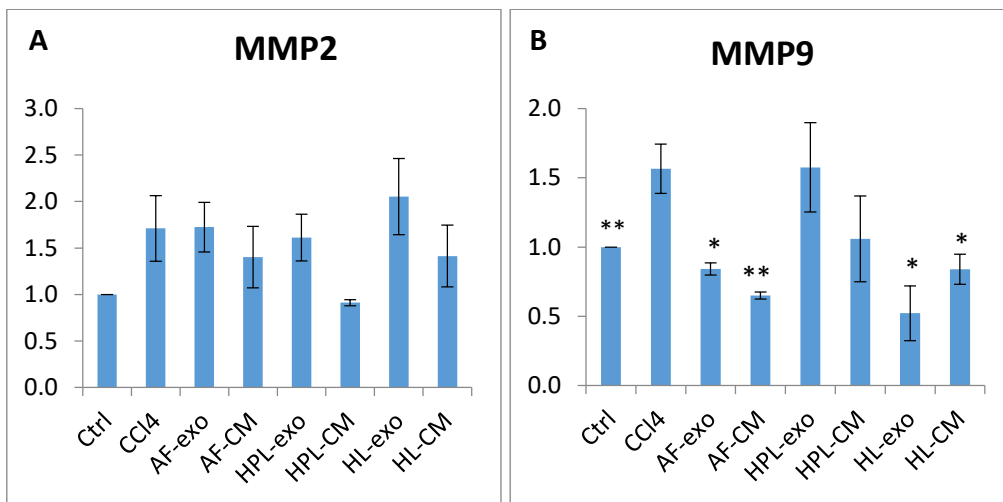
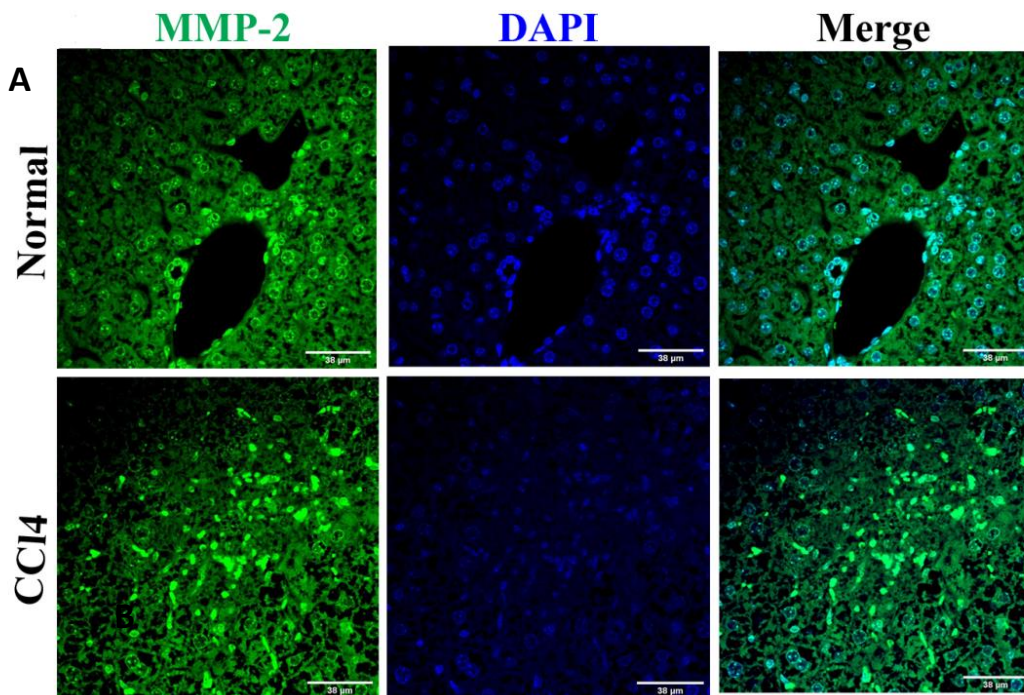


Figure 31: Fold change in expression levels of MMP2 (A) and MMP9 (B) compared to healthy animals (ctrl). Bars represent fold change as emerged from average $\Delta\Delta Ct$ ($\Delta Ct(\text{gene}) - \text{average } \Delta Ct(\text{control})$) of all mice per condition. Error bars represent standard error margin (SEM). One-tailed T-test was performed, comparing each condition with CCl4 (stars above each bar). (* stands for $0.01 < p < 0.05$, ** stands for $0.001 < p < 0.01$, *** stands for $p < 0.001$). Number of samples = 3



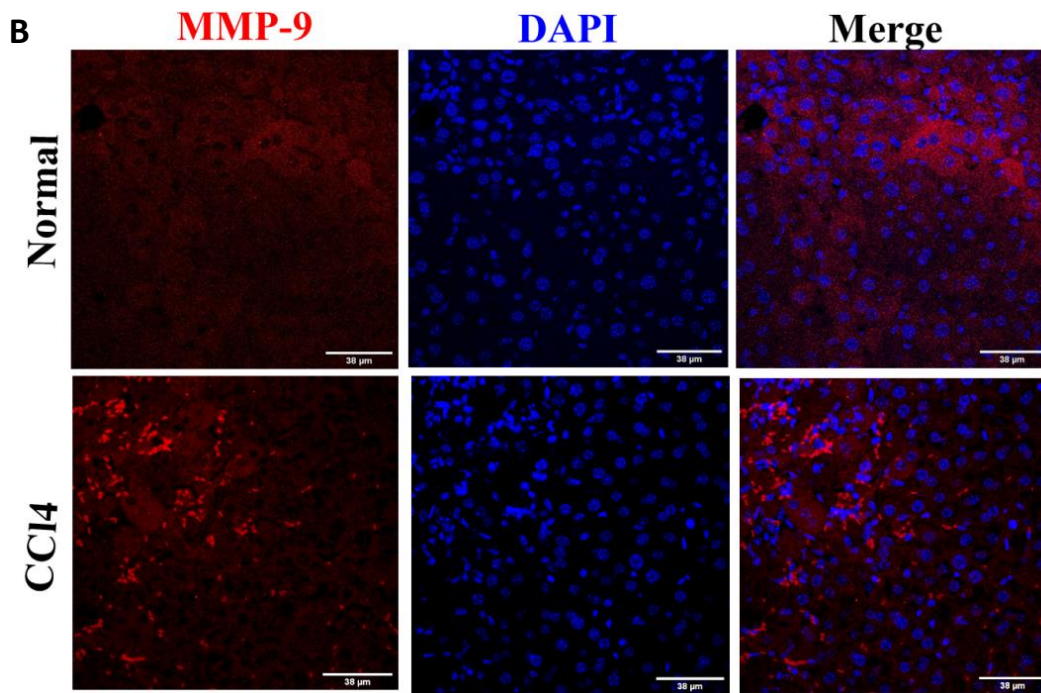


Figure 32: Confocal microscopy images of Control (upper images) and CCl₄ (lower images) mice. Immunofluorescence was performed on mouse liver sections using mouse anti-MMP2 (A, left images) or mouse anti-MMP9, and donkey anti-mouse AlexaFluor 488 (B, left images) and DAPI solution (middle images). Merged images are depicted at the right images. Scale: 30µm.

Matrix metalloproteinases (MMPs) are enzymes, which degrade the ECM proteins, playing a key role in morphogenesis, wound healing, tissue repair and remodeling in response to injury, as well as in the progression of various diseases (137). Liver fibrosis, a basic clinical feature of AHF, is characterized by the imbalance of the main enzymes implicated in the ECM degradation, such as the MMPs and their inhibitors, the tissue inhibitors of metalloproteinases (TIMPs) (138). Activation of HSCs, the main contributors to fibrosis is associated with MMPs upregulation (139). Gene expression levels were determined using Real-Time PCR (fig. 31), and liver sections were stained, in order to visualize the presence of MMP2 and MMP9 (fig. 32).

Gene expression of MMP2 was upregulated during AHF conditions (1.71, SEM=0.35, p=0.058, ns), and this is also shown in the IF figure (fig. 32A). HPL-CM was the only effective treatment that altered the MMP2 levels back to healthy (0.91, SEM=0.03, p=0.090, ns). The rest of the treatments do not exhibit any therapeutic effect: AF-exo (1.73, SEM=0.27, p=0.488, ns), HPL-exo (1.61, SEM=0.25, p=0.416, ns), HL-exo (2.05, SEM=0.41, p=0.281, ns), AF-CM (1.40, SEM=0.33, p=0.278, ns), HL-CM (1.41, SEM=0.33, p=0.286, ns) (fig. 31A).

MMP9 was upregulated in a statistically significant manner during AHF condition (1.56, SEM=0.18, p=0.006, **), shown also in IF images (fig. 32B). Most treatments resulted in healthy levels of MMP9 gene expression: AF-exo (0.84, SEM=0.04, p=0.026, *), HL-exo (0.52, SEM=0.20, p=0.016, *), AF-CM (0.65, SEM=0.02, p=0.004, **), HPL-CM (1.06, SEM=0.31, p=0.114, ns), HL-CM (0.84, SEM=0.11, p=0.013, *). HPL-exo (1.58, SEM=0.32, p=0.487, ns) did not exhibit any efficacy (fig. 31B).

Both gene expression and immunofluorescence confirmed the upregulation of MMP2 and MMP9 in CCl4-induced AHF mice as expected. Several treatments are also assessed as effective in reversing this upregulation, though, further investigation is required in order to safely assess MMP2 and MMP9 protein profile upon treatments.

4.7.6 VEGFA

MFGE8 clearance of inflammation is potentially linked to induction of vascular endothelial growth factor A (VEGFA) (140) which is a critical mediator protein, inducing angiogenesis, vasculogenesis, tissue damage repair and inhibiting apoptosis, so VEGFA was thought to be an important factor to be assessed, as we would expect an upregulation upon treatments. Real-Time PCR (fig. 33) was performed to detect gene expression. Gene expression of VEGFA was only slightly downregulated during AHF (0.84, SEM=0.14, p=0.156, ns), and reached healthy levels upon AF-exosome treatment (1.38, SEM=0.21, p=0.049, *). The rest of the treatments did not exhibit any significant efficacy: HPL-exo (0.92, SEM=0.28, p=0.392, ns), HL-exo (0.97, SEM=0.08, p=0.226, ns), AF-CM (0.89, SEM=0.07, p=0.383, ns), HPL-CM (1.03, SEM=0.01, p=0.117, ns), HL-CM (0.85, SEM=0.16, p=0.479, ns). No clear tendency was observed, so experimental procedures are currently ongoing.

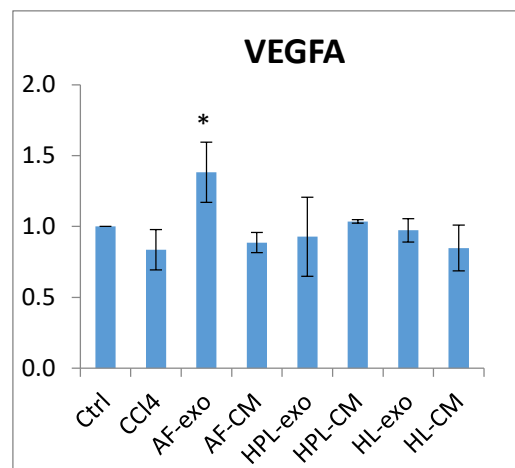


Figure 33: Fold change in expression levels of VEGFA compared to healthy animals (ctrl). Bars represent fold change as emerged from average $\Delta\Delta Ct$ ($\Delta Ct(\text{gene}) - \text{average } \Delta Ct(\text{control})$) of all mice per condition. Error bars represent standard error margin (SEM). One-tailed T-test was performed, comparing each condition with CCl4 (stars above each bar). (* stands for $0.01 < p < 0.05$, ** stands for $0.001 < p < 0.01$, *** stands for $p < 0.001$). Number of samples = 3

4.8 Evaluation of MFGE8 effectiveness against AHF by administration of exogenous rMFGE8 in an *in vivo* mouse model

MFGE8 was found as one of the most significant proteins in the exosomes cargo of AF-MSCs, HPL and HL cells. In order to examine its direct role in the clinical phenotype of AHF, we administered exogenous recombinant MFGE8 protein (rMFGE8) in our *in vivo* model of CCl4-induced AHF mouse model. 15 of a total of 22 (experimental group) Rag1^{-/-} mice were initially injected intraperitoneally with CCl₄ contained in sun oil, in order to induce AHF

phenotype, and control group Rag1^{-/-} mice were injected with PBS in sun oil. The day after, 4 out of the 15 AHF mice (rMFGE8-treated group) were administered 6.5µg of rMFGE8 in PBS per mouse, while the remaining 11 (CCl₄ group) with PBS (see section 3.3.1, Table 4). The third day, mice were sacrificed, blood samples were collected from all of the mice tested, and SGOT and SGPT transaminase levels were measured, in order to determine the levels of liver damage in each condition (fig. 34).

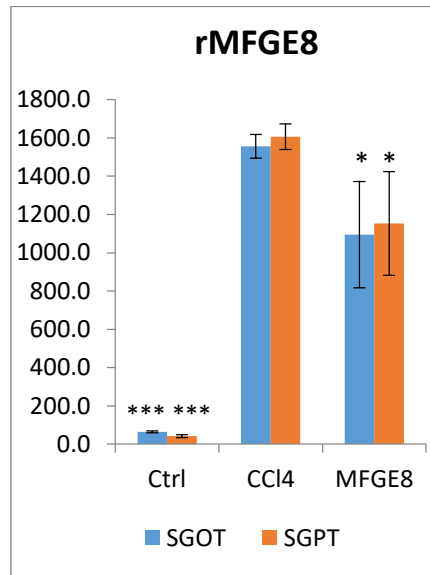


Figure 34: SGOT (blue bars) and SGPT (orange bars) transaminase levels (units/mL) average values and standard error (SEM) bars in each condition: healthy and AHF (CCl₄) animals compared with exogenous rMFGE8. One-tailed T-test was performed, comparing MFGE8-treated mice and control mice with CCl₄ (stars above each bar). (* stands for 0.01<p<0.05, ** stands for 0.001<p<0.01, *** stands for p<0.001).

Tansaminases (SGOT: 1556.8, SEM=61.5, SGPT: 1606.4, SEM=67.3) levels in AHF mice were elevated versus the control mice (SGOT: 64.4, SEM=5.5, p<0.001, ***, SGPT: 42.1, SEM=7.5, p<0.001, ***). Administration of the exogenous recombinant MFGE8 decreased the transaminase levels (SGOT: 1094.3, SEM=277.3, p=0.014, *, SGPT: 1153.8, SEM=271.3, p=0.017, *). This indicated an amelioration of the clinical phenotype, proving that MFGE8 is effective in decreasing transaminase levels. This is the first step of a series of experiments on MFGE8-treated mice that are currently on going in our laboratory, in order to evaluate the effect of MFGE8 on the cell signaling pathways and to compare with the exosomes and CM effects.

5. Discussion

Acute Hepatic Failure (AHF) is a deadly clinical syndrome, which overrides the innate ability of the liver to regenerate, resulting in massive and rapid inflammation, cell apoptosis and necrosis of the liver tissue. Exosomes derived from AF-MSCs, as well as from their hepatic derivatives (HPL and HL cells) are considered to be a novel promising tool against AHF, as they are capable of acting as mediators, reversing the clinical phenotype of AHF. The exact mechanism of this process is largely unknown (**141, 142**).

AF-MSCs exhibit significant advantages against alternative stem cells, including their differentiation potential, absence of ethical issues and low immunogenicity (**78-80**). They were cultured and differentiated into HPL and HL cells, and both the exosomes and the conditioned medium (CM) were isolated and administered to CCl₄-induced AHF mice (**44, 45, 111, 112, 143, 144**). Upon biochemical analysis, SGOT and SGPT transaminases levels were identified in the murine blood serum. MSCs have been evaluated in several clinical trials against liver disease, though there are no clinical results of MSC-exosomes administration in liver diseases, while there is currently a number of trials using exosomes ongoing (**145, 146**). In a previous research of our laboratory, CM derived from AF-MSCs, HPL and HL cells were proved to be effective in reversing the AHF clinical phenotype, reducing the transaminase levels of the murine livers (**111**). Combining the importance of MSC secretome against AHF and the emerging importance of exosomes in the context of therapy against liver disease, our study investigates a novel, emerging and potentially significant therapy against AHF. In this study, we showed that exosomes, when administered intrahepatically, upon targeting the liver tissue and deploying their cargo into the cells, they cause a significant improvement of clinical image, vastly reducing SGOT and SGPT transaminase levels and improving the hepatic histological image. Moreover, exosomes alone reduce transaminases significantly more than their control (secretome excluding exosomes), underlining the crucial role they potentially have in ameliorating the clinical image.

Proteomic analysis of AF-MSC, HPL and HL cell-derived exosomes revealed a huge number of proteins as their cargo, such as several anti-inflammatory proteins, TGF β -related proteins, collagens, keratins and matrix metalloproteinases (MMPs). We already know that disruption of MMPs and TIMPs balance plays a key role in the progression of AHF, and its restoration is accompanied with amelioration of AHF (**147**). Furthermore, collagens and keratins, as ECM components, are related to the severity of cirrhosis and liver failure in conditions like hepatocellular carcinoma (**148**) and play a key role in the development of liver fibrosis in AHF models (**149**). Since the role of most of the proteins included in our exosomes are known in the context of liver disease, we are able to hypothesize about how these sets of molecules could act into the liver cells and which mechanisms they exploit to affect the phenotype.

From the proteins detected in our exosomes, six of them were observed as abundant and at the same time their difference of expression among the three cell types was found to be statistically significant, including components of complement, TGF β -induced gene ig-h3,

MFGE8 and EMILIN1. The latter two are known for their anti-inflammatory, anti-apoptotic, anti-fibrotic and pro-proliferative properties. Using bioinformatics tools, such as Cytoscape and ClueGO, ECM-related pathways, IGF/IGFBP signaling and IL4/IL13 inflammatory pathway were among the most enriched pathways derived from these proteins. Annexin-A1, a significant component of the therapeutic effect, as proved in previous studies on our laboratory (112), is involved in the IL4/IL13 pathway, while MFGE8 is involved in the IGF/IGFBPs axis, according to pathway analysis. MMPs/TIMPs system seems also important, as MMP2 and its inhibitor, TIMP1, are common in all of the three enriched pathways.

MFGE8 binds to its integrin receptor on the cell membrane, integrin $\alpha\beta3$, and this leads to a cascade of intracellular signaling pathways which are able to alter the proliferative, metabolic, communication, inflammatory functions of the target cells, alleviating disease phenotypes, inflammation and apoptosis (150). We sought to find the most common downstream pathways that are affected upon MFGE8-induced activation of integrins. PI3K/AKT and ERK pathways were among the most common, and we focused on investigating whether these pathways are up- or down-regulated during AHF and upon treatments.

Inflammation during AHF is observed by the significantly elevated levels of IL-1b and IL-6. Suppression of inflammation and clearance of cell debris and apoptotic bodies is crucial for the maintenance of liver homeostasis, which is severely impaired during AHF. Kupffer cells play a main role on this process, as under normal conditions, dying cells are specifically recognized by phagocytes and are engulfed, in a procedure called “efferocytosis”, though during liver injury this process is disrupted (151, 152). In our results, CD68 marker (which is expressed in Kupffer cells) is partly increased and restored to near-healthy levels, following a significant decrease observed in AHF. MFGE8, an important protein of the exosomes, is crucial in the development of efferocytosis, as its two sub-domains form a bridge between phagocytic cells, like Kupffer cells, and apoptotic cells, facilitating the engulfment of the latter (153, 154). MFGE8-inclusive exosomes manage to increase the expression of the CD68 marker and, at the same time, they suppress apoptosis and inflammation, which might be the results of the process of efferocytosis, including the severe decrease of the interleukin levels upon treatments, indicating that inflammation resolution might be driven by inhibiting IL-1b and IL-6.

Analysis of the liver tissue gene expression profile, as well as determination of protein levels and visualization of specific effectors of our desired pathways, indicates that upon AHF induction, the whole PI3K/AKT/mTOR pathway is upregulated. This might play a role in the favouring of the inflammation of the liver, and in combination with the inhibition of BCL2 by the pathway, in the induction of apoptosis. All treatments induced PTEN expression, an inhibitory molecule which inactivates PI3K and as a result, the whole pathway is downregulated to the healthy levels. PTEN expression might need more investigation, such as mutating it or blocking it in specific liver cells, in order to assess whether this is the main mediator of the downregulation observed upon treatments or not. MAPK/ERK pathway, on the other hand, does not show any notable effect, at least in our preliminary experiments, though more experimental procedures are needed to draw a conclusion.

MMPs/TIMPs balance is very important for maintaining liver homeostasis, and when this is dysregulated, it can lead to HSCs activation, fibrosis and severe liver damage. MMP2 and MMP9, as well as TIMP1 were found during pathway analysis as common in three of the main pathways that our selected proteins were involved. Both MMP2 and MMP9 are upregulated in AHF, as pro-fibrotic HSCs are activated and MMPs mediate the progression of AHF-related fibrotic phenotype, though only a few treatments were able to reverse this. TGF β , a multi-functional cytokine, followed the same trend, being upregulated during AHF and only some treatments partially downregulating it.

The observations we acquired, led us to a tendency of a clear therapeutic benefit of the exosomes against AHF. As proteomic analysis highlighted a number of proteins which are enriched in exosomes and show some significant characteristics, these proteins should be examined for their ability and for their necessity in reversing AHF phenotype. To assess their ability, an experimental set up has begun, administering an exogenous peptide of recombinant MFGE8 in AHF mice, resulting in a statistically significant reduction of AHF phenotype, although not so strong as when exosomes are administered. This has to be confirmed with more experiments. To examine necessity, a lentiviral vector is being constructed expressing siRNA which silences MFGE8 gene in AF-MSCs. Upon confirmation of MFGE8 k/o exosomes, these could be administered in AHF mice, to compare their therapeutic effect with or without MFGE8. Apart from these, several experiments are necessary to be performed in order to clarify the exact series of the events behind PTEN/PI3K/AKT/mTOR regulation, as well as to examine more the Kupffer cell hypothesis and the overall inflammatory microenvironment of each condition, by performing FACS analysis. Furthermore, the investigation of the role that EMILIN1 plays in the intrinsic pathways of the hepatic cells, upon its administration via exosomes or alone, involving a similar experimental setup as the performed MFGE8 experiments.

6. Bibliography

1. Trefts, E., Gannon, M., Wasserman, D. H., & Author, C. B. (2018). The liver HHS Public Access Author manuscript. <https://doi.org/10.1016/j.cub.2017.09.019>
2. Abdel-Misih, S. R. Z., Bloomston, M., & Bismuth, H. (2010). Liver Anatomy. <https://doi.org/10.1016/j.suc.2010.04.017>
3. Kruepunga, N., Hakvoort, T. B. M., Hikspoors, J. P. J. M., Köhler, S. E., & Lamers, W. H. (2019). Anatomy of rodent and human livers: What are the differences? In *Biochimica et Biophysica Acta - Molecular Basis of Disease* (Vol. 1865, Issue 5, pp. 869–878). Elsevier B.V. <https://doi.org/10.1016/j.bbadis.2018.05.019>
4. Ben-Moshe, S., & Itzkovitz, S. (2019). Spatial heterogeneity in the mammalian liver. In *Nature Reviews Gastroenterology and Hepatology* (Vol. 16, Issue 7, pp. 395–410). Nature Publishing Group. <https://doi.org/10.1038/s41575-019-0134-x>
5. Wang, H., Liang, X., Gravot, G., Thorling, C. A., Crawford, D. H. G., Xu, Z. P., Liu, X., & Roberts, M. S. (2016). Visualizing liver anatomy, physiology and pharmacology using multiphoton microscopy. <https://doi.org/10.1002/jbio.201600083>
6. Juza RM, Pauli EM. Clinical and surgical anatomy of the liver: a review for clinicians. *Clin Anat*. 2014;27(5):764-769. doi:10.1002/ca.22350
7. Tu T, Calabro SR, Lee A, et al. Hepatocytes in liver injury: Victim, bystander, or accomplice in progressive fibrosis?. *J Gastroenterol Hepatol*. 2015;30(12):1696-1704. doi:10.1111/jgh.13065
8. Slevin E, Baiocchi L, Wu N, et al. Kupffer Cells: Inflammation Pathways and Cell-Cell Interactions in Alcohol-Associated Liver Disease. *Am J Pathol*. 2020;190(11):2185-2193. doi:10.1016/j.ajpath.2020.08.014
9. MacParland SA, Liu JC, Ma XZ, et al. Single cell RNA sequencing of human liver reveals distinct intrahepatic macrophage populations. *Nat Commun*. 2018;9(1):4383. Published 2018 Oct 22. doi:10.1038/s41467-018-06318-7
10. Khomich O, Ivanov AV, Bartosch B. Metabolic Hallmarks of Hepatic Stellate Cells in Liver Fibrosis. *Cells*. 2019;9(1):24. Published 2019 Dec 20. doi:10.3390/cells9010024
11. Pan T, Chen Y, Zhuang Y, et al. Synergistic modulation of signaling pathways to expand and maintain the bipotency of human hepatoblasts. *Stem Cell Res Ther*. 2019;10(1):364. Published 2019 Dec 2. doi:10.1186/s13287-019-1463-y
12. Yang L, Wang WH, Qiu WL, Guo Z, Bi E, Xu CR. A single-cell transcriptomic analysis reveals precise pathways and regulatory mechanisms underlying hepatoblast differentiation. *Hepatology*. 2017;66(5):1387-1401. doi:10.1002/hep.29353
13. Michalopoulos, G. K., & Bhushan, B. (2021). Liver regeneration: biological and pathological mechanisms and implications. In *Nature Reviews Gastroenterology and Hepatology* (Vol. 18, Issue 1, pp. 40–55). Nature Research. <https://doi.org/10.1038/s41575-020-0342-4>
14. Haga, S., Ogawa, W., Inoue, H., Terui, K., Ogino, T., Igarashi, R., Takeda, K., Akira, S., Enosawa, S., Furukawa, H., Todo, S., & Ozaki, M. (2005). Compensatory recovery of liver mass by Akt-mediated hepatocellular hypertrophy in liver-specific STAT3-deficient mice. *Journal of Hepatology*, 43(5), 799–807. <https://doi.org/10.1016/j.jhep.2005.03.027>
15. Tao, Y., Wang, M., Chen, E., & Tang, H. (2017). Liver Regeneration: Analysis of the Main Relevant Signaling Molecules. In *Mediators of Inflammation* (Vol. 2017). Hindawi Limited. <https://doi.org/10.1155/2017/4256352>
16. Min, J. S., DeAngelis, R. A., Reis, E. S., Gupta, S., Maurya, M. R., Evans, C., Das, A., Burant, C., Lambris, J. D., & Subramaniam, S. (2016). Systems Analysis of the Complement-Induced Priming Phase of Liver Regeneration. *The Journal of Immunology*, 197(6), 2500–2508. <https://doi.org/10.4049/jimmunol.1600628>
17. Michalopoulos, G. K. (2010). Liver regeneration after partial hepatectomy: Critical analysis of mechanistic dilemmas. *American Journal of Pathology*, 176(1), 2–13. <https://doi.org/10.2353/ajpath.2010.090675>

18. Huck, I., Gunewardena, S., Espanol-Suner, R., Willenbring, H., & Apte, U. (2019). Hepatocyte Nuclear Factor 4 Alpha Activation Is Essential for Termination of Liver Regeneration in Mice. *Hepatology*, 70(2), 666–681. <https://doi.org/10.1002/hep.30405>
19. Yang, D., Dai, Z., Yang, T., Balakrishnan, A., Yuan, Q., Vondran, F. W. R., Manns, M. P., Ott, M., Cantz, T., & Sharma, A. D. (2020). MicroRNA-125b-5p Regulates Hepatocyte Proliferation During the Termination Phase of Liver Regeneration. *Hepatology Communications*, 4(12), 1851–1863. <https://doi.org/10.1002/hep4.1597>
20. Hussey, H. H. (1973). Fulminant hepatic failure. In *Journal of the American Medical Association* (Vol. 226, Issue 10, p. 1227). <https://doi.org/10.1001/jama.226.10.1227>
21. Dong, V., Nanchal, R., & Karvellas, C. J. (2020). Pathophysiology of Acute Liver Failure. In *Nutrition in Clinical Practice* (Vol. 35, Issue 1, pp. 24–29). John Wiley and Sons Inc. <https://doi.org/10.1002/ncp.10459>
22. Grek, A., & Arasi, L. (2016). Acute liver failure. *AACN Advanced Critical Care*, 27(4), 420–429. <https://doi.org/10.4037/aacnacc2016324>
23. EASL Clinical Practical Guidelines on the management of acute (fulminant) liver failure. (2017). *Journal of Hepatology*, 66(5), 1047–1081. <https://doi.org/10.1016/j.jhep.2016.12.003>
24. Krawitz, S., Lingiah, V., & Pysopoulos, N. T. (2018). Acute Liver Failure: Mechanisms of Disease and Multisystemic Involvement. In *Clinics in Liver Disease* (Vol. 22, Issue 2, pp. 243–256). W.B. Saunders. <https://doi.org/10.1016/j.cld.2018.01.002>
25. Fyfe, B., Zalana, F., & Liu, C. (2018). The Pathology of Acute Liver Failure. In *Clinics in Liver Disease* (Vol. 22, Issue 2, pp. 257–268). W.B. Saunders. <https://doi.org/10.1016/j.cld.2018.01.003>
26. Rolando, N., Wade, J., Davalos, M., Wendon, J., Philpott-Howard, J., & Williams, R. (2000). The systemic inflammatory response syndrome in acute liver failure. *Hepatology*, 32(4 I), 734–739. <https://doi.org/10.1053/jhep.2000.17687>
27. Wu Z, Han M, Chen T, Yan W, Ning Q. Acute liver failure: mechanisms of immune-mediated liver injury. *Liver Int.* 2010;30(6):782-794. doi:10.1111/j.1478-3231.2010.02262.x
28. Montrieff T, Koyfman A, Long B. Acute liver failure: A review for emergency physicians. *Am J Emerg Med.* 2019;37(2):329-337. doi:10.1016/j.ajem.2018.10.032
29. Lee WC, Chou HS, Wu TJ, Lee CS, Lee CF, Chan KM. Indicators and outcome of liver transplantation in acute liver decompensation after flares of hepatitis B. *J Viral Hepat.* 2011;18(3):193-199. doi:10.1111/j.1365-2893.2010.01295.x
30. Jaeschke, H. (2015). Acetaminophen: Dose-Dependent Drug Hepatotoxicity and Acute Liver Failure in Patients. *Digestive Diseases*, 33(4), 464–471. <https://doi.org/10.1159/000374090>
31. Katarey, D., & Verma, S. (2016). Drug-induced liver injury. In *Clinical medicine (London, England)* (Vol. 16, Issue Suppl 6, pp. s104–s109). Clin Med (Lond). <https://doi.org/10.7861/clinmedicine.16-6-s104>
32. Stravitz, R. T., & Lee, W. M. (2019). Acute liver failure. In *The Lancet* (Vol. 394, Issue 10201, pp. 869–881). Lancet Publishing Group. [https://doi.org/10.1016/S0140-6736\(19\)31894-X](https://doi.org/10.1016/S0140-6736(19)31894-X)
33. Yong L, Guang B, Yan L. Bioinformatic analysis of differentially expressed genes involved in the hepatitis B virus-associated acute liver failure. *Acta Gastroenterol Belg.* 2018;81(2):288-294.
34. Sedhom, D., D'Souza, M., John, E., & Rustgi, V. (2018). Viral Hepatitis and Acute Liver Failure: Still a Problem. In *Clinics in Liver Disease* (Vol. 22, Issue 2, pp. 289–300). W.B. Saunders. <https://doi.org/10.1016/j.cld.2018.01.005>
35. Mendizabal, M., & Silva, M. O. (2016). Liver transplantation in acute liver failure: A challenging scenario. In *World journal of gastroenterology* (Vol. 22, Issue 4, pp. 1523–1531). Baishideng Publishing Group Inc. <https://doi.org/10.3748/wjg.v22.i4.1523>
36. Messina, A., Luce, E., Hussein, M., & Dubart-Kupperschmitt, A. (2020). Pluripotent-Stem-Cell-Derived Hepatic Cells: Hepatocytes and Organoids for Liver Therapy and Regeneration. In *Cells* (Vol. 9, Issue 2). NLM (Medline). <https://doi.org/10.3390/cells9020420>
37. Adam, R., Karam, V., Cailliez, V., O Grady, J. G., Mirza, D., Cherqui, D., Klempnauer, J., Salizzoni, M., Pratschke, J., Jamieson, N., Hidalgo, E., Paul, A., Andujar, R. L., Lerut, J., Fisher, L., Boudjema, K., Fonddevila, C., Soubrane, O., Bachellier, P., ... Duvoux, C. (2018). 2018 Annual Report of the European Liver Transplant Registry (ELTR) – 50-year evolution of liver transplantation. *Transplant International*, 31(12), 1293–1317. <https://doi.org/10.1111/tri.13358>

38. Meirelles Júnior, R. F. erreir., Salvalaggio, P., Rezende, M. B. run. de, Evangelista, A. S., Guardia, B. D. ell., Matielo, C. E. duard. L., Neves, D. B. asto., Pandullo, F. L. ui., Felga, G. E. duard. G., Alves, J. A. ndr. da S., Curvelo, L. A. mori., Diaz, L. G. ustav. G., Rusi, M. B. alb., Viveiros, M. de M., Almeida, M. D. ia. de, Pedroso, P. T. un., Rocco, R. A. ndre., & Meira Filho, S. P. (2015). Liver transplantation: history, outcomes and perspectives. *Einstein* (São Paulo, Brazil), 13(1), 149–152. <https://doi.org/10.1590/S1679-45082015RW3164>
39. Larsen, F. S. (2019). Artificial liver support in acute and acute-on-chronic liver failure. In *Current Opinion in Critical Care* (Vol. 25, Issue 2, pp. 187–191). Lippincott Williams and Wilkins. <https://doi.org/10.1097/MCC.0000000000000584>
40. Thompson, J., Jones, N., Al-Khafaji, A., Malik, S., Reich, D., Munoz, S., MacNicholas, R., Hassanein, T., Teperman, L., Stein, L., Duarte-Rojo, A., Malik, R., Adhami, T., Asrani, S., Shah, N., Gaglio, P., Duddempudi, A., Borg, B., Jalan, R., ... Subramanian, R. (2018). Extracorporeal cellular therapy (ELAD) in severe alcoholic hepatitis: A multinational, prospective, controlled, randomized trial. *Liver Transplantation*, 24(3), 380–393. <https://doi.org/10.1002/lt.24986>
41. Thompson, J., Jones, N., Al-Khafaji, A., Malik, S., Reich, D., Munoz, S., MacNicholas, R., Hassanein, T., Teperman, L., Stein, L., Duarte-Rojo, A., Malik, R., Adhami, T., Asrani, S., Shah, N., Gaglio, P., Duddempudi, A., Borg, B., Jalan, R., ... Subramanian, R. (2018). Extracorporeal cellular therapy (ELAD) in severe alcoholic hepatitis: A multinational, prospective, controlled, randomized trial. *Liver Transplantation*, 24(3), 380–393. <https://doi.org/10.1002/lt.24986>
42. Terblanche, J., & Hickman, R. (1991). Animal models of fulminant hepatic failure. *Digestive Diseases and Sciences*, 36(6), 770–774. <https://doi.org/10.1007/BF01311235>
43. Liu, L., Zhao, Y., Lin, Y., Zhang, R., Luo, S., Ye, P., & Luo, M. (2019). The antagonistic effect of tamoxifen against d-galactosamine/lipopolysaccharide-induced acute liver failure is associated with reactivation of hepatic nuclear factor- κ B. *Immunopharmacology and Immunotoxicology*, 41(2), 192–198. <https://doi.org/10.1080/08923973.2019.1569044>
44. Frank, D., Savir, S., Gruenbaum, B. F., Melamed, I., Grinshpun, J., Kuts, R., Knyazer, B., Zlotnik, A., Vinokur, M., & Boyko, M. (2020). Inducing acute liver injury in rats via carbon tetrachloride (CCL4) exposure through an orogastric tube. *Journal of Visualized Experiments*, 2020(158). <https://doi.org/10.3791/60695>
45. Ghasemi, M., Azarnia, M., Jamali, M., Mirabolghasemi, G., Nazarian, S., Naghizadeh, M. M., Rajabi, M., & Tahamtani, Y. (2014). Protective effects of Ephedra pachyclada extract on mouse models of carbon tetrachloride- induced chronic and acute liver failure. *Tissue and Cell*, 46(1), 78–85. <https://doi.org/10.1016/j.tice.2013.11.005>
46. Xie, G., Wang, X., Jiang, R., Zhao, A., Yan, J., Zheng, X., Huang, F., Liu, X., Panee, J., Rajani, C., Yao, C., Yu, H., Jia, W., Sun, B., Liu, P., & Jia, W. (2018). Dysregulated bile acid signaling contributes to the neurological impairment in murine models of acute and chronic liver failure. *EBioMedicine*, 37, 294–306. <https://doi.org/10.1016/j.ebiom.2018.10.030>
47. Matkowskyj, K. A., Marrero, J. A., Carroll, R. E., Daniilkovich, A. V, Green, R. M., & Benya, R. V. (1999). Azoxymethane-induced fulminant hepatic failure in C57BL/6J mice: characterization of a new animal model.
48. Minsart, C., Rorive, S., Lemmers, A., Quertinmont, E., & Gustot, T. (2020). N-acetylcysteine and glycyrrhizin combination: Benefit outcome in a murine model of acetaminophen-induced liver failure. *World Journal of Hepatology*, 12(9), 596–618. <https://doi.org/10.4254/WJH.V12.I9.596>
49. Rahman, T. M., Selden, A. C., & Hodgson, H. J. F. (2002). A novel model of acetaminophen-induced acute hepatic failure in rabbits. *Journal of Surgical Research*, 106(2), 264–272. <https://doi.org/10.1006/jsre.2002.6476>
50. Zakrzewski, W., Dobrzyński, M., Szymonowicz, M., & Rybak, Z. (2019). Stem cells: Past, present, and future. In *Stem Cell Research and Therapy* (Vol. 10, Issue 1). BioMed Central Ltd. <https://doi.org/10.1186/s13287-019-1165-5>
51. Maemura, M., Taketsuru, H., Nakajima, Y., Shao, R., Kakihara, A., Nogami, J., Ohkawa, Y., & Tsukada, Y. (2021). Totipotency of mouse zygotes extends to single blastomeres of embryos at the four-cell stage. *Scientific Reports*, 11(1), 11167. <https://doi.org/10.1038/s41598-021-90653-1>

52. Bacakova, L., Zarubova, J., Travnickova, M., Musilkova, J., Pajorova, J., Slepicka, P., Kasalkova, N. S., Svorcik, V., Kolska, Z., Motarjemi, H., & Molitor, M. (2018). Stem cells: their source, potency and use in regenerative therapies with focus on adipose-derived stem cells – a review. In *Biotechnology Advances* (Vol. 36, Issue 4, pp. 1111–1126). Elsevier Inc. <https://doi.org/10.1016/j.biotechadv.2018.03.011>
53. Liu, G., David, B. T., Trawczynski, M., & Fessler, R. G. (2020). Advances in Pluripotent Stem Cells: History, Mechanisms, Technologies, and Applications. In *Stem Cell Reviews and Reports* (Vol. 16, Issue 1, pp. 3–32). Springer. <https://doi.org/10.1007/s12015-019-09935-x>
54. Menon, S., Shailendra, S., Renda, A., Longaker, M., & Quarto, N. (2016). An overview of direct somatic reprogramming: The ins and outs of iPSCs. In *International Journal of Molecular Sciences* (Vol. 17, Issue 1). MDPI AG. <https://doi.org/10.3390/ijms17010141>
55. Dupont, G., Yilmaz, E., Loukas, M., Macchi, V., De Caro, R., & Tubbs, R. S. (2019). Human embryonic stem cells: Distinct molecular personalities and applications in regenerative medicine. *Clinical Anatomy*, 32(3), 354–360. <https://doi.org/10.1002/ca.23318>
56. Ilic, D., & Ogilvie, C. (2017). Concise Review: Human Embryonic Stem Cells—What Have We Done? What Are We Doing? Where Are We Going? In *Stem Cells* (Vol. 35, Issue 1, pp. 17–25). Wiley-Blackwell. <https://doi.org/10.1002/stem.2450>
57. Suman, S., Domingues, A., Ratajczak, J., & Ratajczak, M. Z. (2019). Potential clinical applications of stem cells in regenerative medicine. In *Advances in Experimental Medicine and Biology* (Vol. 1201, pp. 1–22). Springer. https://doi.org/10.1007/978-3-030-31206-0_1
58. Karagiannis, P., Takahashi, K., Saito, M., Yoshida, Y., Okita, K., Watanabe, A., Inoue, H., Yamashita, J. K., Todani, M., Nakagawa, M., Osawa, M., Yashiro, Y., Yamanaka, S., & Osafune, K. (2019). Induced pluripotent stem cells and their use in human models of disease and development. In *Physiological Reviews* (Vol. 99, Issue 1, pp. 79–114). American Physiological Society. <https://doi.org/10.1152/physrev.00039.2017>
59. Takahashi, K., & Yamanaka, S. (2006). Induction of Pluripotent Stem Cells from Mouse Embryonic and Adult Fibroblast Cultures by Defined Factors. *Cell*, 126(4), 663–676. <https://doi.org/10.1016/j.cell.2006.07.024>
60. Klein, D. (2018). iPSCs-based generation of vascular cells: reprogramming approaches and applications. In *Cellular and Molecular Life Sciences* (Vol. 75, Issue 8, pp. 1411–1433). Birkhauser Verlag AG. <https://doi.org/10.1007/s00018-017-2730-7>
61. Yoshihara, M., Oguchi, A., & Murakawa, Y. (2019). Genomic instability of iPSCs and challenges in their clinical applications. In *Advances in Experimental Medicine and Biology* (Vol. 1201, pp. 23–47). Springer. https://doi.org/10.1007/978-3-030-31206-0_2
62. Ren, C., Wang, F., Guan, L.-N., Cheng, X.-Y., Zhang, C.-Y., Geng, D.-Q., & Liu, C.-F. (2019). A compendious summary of Parkinson's disease patient-derived iPSCs in the first decade. *Annals of Translational Medicine*, 7(22), 685–685. <https://doi.org/10.21037/atm.2019.11.16>
63. Jung-Klawitter, S., & Opladen, T. (2018). Induced pluripotent stem cells (iPSCs) as model to study inherited defects of neurotransmission in inborn errors of metabolism. In *Journal of Inherited Metabolic Disease* (Vol. 41, Issue 6, pp. 1103–1116). Springer Netherlands. <https://doi.org/10.1007/s10545-018-0225-9>
64. Sun, C., Wilson, G., Fan, J.-G., & Qiao, L. (2015). Potential Applications of Induced Pluripotent Stem Cells (iPSCs) in Hepatology Research. *Current Stem Cell Research & Therapy*, 10(3), 208–215. <https://doi.org/10.2174/1574888x10666150120105946>
65. Steinle, H., Weber, M., Behring, A., Mau-Holzmann, U., von Ohle, C., Popov, A. F., Schlensak, C., Wendel, H. P., & Avci-Adali, M. (2019). Reprogramming of Urine-Derived Renal Epithelial Cells into iPSCs Using srRNA and Consecutive Differentiation into Beating Cardiomyocytes. *Molecular Therapy - Nucleic Acids*, 17, 907–921. <https://doi.org/10.1016/j.omtn.2019.07.016>
66. Kim, J. J. (2015). Applications of iPSCs in cancer research. *Biomarker Insights*, 2015(Suppl 1), 125–131. <https://doi.org/10.4137/BMI.S20065>
67. Mirzaei, H., Sahebkar, A., Sichani, L. S., Moridikia, A., Nazari, S., Nahand, J. S., Salehi, H., Stenvang, J., Masoudifar, A., Mirzaei, H. R., & Jaafari, M. R. (2018). Therapeutic application of multipotent stem

- cells. In *Journal of Cellular Physiology* (Vol. 233, Issue 4, pp. 2815–2823). Wiley-Liss Inc. <https://doi.org/10.1002/jcp.25990>
68. Dominici, M., Le Blanc, K., Mueller, I., Slaper-Cortenbach, I., Marini, F. C., Krause, D. S., Deans, R. J., Keating, A., Prockop, D. J., & Horwitz, E. M. (2006). Minimal criteria for defining multipotent mesenchymal stromal cells. The International Society for Cellular Therapy position statement. *Cytotherapy*, 8(4), 315–317. <https://doi.org/10.1080/14653240600855905>
 69. Mushahary, D., Spittler, A., Kasper, C., Weber, V., & Charwat, V. (2018). Isolation, cultivation, and characterization of human mesenchymal stem cells. In *Cytometry Part A* (Vol. 93, Issue 1, pp. 19–31). Wiley-Liss Inc. <https://doi.org/10.1002/cyto.a.23242>
 70. Van Pham, P. (2016). Mesenchymal Stem Cells in Clinical Applications. In *Stem Cells in Clinical Applications* (pp. 37–69). Springer International Publishing Switzerland. https://doi.org/10.1007/978-3-319-40073-0_2
 71. Brown, C., McKee, C., Bakshi, S., Walker, K., Hakman, E., Halassy, S., Svinarich, D., Dodds, R., Govind, C. K., & Chaudhry, G. R. (2019). Mesenchymal stem cells: Cell therapy and regeneration potential. In *Journal of Tissue Engineering and Regenerative Medicine* (Vol. 13, Issue 9, pp. 1738–1755). John Wiley and Sons Ltd. <https://doi.org/10.1002/term.2914>
 72. Russell, A. L., Lefavor, R., Durand, N., Glover, L., & Zubair, A. C. (2018). Modifiers of mesenchymal stem cell quantity and quality. *Transfusion*, 58(6), 1434–1440. <https://doi.org/10.1111/trf.14597>
 73. Mattiucci, D., Maurizi, G., Leoni, P., & Poloni, A. (2018). Aging- and Senescence-associated Changes of Mesenchymal Stromal Cells in Myelodysplastic Syndromes. In *Cell Transplantation* (Vol. 27, Issue 5, pp. 754–764). SAGE Publications Ltd. <https://doi.org/10.1177/0963689717745890>
 74. Murphy, S., & Atala, A. (2013). Amniotic fluid and placental membranes: Unexpected sources of highly multipotent cells. *Seminars in Reproductive Medicine*, 31(1), 62–68. <https://doi.org/10.1055/s-0032-1331799>
 75. Savickiene, J., Treigyte, G., Baronaite, S., Valiuliene, G., Kaupinis, A., Valius, M., Arlauskiene, A., & Navakauskiene, R. (2015). Human amniotic fluid mesenchymal stem cells from second- and third-trimester amniocentesis: Differentiation potential, molecular signature, and proteome analysis. *Stem Cells International*, 2015. <https://doi.org/10.1155/2015/319238>
 76. Jain, M., Minocha, E., Tripathy, N. K., Singh, N., Chaturvedi, C. P., & Nityanand, S. (2019). Comparison of the cardiomyogenic potency of human amniotic fluid and bone marrow mesenchymal stem cells. *International Journal of Stem Cells*, 12(3), 1–8. <https://doi.org/10.15283/IJSC18087>
 77. Roubelakis, M. G., Pappa, K. I., Bitsika, V., Zagoura, D., Vlahou, A., Papadaki, H. A., Antsaklis, A., & Anagnou, N. P. (2007). Molecular and proteomic characterization of human mesenchymal stem cells derived from amniotic fluid: Comparison to bone marrow mesenchymal stem cells. *Stem Cells and Development*, 16(6), 931–951. <https://doi.org/10.1089/scd.2007.0036>
 78. Mareschi, K., Castiglia, S., Sanavio, F., Rustichelli, D., Muraro, M., Defede, D., Bergallo, M., & Fagioli, F. (2016). Immunoregulatory effects on T lymphocytes by human mesenchymal stromal cells isolated from bone marrow, amniotic fluid, and placenta. *Experimental Hematology*, 44(2), 138-150.e1. <https://doi.org/10.1016/j.exphem.2015.10.009>
 79. Ullah, M., Liu, D. D., & Thakor, A. S. (2019). Mesenchymal Stromal Cell Homing: Mechanisms and Strategies for Improvement. *IScience*, 15, 421. <https://doi.org/10.1016/J.ISCI.2019.05.004>
 80. Phinney DG, Pittenger MF. Concise Review: MSC-Derived Exosomes for Cell-Free Therapy [published correction appears in *Stem Cells*. 2017 Sep;35(9):2103]. *Stem Cells*. 2017;35(4):851-858. doi:10.1002/stem.2575
 81. Madrigal M, Rao KS, Riordan NH. A review of therapeutic effects of mesenchymal stem cell secretions and induction of secretory modification by different culture methods. *J Transl Med*. 2014;12:260. Published 2014 Oct 11. doi:10.1186/s12967-014-0260-8
 82. Gnecci M, Danieli P, Malpasso G, Ciuffreda MC. Paracrine Mechanisms of Mesenchymal Stem Cells in Tissue Repair. *Methods Mol Biol*. 2016;1416:123-146. doi:10.1007/978-1-4939-3584-0_7
 83. Harrell CR, Jovicic N, Djonov V, Arsenijevic N, Volarevic V. Mesenchymal Stem Cell-Derived Exosomes and Other Extracellular Vesicles as New Remedies in the Therapy of Inflammatory Diseases. *Cells*. 2019;8(12):1605. Published 2019 Dec 11. doi:10.3390/cells8121605

84. Takeuchi R, Katagiri W, Endo S, Kobayashi T. Exosomes from conditioned media of bone marrow-derived mesenchymal stem cells promote bone regeneration by enhancing angiogenesis. *PLoS One*. 2019;14(11):e0225472. Published 2019 Nov 21. doi:10.1371/journal.pone.0225472
85. Kichenbrand C, Velot E, Menu P, Moby V. Dental Pulp Stem Cell-Derived Conditioned Medium: An Attractive Alternative for Regenerative Therapy. *Tissue Eng Part B Rev*. 2019;25(1):78-88. doi:10.1089/ten.TEB.2018.0168
86. Vizoso FJ, Eiro N, Cid S, Schneider J, Perez-Fernandez R. Mesenchymal Stem Cell Secretome: Toward Cell-Free Therapeutic Strategies in Regenerative Medicine. *Int J Mol Sci*. 2017;18(9):1852. Published 2017 Aug 25. doi:10.3390/ijms18091852
87. Gurunathan, S., Kang, M.-H., Jeyaraj, M., Qasim, M., & Kim, J.-H. (2019). Review of the Isolation, Characterization, Biological Function, and Multifarious Therapeutic Approaches of Exosomes. *Cells*, 8(4), 307. <https://doi.org/10.3390/CELLS8040307>
88. Liu, Y., Lin, L., Zou, R., Wen, C., Wang, Z., & Lin, F. (2018). MSC-derived exosomes promote proliferation and inhibit apoptosis of chondrocytes via lncRNA-KLF3-AS1/miR-206/GIT1 axis in osteoarthritis. *Cell Cycle*, 17(21–22), 2411. <https://doi.org/10.1080/15384101.2018.1526603>
89. Lee, W. M., Stravitz, R. T., & Larson, A. M. (2012). Introduction to the revised American Association for the Study of Liver Diseases position paper on acute liver failure 2011. In *Hepatology* (Vol. 55, Issue 3, pp. 965–967). John Wiley & Sons, Ltd. <https://doi.org/10.1002/hep.25551>
90. K, S., & S, K. (2014). MSC microvesicles for the treatment of lung disease: a new paradigm for cell-free therapy. *Antioxidants & Redox Signaling*, 21(13), 1905–1915. <https://doi.org/10.1089/ARS.2013.5784>
91. Y, J., Y, N., K, W., C, L., & F, E. (2017). Mesenchymal Stem Cell-Derived Microvesicles Modulate Lipopolysaccharides-Induced Inflammatory Responses to Microglia Cells. *Stem Cells* (Dayton, Ohio), 35(3), 812–823. <https://doi.org/10.1002/STEM.2541>
92. Vishnubhatla, I., Corteling, R., Stevanato, L., Hicks, C., & Sinden, J. (2014). The Development of Stem Cell-Derived Exosomes as a Cell-Free Regenerative Medicine: <https://doi.org/10.5772/58597>, 3. <https://doi.org/10.5772/58597>
93. P, W., B, Z., H, S., H, Q., & W, X. (2018). MSC-exosome: A novel cell-free therapy for cutaneous regeneration. *Cytotherapy*, 20(3), 291–301. <https://doi.org/10.1016/J.JCYT.2017.11.002>
94. Lou, G., Chen, Z., Zheng, M., & Liu, Y. (2017). Mesenchymal stem cell-derived exosomes as a new therapeutic strategy for liver diseases. *Experimental and Molecular Medicine*, 49(6). <https://doi.org/10.1038/EMM.2017.63>
95. Psaraki A, Ntari L, Karakostas C, Korrou-Karava D, Roubelakis MG. Extracellular vesicles derived from Mesenchymal Stem/Stromal Cells: the regenerative impact in liver diseases [published online ahead of print, 2021 Aug 27]. *Hepatology*. 2021;10.1002/hep.32129. doi:10.1002/hep.32129
96. DH, H., HK, K., J, L., HH, K., GH, P., SH, Y., JY, J., H, C., JH, L., S, S., YW, Y., & BS, C. (2020). Mesenchymal Stem/Stromal Cell-Derived Exosomes for Immunomodulatory Therapeutics and Skin Regeneration. *Cells*, 9(5). <https://doi.org/10.3390/CELLS9051157>
97. S, Z., SJ, C., RC, L., JHP, H., SK, L., & WS, T. (2018). MSC exosomes mediate cartilage repair by enhancing proliferation, attenuating apoptosis and modulating immune reactivity. *Biomaterials*, 156, 16–27. <https://doi.org/10.1016/J.BIOMATERIALS.2017.11.028>
98. Nakamura Y, Miyaki S, Ishitobi H, et al. Mesenchymal-stem-cell-derived exosomes accelerate skeletal muscle regeneration. *FEBS Lett*. 2015;589(11):1257-1265. doi:10.1016/j.febslet.2015.03.031
99. J, Z., X, L., J, H., F, C., S, Q., X, S., L, G., J, X., & B, X. (2019). Mesenchymal stromal cell-derived exosomes attenuate myocardial ischaemia-reperfusion injury through miR-182-regulated macrophage polarization. *Cardiovascular Research*, 115(7), 1205–1216. <https://doi.org/10.1093/CVR/CVZ040>
100. H, C., S, C., R, X., L, C., X, S., J, W., J, Q., Y, Z., & J, M. (2020). Hypoxia-challenged MSC-derived exosomes deliver miR-210 to attenuate post-infarction cardiac apoptosis. *Stem Cell Research & Therapy*, 11(1). <https://doi.org/10.1186/S13287-020-01737-0>
101. W, Z., Y, Z., X, C., T, N., H, C., Q, G., Y, Z., P, L., Y, Z., C, L., Y, C., T, S., & C, J. (2021). Pancreatic cancer-targeting exosomes for enhancing immunotherapy and reprogramming tumor microenvironment. *Biomaterials*, 268. <https://doi.org/10.1016/J.BIOMATERIALS.2020.120546>

102. C, M., V, R., Y, Y., H, B., J, von der O., & R, H. (2019). Taxol-Loaded MSC-Derived Exosomes Provide a Therapeutic Vehicle to Target Metastatic Breast Cancer and Other Carcinoma Cells. *Cancers*, 11(6). <https://doi.org/10.3390/CANCERS11060798>
103. L, R., AF, K., A, S., & S, R. (2021). Mesenchymal stem cell (MSC)-derived exosomes as a cell-free therapy for patients Infected with COVID-19: Real opportunities and range of promises. *Chemistry and Physics of Lipids*, 234. <https://doi.org/10.1016/J.CHEMPHYSLIP.2020.105009>
104. S, A.-K., & EM, A. (2020). Potential application of mesenchymal stem cells and their exosomes in lung injury: an emerging therapeutic option for COVID-19 patients. *Stem Cell Research & Therapy*, 11(1). <https://doi.org/10.1186/S13287-020-01963-6>
105. Li, T., Yan, Y., Wang, B., Qian, H., Zhang, X., Shen, L., Wang, M., Zhou, Y., Zhu, W., Li, W., & Xu, W. (2013). Exosomes derived from human umbilical cord mesenchymal stem cells alleviate liver fibrosis. *Stem Cells and Development*, 22(6), 845–854. <https://doi.org/10.1089/SCD.2012.0395>
106. Tan, C. Y., Lai, R. C., Wong, W., Dan, Y. Y., Lim, S. K., & Ho, H. K. (2014). Mesenchymal stem cell-derived exosomes promote hepatic regeneration in drug-induced liver injury models. *Stem Cell Research and Therapy*, 5(3). <https://doi.org/10.1186/SCRT465>
107. Jiang, W., Tan, Y., Cai, M., Zhao, T., Mao, F., Zhang, X., Xu, W., Yan, Z., Qian, H., & Yan, Y. (2018). Human umbilical cord MSC-derived exosomes suppress the development of CCl4-induced liver injury through antioxidant effect. *Stem Cells International*, 2018. <https://doi.org/10.1155/2018/6079642>
108. Liu, Y., Lin, L., Zou, R., Wen, C., Wang, Z., & Lin, F. (2018). MSC-derived exosomes promote proliferation and inhibit apoptosis of chondrocytes via lncRNA-KLF3-AS1/miR-206/GIT1 axis in osteoarthritis. *Cell Cycle*, 17(21–22), 2411. <https://doi.org/10.1080/15384101.2018.1526603>
109. M, S., Q, X., Z, W., Y, C., Y, S., X, C., M, C., B, Z., Y, Z., R, Y., Y, S., & H, B. (2020). Exosomes derived from human umbilical cord mesenchymal stem cells ameliorate IL-6-induced acute liver injury through miR-455-3p. *Stem Cell Research & Therapy*, 11(1). <https://doi.org/10.1186/S13287-020-1550-0>
110. Zhao S, Liu Y, Pu Z. Bone marrow mesenchymal stem cell-derived exosomes attenuate D-GalN/LPS-induced hepatocyte apoptosis by activating autophagy in vitro. *Drug Des Devel Ther*. 2019;13:2887-2897. Published 2019 Aug 19. doi:10.2147/DDDT.S220190
111. Zagoura DS, Roubelakis MG, Bitsika V, et al. Therapeutic potential of a distinct population of human amniotic fluid mesenchymal stem cells and their secreted molecules in mice with acute hepatic failure. *Gut*. 2012;61(6):894-906. doi:10.1136/gutjnl-2011-300908
112. Zagoura D, Trohatou O, Makridakis M, et al. Functional secretome analysis reveals Annexin-A1 as important paracrine factor derived from fetal mesenchymal stem cells in hepatic regeneration. *EBioMedicine*. 2019;45:542-552. doi:10.1016/j.ebiom.2019.07.009
113. Li, H., Guan, K., Li, X., Ma, Y., & Zhou, S. (2019). MFG-E8 induced differences in proteomic profiles in mouse C 2 C 12 cells and its effect on PI3K/Akt and ERK signal pathways. *International Journal of Biological Macromolecules*, 124, 681–688. <https://doi.org/10.1016/J.IJBIOMAC.2018.11.265>
114. An, S. Y., Jang, Y. J., Lim, H. J., Han, J., Lee, J., Lee, G., Park, J. Y., Park, S. Y., Kim, J. H., Do, B. R., Han, C., Park, H. K., Kim, O. H., Song, M. J., Kim, S. J., & Kim, J. H. (2017). Milk Fat Globule-EGF Factor 8, Secreted by Mesenchymal Stem Cells, Protects Against Liver Fibrosis in Mice. *Gastroenterology*, 152(5), 1174–1186. <https://doi.org/10.1053/j.gastro.2016.12.003>
115. Jang, Y. J., An, S. Y., & Kim, J. H. (2017). Identification of MFG8 in mesenchymal stem cell secretome as an anti-fibrotic factor in liver fibrosis. *BMB Reports*, 50(2), 58–59. <https://doi.org/10.5483/BMBRep.2017.50.2.012>
116. Zhang, L., Tian, R., Yao, X., Zhang, X. J., Zhang, P., Huang, Y., She, Z. G., Li, H., Ji, Y. X., & Cai, J. (2021). Milk Fat Globule–Epidermal Growth Factor–Factor 8 Improves Hepatic Steatosis and Inflammation. *Hepatology*, 73(2), 586–605. <https://doi.org/10.1002/hep.31277>
117. Sastre J, Dávila I. Dupilumab: A New Paradigm for the Treatment of Allergic Diseases. *J Investig Allergol Clin Immunol*. 2018;28(3):139-150. doi:10.18176/jiaci.0254
118. Nguyen JK, Austin E, Huang A, Mamalis A, Jagdeo J. The IL-4/IL-13 axis in skin fibrosis and scarring: mechanistic concepts and therapeutic targets. *Arch Dermatol Res*. 2020;312(2):81-92. doi:10.1007/s00403-019-01972-3
119. Vaz de Paula CB, de Azevedo MLV, Nagashima S, et al. IL-4/IL-13 remodeling pathway of COVID-19 lung injury. *Sci Rep*. 2020;10(1):18689. Published 2020 Oct 29. doi:10.1038/s41598-020-75659-5

120. Gao S, Zhou J, Liu N, et al. Curcumin induces M2 macrophage polarization by secretion IL-4 and/or IL-13. *J Mol Cell Cardiol.* 2015;85:131-139. doi:10.1016/j.yjmcc.2015.04.025
121. Capuano A, Fogolari F, Bucciotti F, et al. The $\alpha 4\beta 1$ /EMILIN1 interaction discloses a novel and unique integrin-ligand type of engagement. *Matrix Biol.* 2018;66:50-66. doi:10.1016/j.matbio.2017.10.001
122. Imhof T, Korkmaz Y, Koch M, Sengle G, Schiavinato A. EMILIN proteins are novel extracellular constituents of the dentin-pulp complex. *Sci Rep.* 2020;10(1):15320. Published 2020 Sep 18. doi:10.1038/s41598-020-72123-2
123. Li A, Yuan JF, Gong Q, et al. Effects of *Eucommia ulmoides* extract against renal injury caused by long-term high purine diets in rats. *Food Funct.* 2021;12(12):5607-5620. doi:10.1039/d0fo02802a
124. Datta R, Lizama CO, Soltani AK, et al. Autoregulation of insulin receptor signaling through MFG8 and the $\alpha v\beta 5$ integrin. *Proc Natl Acad Sci U S A.* 2021;118(18):e2102171118. doi:10.1073/pnas.2102171118
125. Ren JJ, Huang TJ, Zhang QQ, et al. Insulin-like growth factor binding protein related protein 1 knockdown attenuates hepatic fibrosis via the regulation of MMPs/TIMPs in mice. *Hepatobiliary Pancreat Dis Int.* 2019;18(1):38-47. doi:10.1016/j.hbpd.2018.08.008
126. Gao, Y. Y., Zhang, Z. H., Zhuang, Z., Lu, Y., Wu, L. Y., Ye, Z. nan, Zhang, X. S., Chen, C. L., Li, W., & Hang, C. H. (2018). Recombinant milk fat globule-EGF factor-8 reduces apoptosis via integrin $\beta 3$ /FAK/PI3K/AKT signaling pathway in rats after traumatic brain injury. *Cell Death and Disease*, 9(9). <https://doi.org/10.1038/S41419-018-0939-5>
127. Xu, X., Zhang, A., Zhu, Y., He, W., Di, W., Fang, Y., & Shi, X. (2018). MFG-E8 reverses microglial-induced neurotoxic astrocyte (A1) via NF- κ B and PI3K-Akt pathways. *Journal of Cellular Physiology*, 234(1), 904–914. <https://doi.org/10.1002/JCP.26918>
128. Khalifeh-Soltani, A., Gupta, D., Ha, A., Podolsky, M. J., Datta, R., & Atabai, K. (2018). The Mfge8- $\alpha 8\beta 1$ -PTEN pathway regulates airway smooth muscle contraction in allergic inflammation. *FASEB Journal*, 32(11), 5927–5936. <https://doi.org/10.1096/FJ.201800109R>
129. Li, H., Xu, W., Ma, Y., Zhou, S., & Xiao, R. (2018). Milk fat globule membrane protein promotes C2C12 cell proliferation through the PI3K/Akt signaling pathway. *International Journal of Biological Macromolecules*, 114, 1305–1314. <https://doi.org/10.1016/J.IJBIOMAC.2018.04.026>
130. Modica, T. M. E., Maiorani, O., Sartori, G., Pivetta, E., Doliana, R., Capuano, A., Colombatti, A., & Spessotto, P. (2017). The extracellular matrix protein EMILIN1 silences the RAS-ERK pathway via $\alpha 4\beta 1$ integrin and decreases tumor cell growth. *Oncotarget*, 8(16), 27034–27046. <https://doi.org/10.18632/ONCOTARGET.15067>
131. Cooper LF, Ravindran S, Huang CC, Kang M. A Role for Exosomes in Craniofacial Tissue Engineering and Regeneration. *Front Physiol.* 2020;10:1569. Published 2020 Jan 14. doi:10.3389/fphys.2019.01569
132. Braicu C, Tomuleasa C, Monroig P, Cucuianu A, Berindan-Neagoe I, Calin GA. Exosomes as divine messengers: are they the Hermes of modern molecular oncology?. *Cell Death Differ.* 2015;22(1):34-45. doi:10.1038/cdd.2014.130
133. Masyuk AI, Masyuk TV, Larusso NF. Exosomes in the pathogenesis, diagnostics and therapeutics of liver diseases. *J Hepatol.* 2013;59(3):621-625. doi:10.1016/j.jhep.2013.03.028
134. Ge, Z., Chen, Y., Wang, B., Zhang, X., Yan, Y., Zhou, L., Zhang, Y., & Xie, Y. (2020). MFG8 attenuates Ang-II-induced atrial fibrosis and vulnerability to atrial fibrillation through inhibition of TGF- $\beta 1$ /Smad2/3 pathway. *Journal of Molecular and Cellular Cardiology*, 139, 164–175. <https://doi.org/10.1016/J.YJMCC.2020.01.001>
135. Fujiwara, C., Uehara, A., Sekiguchi, A., Uchiyama, A., Yamazaki, S., Ogino, S., Yokoyama, Y., Torii, R., Hosoi, M., Suto, C., Tsunekawa, K., Murakami, M., Ishikawa, O., & Motegi, S. ichiro. (2019). Suppressive Regulation by MFG-E8 of Latent Transforming Growth Factor β -Induced Fibrosis via Binding to αv Integrin: Significance in the Pathogenesis of Fibrosis in Systemic Sclerosis. *Arthritis and Rheumatology*, 71(2), 302–314. <https://doi.org/10.1002/ART.40701>
136. Carnevale, D., Facchinello, N., Iodice, D., Bizzotto, D., Perrotta, M., De Stefani, D., Pallante, F., Carnevale, L., Ricciardi, F., Cifelli, G., Da Ros, F., Casaburo, M., Fardella, S., Bonaldo, P., Innocenzi, G., Rizzuto, R., Braghetta, P., Lembo, G., & Bressan, G. M. (2018). Loss of emilin-1 enhances arteriolar myogenic tone through TGF- β (transforming growth factor- β)-dependent transactivation of EGFR

- (epidermal growth factor receptor) and is relevant for hypertension in mice and humans. *Arteriosclerosis, Thrombosis, and Vascular Biology*, 38(10), 2484–2497. <https://doi.org/10.1161/ATVBAHA.118.311115>
137. Nagase H, Visse R, Murphy G. Structure and function of matrix metalloproteinases and TIMPs. *Cardiovasc Res*. 2006;69(3):562-573. doi:10.1016/j.cardiores.2005.12.002
 138. Ortiz C, Schierwagen R, Schaefer L, Klein S, Trepats X, Trebicka J. Extracellular Matrix Remodeling in Chronic Liver Disease [published online ahead of print, 2021 Jul 23]. *Curr Tissue Microenviron Rep*. 2021;1-12. doi:10.1007/s43152-021-00030-3
 139. Benyon RC, Hovell CJ, Da Gaça M, Jones EH, Iredale JP, Arthur MJ. Progelatinase A is produced and activated by rat hepatic stellate cells and promotes their proliferation. *Hepatology*. 1999;30(4):977–986. doi: 10.1002/hep.510300431
 140. Howangyin KY, Zlatanova I, Pinto C, et al. Myeloid-Epithelial-Reproductive Receptor Tyrosine Kinase and Milk Fat Globule Epidermal Growth Factor 8 Coordinately Improve Remodeling After Myocardial Infarction via Local Delivery of Vascular Endothelial Growth Factor. *Circulation*. 2016;133(9):826-839. doi:10.1161/CIRCULATIONAHA.115.020857
 141. Wu HY, Zhang XC, Jia BB, et al. Exosomes derived from human umbilical cord mesenchymal stem cells alleviate acetaminophen-induced acute liver failure through activating ERK and IGF-1R/PI3K/AKT signaling pathway. *J Pharmacol Sci*. 2021;147(1):143-155. doi:10.1016/j.jphs.2021.06.008
 142. Wu HH, Lee OK. Exosomes from mesenchymal stem cells induce the conversion of hepatocytes into progenitor oval cells. *Stem Cell Res Ther*. 2017;8(1):117. Published 2017 May 23. doi:10.1186/s13287-017-0560-z
 143. Liu J, Tan H, Sun Y, Zhou S, Cao J, Wang F. The preventive effects of heparin-superoxide dismutase on carbon tetrachloride-induced acute liver failure and hepatic fibrosis in mice. *Mol Cell Biochem*. 2009;327(1-2):219-228. doi:10.1007/s11010-009-0060-2
 144. Chen X, Gong X, Jiang R, et al. Resolvin D1 attenuates CCl4-induced acute liver injury involving up-regulation of HO-1 in mice. *Immunopharmacol Immunotoxicol*. 2016;38(2):61-67. doi:10.3109/08923973.2015.1115517
 145. Zhang S, Hou Y, Yang J, et al. Application of mesenchymal stem cell exosomes and their drug-loading systems in acute liver failure. *J Cell Mol Med*. 2020;24(13):7082-7093. doi:10.1111/jcmm.15290
 146. Tsuchiya A, Takeuchi S, Watanabe T, et al. Mesenchymal stem cell therapies for liver cirrhosis: MSCs as "conducting cells" for improvement of liver fibrosis and regeneration. *Inflamm Regen*. 2019;39:18. Published 2019 Sep 9. doi:10.1186/s41232-019-0107-z
 147. Moslem M, Valojerdi MR, Pournasr B, Muhammadnejad A, Baharvand H. Therapeutic potential of human induced pluripotent stem cell-derived mesenchymal stem cells in mice with lethal fulminant hepatic failure. *Cell Transplant*. 2013;22(10):1785-1799. doi:10.3727/096368912X662462
 148. Gu J, Zhang E, Liang B, et al. Liver Collagen Contents Are Closely Associated with the Severity of Cirrhosis and Posthepatectomy Liver Failure in Patients with Hepatocellular Carcinoma and Child-Pugh Grade A Liver Function. *Ann Surg Oncol*. 2021;28(8):4227-4235. doi:10.1245/s10434-020-09557-5
 149. He Y, Jin L, Wang J, Yan Z, Chen T, Zhao Y. Mechanisms of fibrosis in acute liver failure. *Liver Int*. 2015;35(7):1877-1885. doi:10.1111/liv.12731
 150. Liu F, Chen Y, Hu Q, et al. MFGE8/Integrin β 3 pathway alleviates apoptosis and inflammation in early brain injury after subarachnoid hemorrhage in rats. *Exp Neurol*. 2015;272:120-127. doi:10.1016/j.expneurol.2015.04.016
 151. Weiskirchen, R., Tabas, I., Diehl, L., Horst, A. K., & Tiegs, G. (2019). Contribution of Macrophage Efferocytosis to Liver Homeostasis and Disease. *Frontiers in Immunology* | www.frontiersin.org, 10. <https://doi.org/10.3389/fimmu.2019.02670>
 152. Wang, H., Wang, G., Ansari, G. A. S., Firoze, M., & Id, K. (2018). Trichloroethene metabolite dichloroacetyl chloride induces apoptosis and compromises phagocytosis in Kupffer Cells: Activation of inflammasome and MAPKs. <https://doi.org/10.1371/journal.pone.0210200>
 153. Z, P., EK, D., C, L., L, P., S, L., X, W., JA, J., S, K., & AD, F. (2019). Bacillus anthracis Edema Toxin Inhibits Efferocytosis in Human Macrophages and Alters Efferocytic Receptor Signaling. *International Journal of Molecular Sciences*, 20(5). <https://doi.org/10.3390/IJMS20051167>

154. A, D., S, G., M, S., S, C., NS, A., NL, P., ES, W., JF, S., CK, S., & S, R. (2016). Correction of MFG-E8 Resolves Inflammation and Promotes Cutaneous Wound Healing in Diabetes. *Journal of Immunology* (Baltimore, Md. : 1950), 196(12), 5089–5100. <https://doi.org/10.4049/JIMMUNOL.1502270>